

Calibration Procedures for Seismic and Deflection-Based Devices

by

Vivek Tandon, Ph.D.

and

Soheil Nazarian, Ph.D., P.E.

Research Project 7-2984

Conducted for

Texas Department of Transportation

Research Report 2984 - 2F

December 1998

**The Center for Highway Materials Research
The University of Texas at El Paso
El Paso, TX 79968-0516**

TECHNICAL REPORT STANDARD TITLE PAGE

1. Report No. TX - 98 2984 - 2F		2. Government Accession No.		3. Recipient's Catalog No.	
4. Title and Subtitle Calibration Procedures for Seismic and Deflection-Based Devices				5. Report Date December 1998	
				6. Performing Organization Code	
7. Authors V. Tandon and S. Nazarian				8. Performing Organization Report No. Research Report 2984-2F	
9. Performing Organization Name and Address Center for Highway Materials Research The University of Texas at El Paso El Paso, Texas 79968-0516				10. Work Unit No.	
				11. Contract or Grant No. Study No. 7-2984	
12. Sponsoring Agency Name and Address Texas Department of Transportation P.O. Box 5051 Austin, Texas 78763				13. Type of Report and Period Covered Final Report 9/96 - 8/98	
				14. Sponsoring Agency Code	
15. Supplementary Notes Research Performed in Cooperation with TxDOT Research Study Title: Development of Instrumentation Testing and Calibration Procedures and Facilities					
16. Abstract TxDOT has acquired fifteen Falling Weight Deflectometers (FWD), one Seismic Pavement Analyzer (SPA), and five Portable Seismic Pavement Analyzers (PSPA) for evaluating the structural integrity of pavements. These nondestructive testing devices use different types of sensor for measuring deflection, deformation and load with time. The accuracy and precision levels of these devices reduce over the years due to wear and tear of the testing devices. Thus, it is essential to develop calibration procedures for these sensors. The primary function of the FWD device is to measure a deflection basin due to a load imparted to the pavement. Velocity transducers (a.k.a. geophones) are used to determine the deflection and load cells are utilized to measure the applied load. The SPA uses several accelerometers and geophones to measure the propagation of waves and deformation of pavements due to imparted loads. Load cells are used to measure the loads applied to the pavement. The PSPA only uses accelerometers to measure wave propagation patterns. Calibration procedures for three different sensors: a) accelerometers, b) geophones, and c) load cells, which are essential for accurate and precise structural evaluation of pavements, have been developed as part of this study. The unique features of the proposed procedures are that: 1) each sensor is calibrated in place as a system, 2) none of the devices have to be disassembled for calibration, and 3) any desired frequency range and amplitude can be conveniently reproduced.					
17. Key Words FWD, PSPA, SPA, Geophone, Accelerometer, Calibration, Load Cell.			18. Distribution Statement No restrictions. This document is available to the public through the National Technical Information Service, 5285 Port Royal Road, Springfield, Virginia 22161		
19. Security Classified (of this report) Unclassified		20. Security Classified (of this page) Unclassified		21. No. of Pages 109	22. Price

The contents of this report reflect the view of the authors, who are responsible for the facts and the accuracy of the data presented herein. The contents do not necessarily reflect the official views or policies of the Texas Department of Transportation. This report does not constitute a standard, specification, or regulation.

The material contained in this report is experimental in nature and is published for informational purposes only. Any discrepancies with official views or policies of the Texas Department of Transportation should be discussed with the appropriate Austin Division prior to implementation of the procedures or results.

**NOT INTENDED FOR CONSTRUCTION, BIDDING, OR
PERMIT PURPOSES**

Vivek Tandon, Ph.D.
Soheil Nazarian, Ph.D., P.E. (69263)

Acknowledgments

The authors would like to express their sincere appreciation to Mr. Carl Bertrand of Design Division of the Texas Department of Transportation for his ever-present support. Many thanks are also due to Mr. Randy Beck of the Design Division for providing expertise in debugging the FWD system. The authors would like to thank the El Paso and Odessa District personnel for providing us with the FWD devices

The authors would also like to thank the undergraduate research assistants who worked on this project. Specifically, the recognition is extended to Cijifredo Zuniga, and Javier Dominguez for their enthusiasm in performing all the necessary tests for this project and their help in the preparation of this report.

This was a joint project between UTEP and the University of Texas at Arlington. The constant interaction with Dr. Roger Walker of UT-Arlington was very beneficial and constructive.

This page replaces an intentionally blank page in the original.

-- CTR Library Digitization Team

Abstract

TxDOT has acquired fifteen Falling Weight Deflectometers (FWD), one Seismic Pavement Analyzer (SPA), and five Portable Seismic Pavement Analyzers (PSPA) for evaluating the structural integrity of pavements. These nondestructive testing devices use different types of sensor for measuring deflection, deformation and load with time. The accuracy and precision levels of these devices reduce over the years due to wear and tear of the testing devices. Thus, it is essential to develop calibration procedures for these sensors.

The primary function of the FWD device is to measure a deflection basin due to a load imparted to the pavement. Velocity transducers (a.k.a. geophones) are used to determine the deflection and load cells are utilized to measure the applied load. The SPA uses several accelerometers and geophones to measure the propagation of waves and deformation of pavements due to imparted loads. Load cells are used to measure the loads applied to the pavement. The PSPA only uses accelerometers to measure wave propagation patterns.

Calibration procedures for three different sensors: a) accelerometers, b) geophones, and c) load cells, which are essential for accurate and precise structural evaluation of pavements, have been developed as part of this study. The unique features of the proposed procedures are that: 1) each sensor is calibrated in place as a system, 2) none of the devices have to be disassembled for calibration, and 3) any desired frequency range and amplitude can be conveniently reproduced.

This page replaces an intentionally blank page in the original.

-- CTR Library Digitization Team

Implementation Statement

The calibration methods proposed in this study can be immediately implemented by the TxDOT. The proper calibration of the sensors used in the nondestructive testing devices is essential in obtaining high-quality data, and ensuring that similar equipment yield comparable results throughout the State.

A prototype slab that can accommodate the necessary instrumentation for most calibration setups has been developed at UTEP during the course of this study. It is proposed that such facility be replicated in Austin for use by TxDOT.

This page replaces an intentionally blank page in the original.

-- CTR Library Digitization Team

Table of Contents

Acknowledgments	vii
Abstract	ix
Implementation Statement	xi
List of Tables	xv
List of Figures	xvii
Chapter 1	
Introduction	1
Problem Statement	1
Research Objective and Approach	1
Chapter 2	
Falling Weight Deflectometer	3
SHRP Calibration Method	3
Relative Calibration Procedure	4
Reference Calibration Procedure for Geophone and the Load Cells	4
Texas Calibration Method	5
Proposed Calibration System for Geophones	6
Laboratory Reference Geophone Calibration	6
Proposed Calibration Setup for the Load Cell	15
Laboratory Calibration of Reference Load Cells	15
Field Calibration of the FWD Load Cells	17
Characteristics of Geophones	17
Calibration with Texas System	20

Chapter 3

Portable Seismic Pavement Analyzer	23
Description of PSPA Data Analysis Procedures	24
Proposed Calibration of Accelerometers	29
Phase Shift Calibration	29
Amplitude Calibration	36

Chapter 4

Seismic Pavement Analyzer	43
Description of SPA Data Analysis Procedure	43
Impulse-Response Method	44
Spectral-Analysis-of-Surface-Wave (SASW) Method	46
Proposed Calibration of Accelerometers	47
Phase Shift Calibration	47
Amplitude Calibration	54
Proposed Calibration of Geophones	56
Phase Shift Calibration	56
Amplitude Calibration	56
Proposed Calibration of Load Cells	56

References	63
------------------	----

Appendix A

Specifications of Equipment Used	65
--	----

List of Tables

Table 2.1 Characteristics of Geophones Used in This Study	20
Table 3.1 Poles and Zeros Obtained from Curve Fitting of the Data of Figure 3.10	36
Table 3.2 Poles and Zeros Obtained from Curve Fitting of Spectra Shown in Figure 3.14	41
Table 4.1 Poles and Zeros Obtained from Fitting a Curve to Data Shown in Figure 4.10	52
Table 4.2 Poles and Zeros Obtained from Fitting a Curve to Data Shown in Figure 4.12	54

This page replaces an intentionally blank page in the original.

-- CTR Library Digitization Team

List of Figures

Figure 2.1	A Schematic of Proximitor Calibration Test Setup	7
Figure 2.2	A Typical Calibration Curve of Proximitor	8
Figure 2.3	A Schematic of Laboratory Test Setup for Geophone Calibration	9
Figure 2.4	A Typical Frequency Response and Coherence Function from Calibration of a Geophone	10
Figure 2.5	Calibration Curves of Geophones	12
Figure 2.6	A Schematic of Field Calibration of FWD Geophone	13
Figure 2.7	Field Calibration of FWD Geophone	14
Figure 2.8	A Calibration Curve of FWD Geophone	15
Figure 2.9	A Schematic of Load Cell Calibration in the Laboratory	16
Figure 2.10	A Typical Calibration Curve of Load Cell	18
Figure 2.11	A Schematic of FWD Load Cell Calibration	19
Figure 2.12	Comparison of Calibration Factors from SHRP and Texas Protocols	21
Figure 2.13	Comparison of Raw Geophone Outputs Under a 30 mSec Impulse	22
Figure 2.14	Comparison of Deflections Obtained from Geophones Under 30 mSec Impulse	22
Figure 3.1	Schematic of Portable Seismic Pavement Analyzer	24
Figure 3.2	Typical Time Records from High-Frequency Seismic Field Tests	25
Figure 3.3	Spectral Functions from USW Tests	26
Figure 3.4	Typical Dispersion Curve from an Asphalt Concrete Layer	28
Figure 3.5	A Typical Frequency Response Obtained with IE Method	29
Figure 3.6	A Schematic Diagram of PSPA Calibration System	30
Figure 3.7	Response of Accelerometer Outside PSPA Holder	32
Figure 3.8	Responses of a Typical PSPA Accelerometer before and after Placed inside the Sensor Holder	33
Figure 3.9	Comparison of Response of Accelerometers 1 and 2 of PSPA	34
Figure 3.10	Ratio of Frequency Response Curves of Accelerometer 1 and 2	35
Figure 3.11	A Schematic of Test Setup for Amplitude Calibration of Accelerometer	37
Figure 3.12	A Typical Frequency Response of Built-in Accelerometer of Piezo Shaker	38
Figure 3.13	A Typical Frequency Response of PSPA Accelerometer	39
Figure 3.14	Calibration Curves for PSPA Accelerometer	40
Figure 3.15	Calibrated Response of PSPA Accelerometer	42

Figure 4.1	A Schematic of Seismic Pavement Analyzer	44
Figure 4.2	Typical Normalized Time Records Obtained with SPA	45
Figure 4.3	Typical Spectral Functions Used in Impulse-Response Test	46
Figure 4.4	Typical Amplified Signal Used in Ultrasonic-Body-Waves Test	48
Figure 4.5	Spectral Functions Used in SASW Method	49
Figure 4.6	Typical Dispersion Curves from SASW Testing	50
Figure 4.7	Typical Modulus Profile from SASW Tests	50
Figure 4.8	A Schematic of Field Calibration of SPA Accelerometer or Geophone	51
Figure 4.9	Comparison of Phase Spectra of Accelerometers 2 and 3 of SPA	53
Figure 4.10	Phase Calibration Spectrum for Accelerometers 2 and 3 Pair	53
Figure 4.11	Amplitude Ratio Spectrum of Accelerometer 1 of SPA	55
Figure 4.12	Amplitude Calibration of SPA Accelerometer 1	55
Figure 4.13	Comparison of Response of Geophones 2 and 3 of SPA	57
Figure 4.14	Ratio of Frequency Response Curves of Geophones 2 and 3	57
Figure 4.15	Field Calibration of SPA Geophone 1	58
Figure 4.16	Calibration Amplitude Spectra for Geophone 1 of SPA	59
Figure 4.17	A Schematic of Test Setup for SPA Load Cell Calibration	60
Figure 4.18	A Typical Load Time-History from the Calibration and SPA Load Cells	61
Figure 4.19	A Typical Calibration Curve of SPA Low-Frequency Load Cell	61
Figure 4.20	A Typical Calibration Curve of SPA High-Frequency Load Cell	62

Chapter 1

Introduction

Problem Statement

Nondestructive devices are being used by the Texas DOT for pavement evaluation. TxDOT has acquired fifteen Falling Weight Deflectometers (FWD), one Seismic Pavement Analyzer (SPA), and five Portable Seismic Pavement Analyzers (PSPA) for evaluating the structural integrity of pavements. These nondestructive testing devices use different types of sensor for measuring deflection, deformation and load with time. The accuracy and precision levels of these devices reduce over the years due to wear and tear of the testing devices. Thus, it is essential to develop calibration procedures for these sensors.

The primary function of the FWD device is to measure a deflection basin due to a load imparted to the pavement. Velocity transducers (a.k.a. geophones) are used to determine the deflection and load cells are utilized to measure the applied load. The SPA uses several accelerometers and geophones to measure the propagation of waves and deformation of pavements due to imparted loads. Load cells are used to measure the loads applied to the pavement. The PSPA only uses accelerometers to measure wave propagation patterns.

Calibration procedures for three different sensors: a) accelerometers, b) geophones, and c) load cells, which are essential for accurate and precise structural evaluation of pavements, have been developed as part of this study.

Research Objective and Approach

The main objective of this study was to develop calibration procedures for three types of sensors used in FWD, SPA and PSPA. Although similar sensors are used in different devices, the amplitude levels and the frequency ranges utilized in the analysis differ from one testing device to another. Hence, it is essential to develop calibration procedures for each sensor in each testing device.

The main objectives of this research have been accomplished by identifying the role of each sensor in evaluating the structural integrity of pavements, and devising methods to ensure that the information obtained from the sensor is accurate and precise.

In view of the above discussion, this study was divided into three phases. In the first phase, calibration procedures for sensors used in the FWD devices were developed. In the second and third phases, calibration procedures for sensors used in the SPA and PSPA were developed.

For each phase, current calibration test methods for each sensor were identified, evaluated and modified. New calibration procedures were developed when necessary. The calibration procedures were developed keeping in view two objectives. Each calibration procedure should be able to identify the accuracy and precision of the sensor calibrated. In addition, the calibration procedure should be practical and easy so that they can be routinely performed by the TxDOT personnel.

This report is divided into five chapters. In the first chapter, the problem statement and research objectives are reported. The second chapter consists of a review of the existing calibration procedures for sensors used in the FWD, along with several modifications to the existing procedures to make them more robust and convenient. The third and fourth chapters include the newly-devised calibration procedures for the sensors used in the PSPA and SPA, respectively. The fifth chapter summarizes the findings of the report, and provide suggestions for future activities to more smoothly implement the procedures in TxDOT activities.

Chapter 2

Falling Weight Deflectometer

Most highway agencies use the FWD for evaluating the structural integrity of their pavements. Over the last decade or so, TxDOT has acquired a fleet of fifteen FWDs, and successfully used them for pavement evaluations. The primary function of the FWD is to measure a deflection basin due to a load imparted to the pavement. Deflection basin measured in the field is used to back-calculate modulus profiles of pavement sections. Various computer programs are available for back-calculation process.

It is critical to accurately determine the deflection basins and imparted loads in the field. Nazarian and Stokoe (1986) indicate that a small error in deflections measured in the field may yield significantly erroneous modulus values. Hence, a reliable method for evaluating the accuracy of the sensors used for determining deflections, is needed.

Two different calibration systems for evaluating the accuracy and precision of the FWD have been developed. One of them, developed by the Strategic Highway Research Program (SHRP), performs the relative as well as reference calibration of the geophones. The second method is a so-called Texas Calibration Method which was developed at the University of Texas at El Paso (UTEP) for the TxDOT. Both of these methods have been recently included in the ASTM standards for the FWD testing. These methods are discussed in the following sections.

SHRP Calibration Method

Under the SHRP calibration method, two types of calibrations are performed: 1) a reference calibration and 2) a relative calibration. The SHRP reference calibration compares a deflection measured with an FWD reading against an independent reference sensor that meets benchmarks traceable to the National Institute of Standards and Technology. The relative calibration, which SHRP standardized, ensures that the FWD sensors provide consistent results and function correctly. A brief description of these procedures is included in this section. A detailed description of these procedures can be found in ASTM D4694.

Relative Calibration Procedure

The goal of the relative calibration procedure is to ensure that all sensors reproduce the same deflection under a given impact. The relative deflection calibration requires a sensor holding tower. The tower must have sufficient positions to accommodate all sensors used in an FWD. The sensors are stacked one above the other along a vertical axis. During the calibration, the sensors are rotated so that each sensor occupies every level in the tower. At each tower position, five deflections are recorded for each sensor. Deflection magnitudes of about 400 μm (15 mils) are desired. Deflection ratios are determined for each sensor by dividing the average for all the sensors by the average of that sensor. If any of the resulting ratios are greater than 1.003 or less than 0.997, all sensor calibration factors should be adjusted.

To ensure that small deflections are monitored to a reasonable degree of accuracy, the above procedure is repeated at a distance of 1 to 1.5 m (3 to 5 feet) from the load plate. Deflection magnitudes between 50 μm to 100 μm (2 to 4 mils) are desired. If the average difference between any two sensor readings is 2 μm (0.08 mils) or less, the calibration factors should not be altered. On the other hand, if the differences in average deflections are greater than 2 μm (0.08 mils), the device should be repaired and re-calibrated according to the manufacturer's recommendations.

Reference Calibration Procedure for Geophone and the Load Cells

The relative calibration ensures that all geophone readings are consistent. But it does not ensure that the deflections are accurate. The reference calibration is conducted to determine the accuracy of sensors. The SHRP reference calibration system uses a Linear Variable Differential Transformer (LVDT) as the reference deflection measurement device, because it can be accurately and independently calibrated with a micrometer. The LVDT and the geophones are mounted in special holders so that the magnetized tip of the LVDT core is always in contact with the top of the holder for the geophone, and hence is always subjected to the same movement as the geophone. The LVDT is mounted at the end of a wide-flange beam. The geophone holder is designed to rest on the pavement. During the calibration process, each geophone is taken out of the holder and placed in the holder under the reference calibration beam. The geophone calibration data are collected at two deflection levels similar to that of relative calibration procedure. Ten sets of deflection data are collected for each deflection level. The calibration factors are then calculated for each geophone. The new calibration factors should be used for future analysis.

The load cell calibration is performed by using a reference load cell. The reference load cell consists of an aluminum case, 30 cm (11.8 inches) in diameter, and 8.3 cm (3.25 inches) high, with four measuring links equally spaced on a 19 cm (7.5 inches) circle. A ribbed rubber sheet, identical to that on the bottom of the FWD loading plate, is glued to the bottom of the reference load cell to ensure uniform pressure on the pavement surface. For each FWD, load cell calibration is performed at four load levels, with ten tests at each level. A relationship is developed between the FWD load cell and the reference load cell. The developed relationship can then be used for modifying the FWD load cell readings.

This method of the calibration has two disadvantages. First, the geophone (a deflection measurement sensor) is taken out of the holder and placed on a rigid frame. As such, with this

method of calibration, one does not calibrate the geophone system but the geophone. It is possible that the geophone is working properly, however, the spring holding mechanism is worn out. In that situation, the calibration of geophone will show no problems but the results obtained from the FWD system may not be accurate. Second, the accuracy of the system is determined at two levels of deflections 400 μm and 50 μm . However, the deflections measured in the field can be as high as 2500 μm (100 mils). Problems associated with the higher deflections could not be identified with this method of calibration.

In recent years, highway agencies have started focusing on the issue of using the whole time history record of the geophone rather than using only peak deflections. For accurate and precise measurement of the deflection time history, it is essential to evaluate the performance for a frequency range and multiple deflection levels. This standard is not capable of performing the calibration for a range of frequencies and deflections.

Texas Calibration Method

A portable reference calibration system, that can be used in the field, has also been developed at UTEP. This calibration system consists of at least two-well calibrated geophones, three load cells, a load-bearing plate, and a data acquisition system (Nazarian et al., 1991). The system allows the simultaneous calibration of several FWD geophones. The well-calibrated geophones are placed next to the FWD geophones with the help of modeling clay or vacuum grease. After the placement of the geophones, the load is dropped ten times from each drop height. The deflection measured from the FWD geophones and the calibration system geophones are compared to identify the accuracy of the individual geophone similar to the SHRP procedure.

One advantage of this calibration system is that the FWD geophones are not removed from the FWD holders, and therefore, it provides the calibration of the geophone system (not the geophone alone). The disadvantages of the system are that 1) this method can only calibrate for peak deflections, and 2) this method of calibration cannot be applied to the FWD central geophone located on top of the loading plate.

The load cell calibration procedure is similar to the SHRP procedure except that the three dynamic load cells, sandwiched between two steel plates, have been used in the Texas Calibration method. The load cells are affixed to the bottom plate and the load is transferred to them through the top plate. The summation of peak loads obtained from the three load cells is compared with the load measured by the FWD load cell.

Based on the shortcomings of the two systems described, a more comprehensive calibration system is needed. The system should be capable of calibrating geophones over the ranges of frequency and deflection observed in the field such that the whole time history of a deflection basin can be obtained accurately and precisely. The modified calibration method should also be capable of identifying the problems associated with the FWD holding system or the geophones. Thus, the highway agencies can determine when to replace the geophone holders or the geophones.

Proposed Calibration System for Geophones

The proposed calibration takes advantage of the laboratory calibration procedures developed during the assessment of the Texas Calibration Protocol described above. The laboratory procedures are extensively modified so that they can be directly applicable to the field calibration. In the Texas Calibration Procedure, several reference geophones are calibrated in the laboratory so that they can be used in the field to verify the FWD geophone's accuracy and precision. In the proposed setup, the geophone calibration setup is transported in the field so that the FWD geophones can be directly calibrated. The new calibration protocol has a field and a laboratory component as described next.

Laboratory Reference Geophone Calibration

In the laboratory calibration setup, a proximator and a reference geophone is calibrated. A proximator is a non-contact transducer which monitors the movement of a target by converting the change in the eddy current field to change in voltage (Tandon,1990). As shown in Figure 2.1, a proximator transducer system consists of a probe, an extension cable and a proximator. The proximator can be accurately and independently calibrated with an accurate micrometer. The proximators have several distinct advantage over other displacement measuring devices. They are reasonably priced, non-contact, very accurate, quite sensitive, and maintain their accuracy up to high frequency. The accuracy and precision of proximators was experimentally verified in Project 913. The specifications of proximator used in this study are given in Appendix A. Even though, the proximators are quite stable and their calibration factors do not change much with time, they are quite sensitive to the properties of the target used. Therefore, they should be re-calibrated whenever a new target material is used.

A schematic of the laboratory test setup, for the calibration of a proximator, is shown in the Figure 2.1. The proximator is calibrated using a voltmeter, a micrometer, a moving part, and a proximator transducer system. The micrometer selected for this study has a Least Count of 0.001 mm (0.00005 inches). Although a higher resolution micrometer may be desirable, the cost of acquiring such devices may not be justifiable. The voltmeter used in the calibration is an ordinary voltmeter and can be obtained from any electronics shop. The moving part allows the movement of the target smoothly. The target used in this study is made of ANSI 4140 steel material.

The calibration of the proximator system is performed by moving the target close to the proximator probe such that the probe is almost touching the target. After its reading is zeroed for convenience, the micrometer is moved 0.001 mm away from the target and the voltmeter reading is taken. This process is repeated in the increments of 0.001 mm until the target goes out of the range of the probe. The results obtained from this procedure are plotted in Figure 2.2. The movement of the micrometer is plotted on the X-axis and the voltage output is plotted on the Y-Axis. A linear fit to the data shows that the calibration factor is 8.568 V/mm (217 V/in.). The nominal calibration factor provided by the manufacturer is about 8 V/mm (200 V/in.). The figure shows that the calibration is quite linear throughout the displacement range of the proximator (R^2 of 0.99). This calibrated proximator can then be used for the calibration of the Reference geophone.

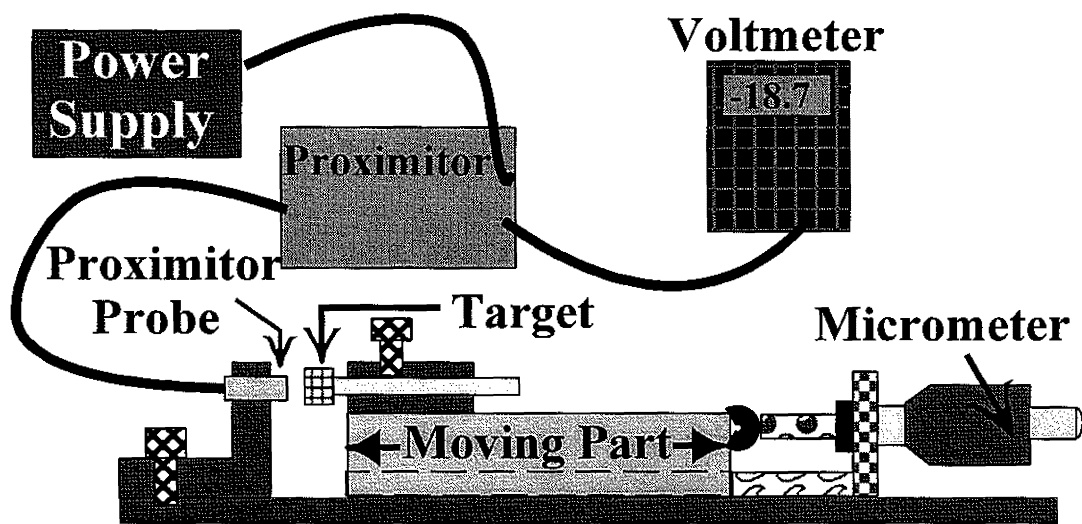


Figure 2.1 A Schematic of Proximitors Calibration Test Setup

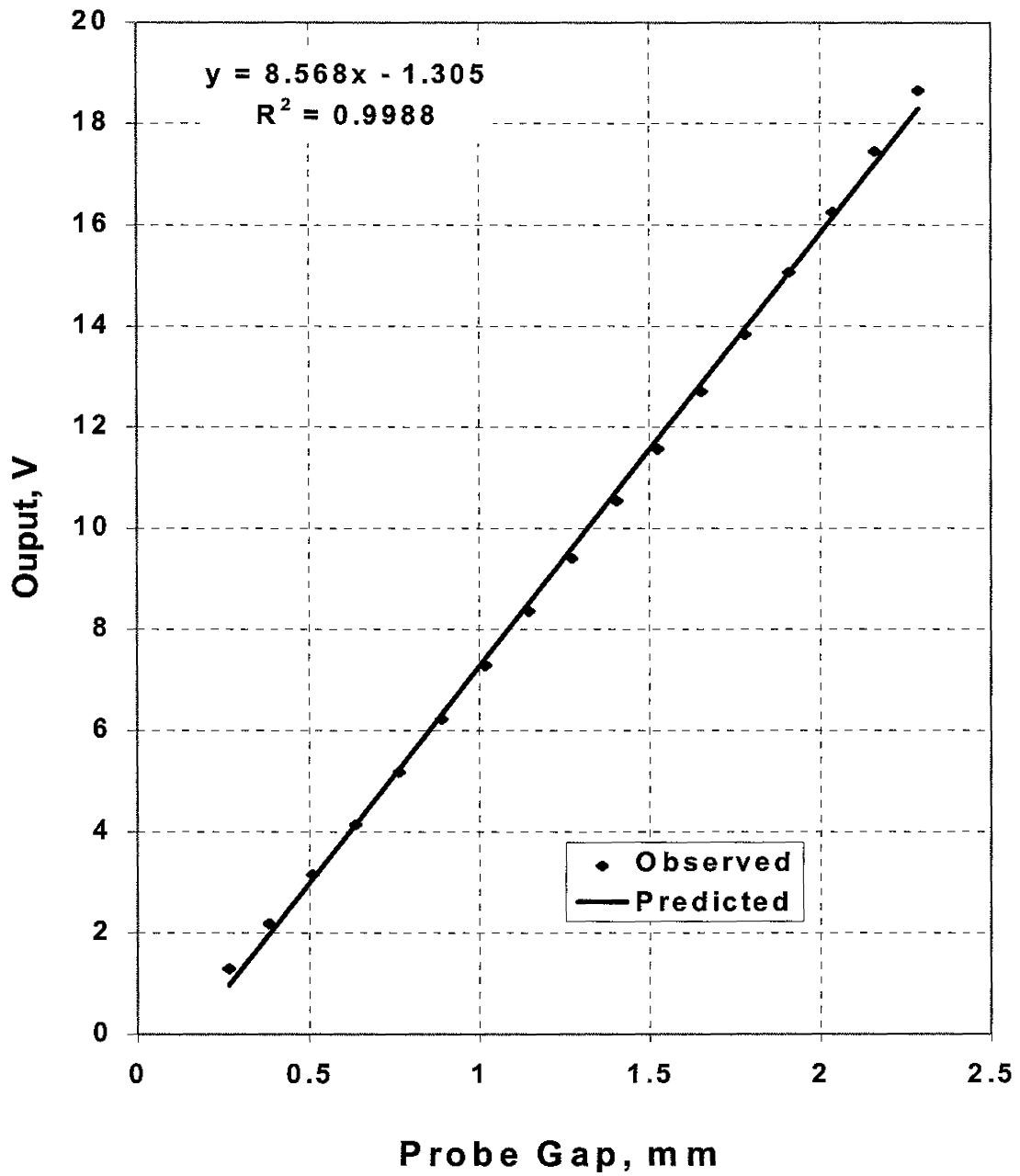


Figure 2.2 A Typical Calibration Curve of Proximity

A schematic of the test setup for a calibration of the reference geophone is shown in Figure 2.3. The test setup requires a dynamic signal analyzer equipped with a random function generator, a shaker with an amplifier, a proximator transducer system and a geophone. The specifications for the devices used are included in Appendix A. The geophone is securely placed on top of the shaker as shown in the figure. A target is placed on the top of the geophone assembly such that the movement induced in the geophone and in the target (for proximator probe) is the same. This assembly is placed below the proximator probe such that the gap between the probe and geophone is maximum (i.e., the gap between the probe and the target is not more than the measurement limit of the proximator).

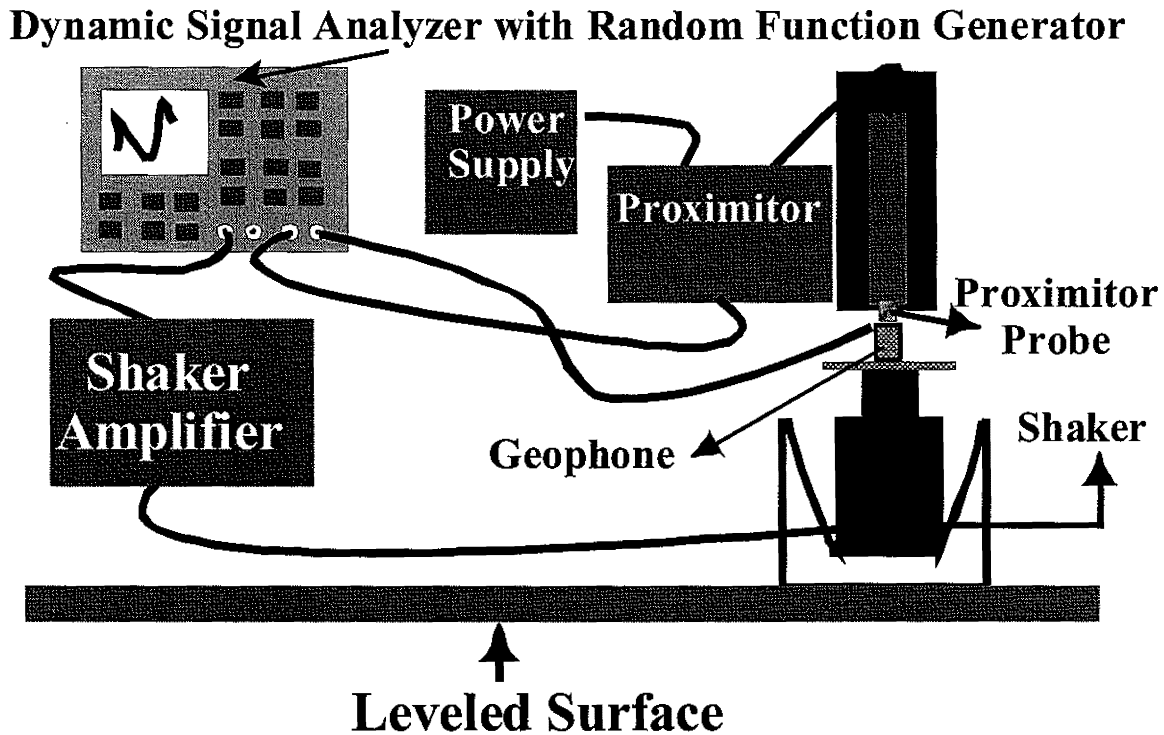


Figure 2.3 A Schematic of Laboratory Test Setup for Geophone Calibration

A random signal in the frequency range of 0 to 50 Hz is sent to the shaker via the shaker amplifier. The voltage outputs from both sensors are input into a dynamic signal analyzer. The frequency response and the coherence function from the outputs of the two signals are determined (Figure 2.4).

Typical output from one sensor is shown in Figure 2.4. As expected, the response is rather flat up to a frequency of about 5 Hz and rapidly increases above that frequency. The coherence function is practically equal to 1, corresponding to an extremely high signal-to-noise ratio. Below a frequency of about 1 Hz, the coherence values are significantly lower than 1, indicating low quality data. This can be remedied by replacing the random input signal to the shaker with a swept sine

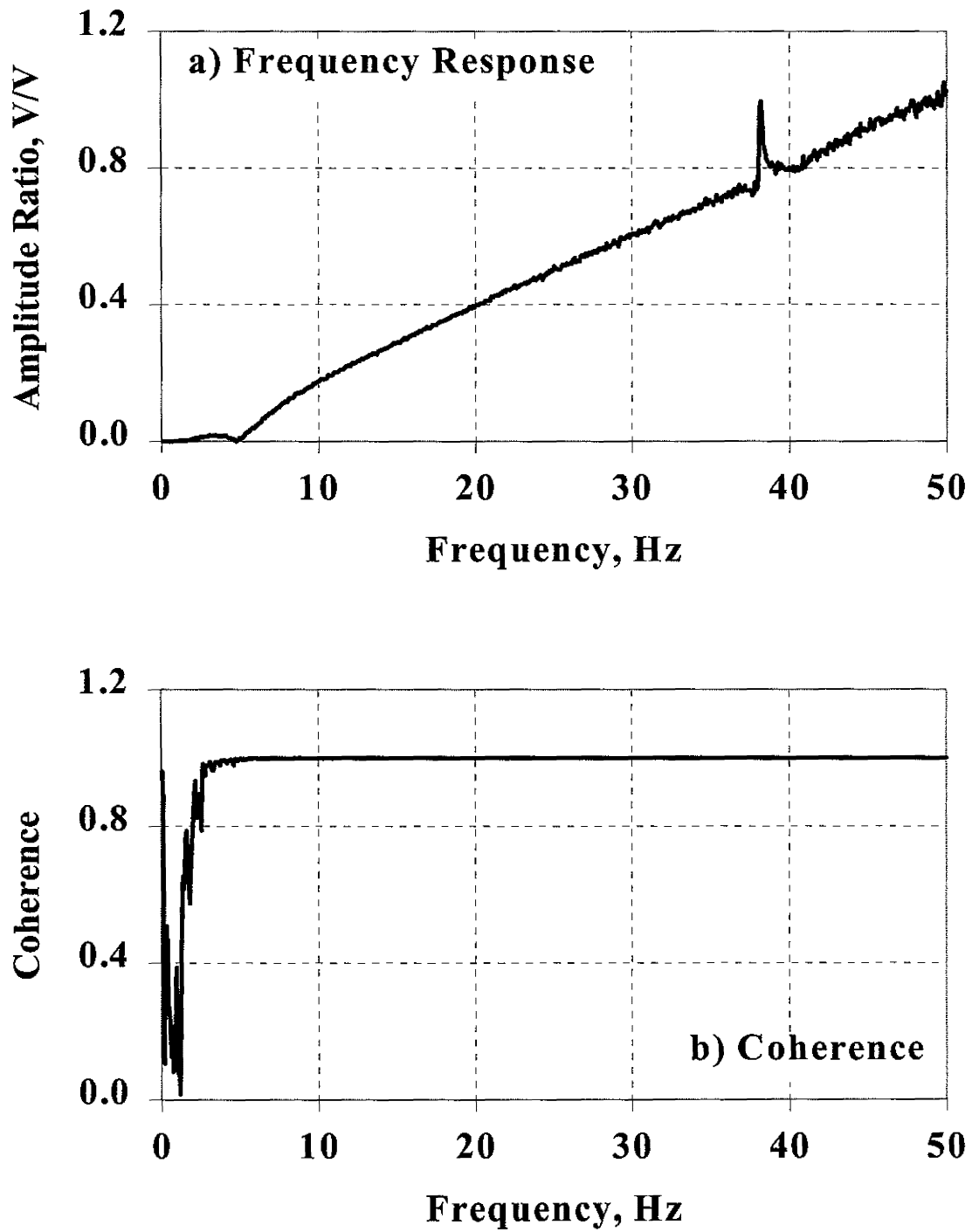


Figure 2.4 A Typical Frequency Response and Coherence Function from Calibration of a Geophone

signal during the calibration process. The modified setup will increase the calibration period by a factor in excess of 10. Many years of experience has shown that the difference in the extracted calibration parameters from the random signal and swept sine inputs are negligible. The localized peak at about 38 Hz in Figure 2.4a may be related to the setup. Since it is very localized, it would not impact the calibration parameters.

To determine the calibration parameters of the geophone, the frequency response is integrated (as the output of a geophone is velocity, and a proximator is deflection). The integrated signal is divided by the calibration factor of the proximator to obtain the calibration curve of the reference geophone.

The calibration curves after the data reduction are shown in the Figure 2.5. In Figure 2.5a, the variation in amplitude with frequency is shown. The amplitude above a frequency of 15 Hz is constant. However, below that frequency, the amplitude drastically decreases. The variation in phase with frequency is shown in Figure 2.5b. A phase shift of 180 degrees is observed in the first 15 Hz of the phase spectrum. Both graphs exhibit the classical behaviors of a single-degree-of-freedom system. By fitting a curve to the data, the natural frequency, damping ratio and the gain factor are determined. More information will be provided later in this chapter.

A typical FWD geophone was disconnected from the trailer, and was calibrated in the laboratory. The results are included in Figure 2.5 as well. The calibration curves are similar to the reference geophone. The constant amplitude at higher frequencies are smaller than the reference geophone. This indicates that the FWD sensor is less sensitive than the reference one. The phase characteristics from the two geophones are fairly similar, indicating that the natural frequencies and damping ratios are fairly similar.

Field FWD Geophone Calibration

The calibration setup developed in the laboratory can be transported to the field. The difference is that the proximator is replaced by the reference geophone, and the data analyses steps are modified.

A 41 cm by 29 cm utility box was incorporated in a 140 mm thick PCC slab as shown in Figure 2.6. The shaker can be placed in the utility box below the ground level. The depth of the box was selected to ensure that the top of the shaker table is flushed with the surface of the slab. In that manner, the FWD geophone holder can easily be placed on the top of the shaker without any disassembly. The surface on which the shaker is placed should be leveled to minimize any eccentric movement of the reference or the FWD geophone.

A well-calibrated geophone is securely embedded in a shaker as a reference. The FWD geophone is then lowered onto the shaker in its holder using the FWD raise-lower mechanism. A random signal can be send to the shaker via an amplifier. The data can be recorded using a setup similar to that of the laboratory calibration. A DC offset voltage should be added to the source generation subroutine. The DC offset is needed to Counter balance the weight of the FWD holder on top of the shaker.

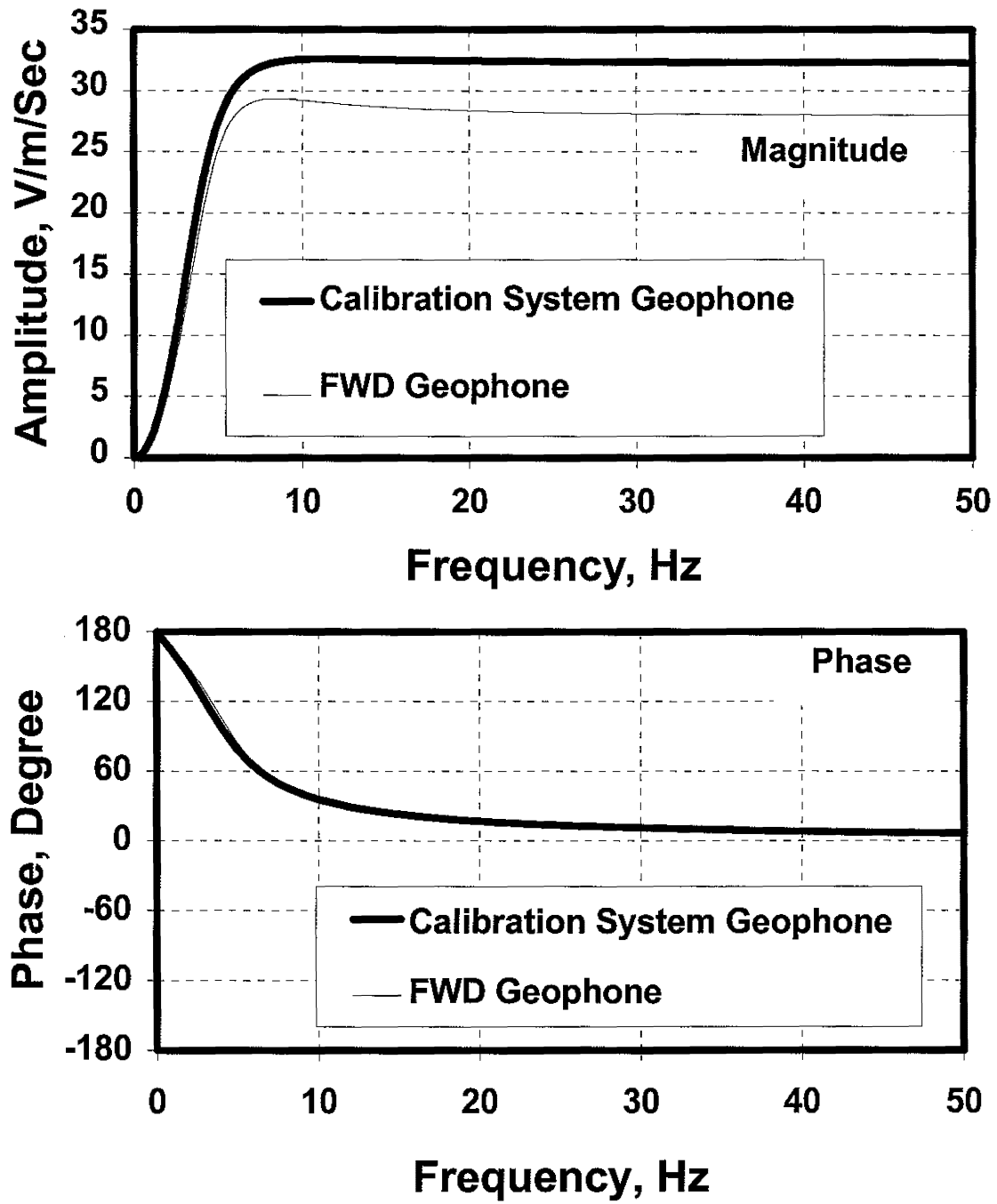


Figure 2.5 Calibration Curves of Geophones

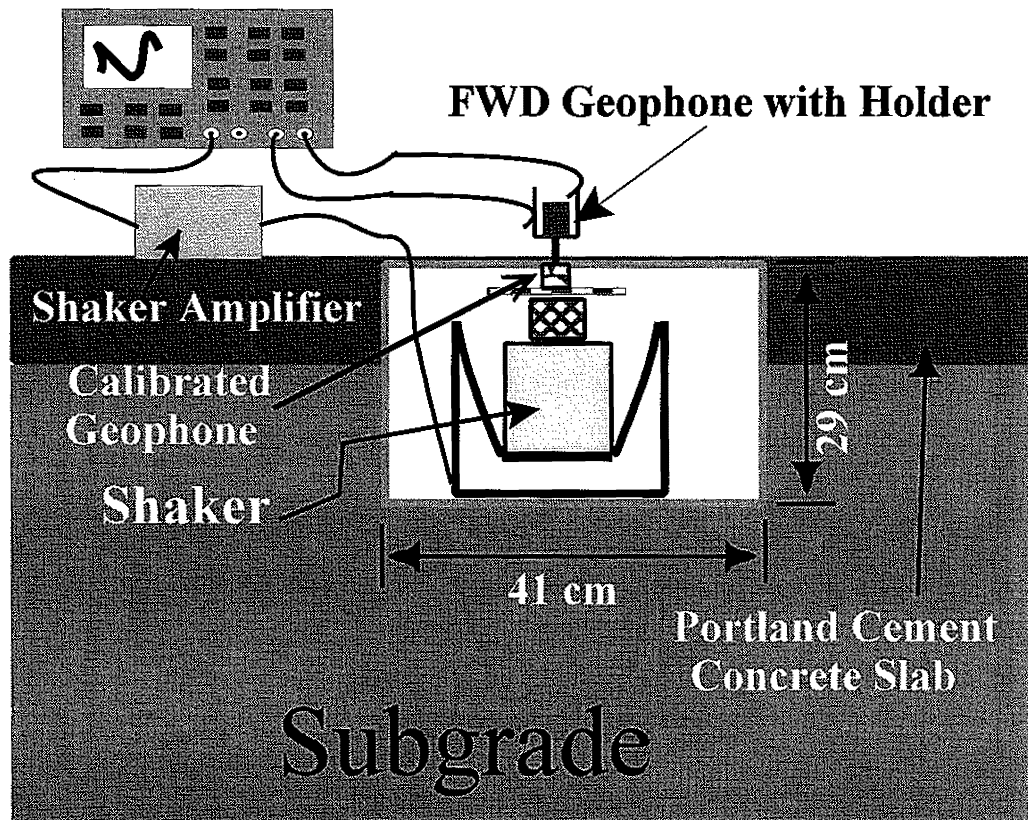


Figure 2.6 A Schematic of Field Calibration of FWD Geophone

The result obtained from one test is shown in Figure 2.7. The amplitude spectrum of the ratio of the outputs of the FWD geophone and the reference geophone is shown in the figure. In Figure 2.7, if the calibration curve of the FWD geophone was identical to the reference geophone, the amplitude ratio would have been independent of frequency and equal to unity. The sharp drop in amplitude ratio below a frequency of 5 Hz indicates that the natural frequency of the FWD geophone is somewhat lower than that of the reference geophone. A peak amplitude at 5 Hz indicates that the FWD geophone is less damped than the reference geophone. The constant amplitude ratio of 0.9 in the range of frequencies of 10 to 30 Hz indicates that the FWD geophone has a gain which is about 10 percent less than that of the calibration geophone.

Also shown in Figure 2.7 are the results from the same experiment but when the FWD geophone was removed from its holder and securely placed on top of the shaker. The difference between the two curves can be attributed to the interaction between the holder and the shaker. The two curves follow each other quite well up to a frequency of 30 Hz. At higher frequencies the differences on the order of 3 to 5 percent can be observed. Such differences may adversely affect the deflections measured with the FWD, especially when full-waveform analysis has to be carried out.

If the frequency response curve shown in Figure 2.7 is multiplied by the calibration curve of the reference geophone obtained in the laboratory, the calibration curve for the FWD geophone can be obtained (Figure 2.8). The calibration curve of the FWD geophone looks very similar to that shown in Figure 2.5. The results of the calibration test setup indicate that the FWD geophone can be calibrated in the field with the same test setup used in the laboratory.

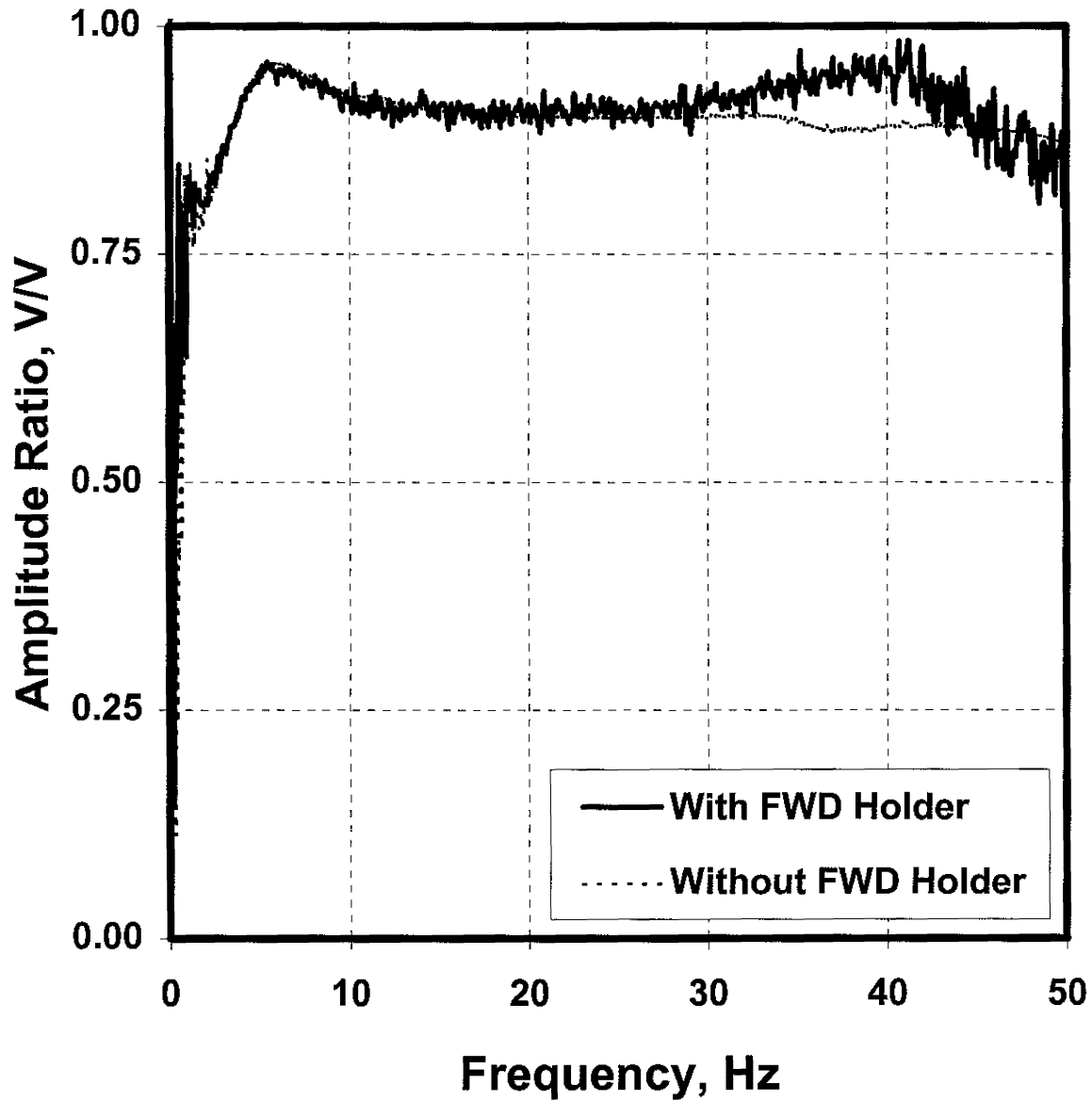


Figure 2.7 Field Calibration of FWD Geophone

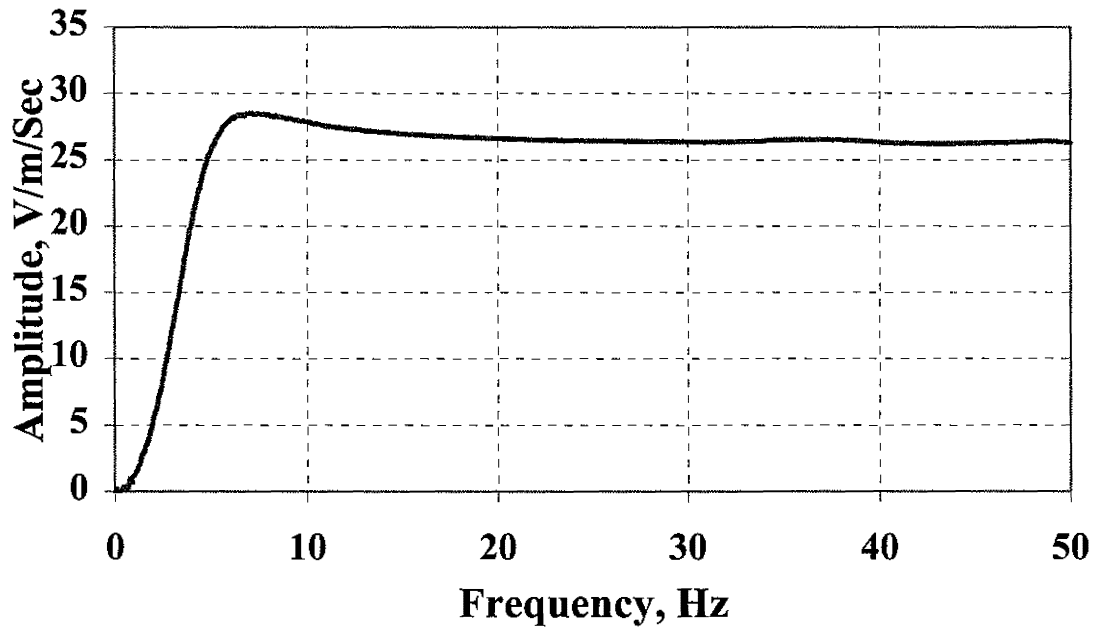


Figure 2.8 A Calibration Curve of FWD Geophone

Proposed Calibration Setup for the Load Cell

The SHRP and the Texas Calibration methods for the load cell are included in the ASTM standard D4694. The proposed calibration setup uses the same concept. Again the reference load cells to be used are calibrated in the laboratory first. The calibrated load cells are then used in the field to calibrate the FWD load cells.

Laboratory Calibration of Reference Load Cells

The calibration of the reference dynamic load cells in the laboratory is necessary to ensure that the behavior of the load cells does not change by mounting them on the load cell plate. The laboratory calibration of the dynamic load cells, as shown in Figure 2.9, is done with the assistance of an MTS system. The load cell of the MTS system contains a calibration that is traceable to the National

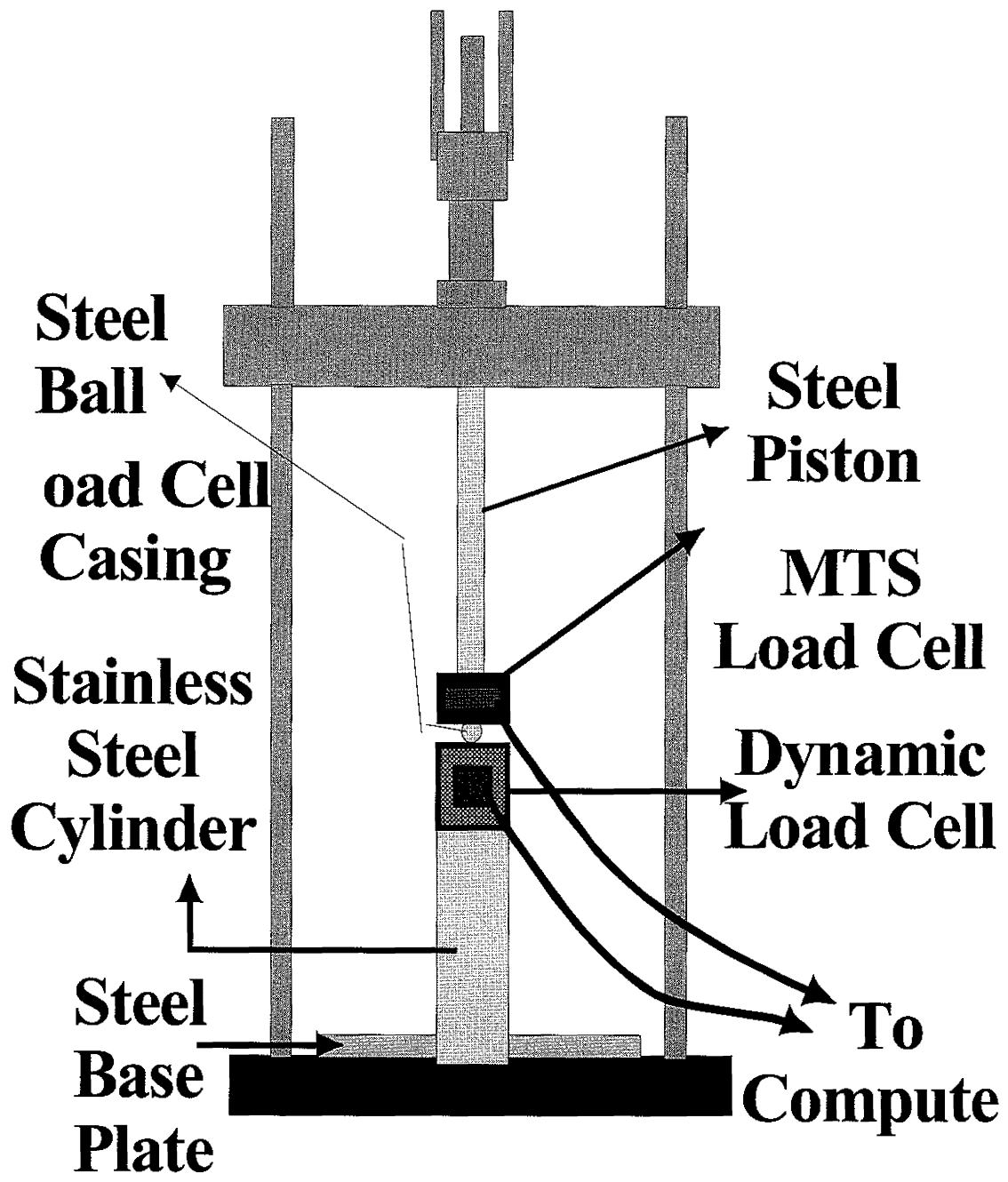


Figure 2.9 A Schematic of Load Cell Calibration in the Laboratory

Institute of Standards and Technology (formerly known as NBS). The encased load cell is placed between the upper and lower platens of the MTS system. A seating load of 450 N (100 lbs) is applied to ensure proper contact between the load cell and the platens. Impulse loads of different magnitude with a duration of about 100 msec are applied. The magnitude of the impulse load is increased. The peak load obtained from the MTS load cell and the peak voltage obtained from the dynamic load cells are recorded for five cycles at each load magnitude. The results from all cycles and load levels are correlated to determine the calibration constant of the load cell.

The results from one test are shown in Figure 2.10. The X-axis is the applied load as measured by the MTS load cell, and the Y-axis is the voltage measured from the dynamic load cell. A least-squares best-fit line through the data points yield a calibration ratio of 0.175 V/KN (or 7.8E-4 V/lbs) with an R^2 value of 0.99. Similarly, the other two reference load cells can be calibrated in the laboratory. The three calibration factors can then be used to determine the calibration factor of the FWD load cell.

Field Calibration of the FWD Load Cells

The field calibration of the load cells can be performed using the Texas Calibration method with slight modifications, as shown in Figure 2.11. One of the modifications is that the bottom and top plates of the calibration plates were made of stainless steel rather than aluminum. The another change is that a recess is made in the PCC slab to accommodate the calibration plates. The depth of the recess is such that the top plate is flushed with the slab surface. The advantage of this method, aside from convenience, is that lateral movement of bottom and top plate is minimized. The procedure for calibration is similar to the Texas Calibration method, and can be found in TxDOT Report 913.

Comparison of FWD Calibration Results

A TxDOT FWD was loaned to UTEP for comparison of calibration methods and evaluation of the proposed calibration test setup. The results from the comparison are reported in the following sections. First the characteristics of the geophone are reported, and then the results obtained from the SHRP, the Texas and the newly proposed protocols are compared.

Characteristics of Geophones

The characteristics of the geophones were obtained using the calibration curves of the geophones measured as per the proposed test setup. The calibration curves of the two geophones are shown in Figure 2.5. The responses of the two geophones were similar. Basically, a polynomial with 2 poles and 2 zeros were fitted to the data. The poles and zeros obtained were then used to calculate the natural frequency, damping ratio, and gain for each geophone. The characteristics of the two geophones are summarized in Table 2.1. The geophone used in the calibration system is slightly more sensitive and slightly more damped than the FWD one. This exercise shows that the FWD sensors can be readily calibrated.

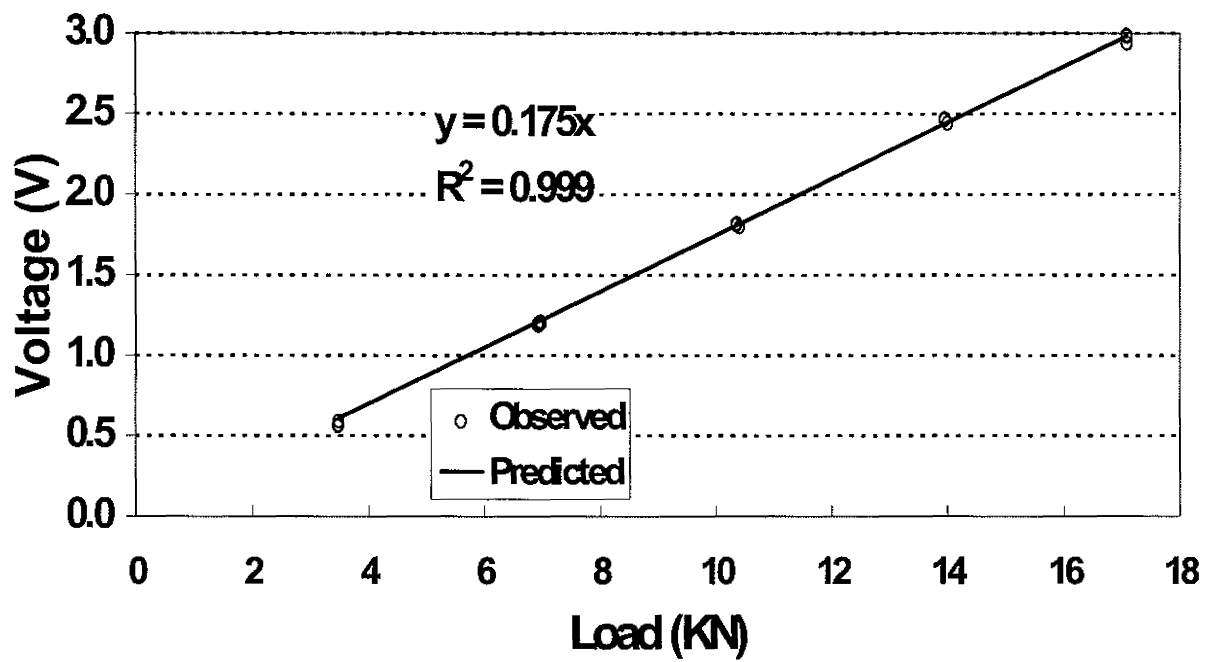


Figure 2.10 A Typical Calibration Curve of Load Cell

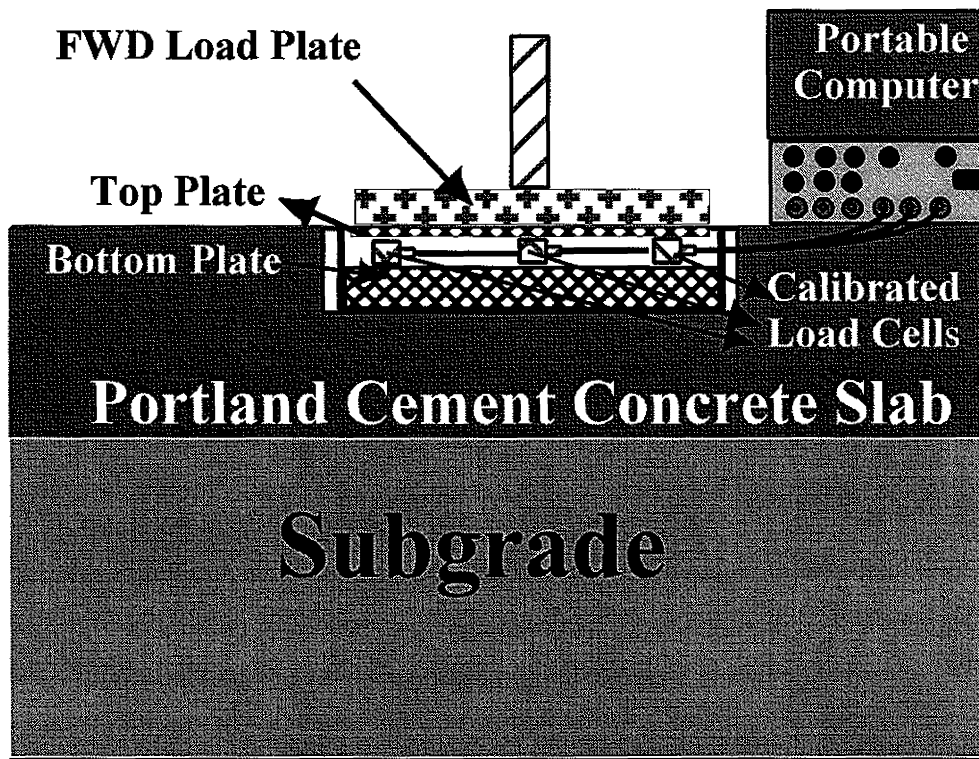


Figure 2.11 A Schematic of FWD Load Cell Calibration

Table 2.1 Characteristics of Geophones Used in This Study

Geophone	Natural Frequency, Hz	Damping Ratio, percent	Gain, v/m/sec
FWD	4.67	58.8	27.9
Calibration System	4.42	65.4	32.2

Calibration with Texas System

The results from typical calibration of an FWD using the Texas System are summarized in Figure 2.12. Two methods of calibration were used. In the first method, the geophone of the calibration system was placed next to the FWD sensor while it was in its holder. In the second experiment, a holder, similar to the one used in the SHRP calibration protocol, was secured to a slab. The FWD geophone and the geophone of the calibration system were rigidly attached to the holder. As reflected in Figure 2.12, the calibration factor for the FWD geophone changed from 0.93 to 0.97 when the placement system changed. The difference can be attributed to the interaction between the FWD sensor and the sensor holder (as shown in Figure 2.7). The levels of the deflection obtained from the tests were not similar. The reason is that in the SHRP protocol the loading plate is moved until the sensor experiences a deflection of about 400 μm . However, in the Texas Calibration Process sensors are calibrated in their respective holders. This experiment clearly demonstrates the importance of calibrating the FWD sensors in its original holders along the range of deflections they usually experience.

Calibration with Proposed System

Following the SHRP recommendation, the calibration has to be performed on a thin concrete slab with a very weak subgrade. Our interview of the operators of the four SHRP regional centers (under Project 2935) indicated that most centers had carefully designed their slabs to obtain desired deflections. Vibration isolation between the block holding the LVDT and the slab was of concern. To minimize the cost of construction, and to improve the stability of the calibration facility, it may be desirable to use a shaker to apply a half sine-wave impulse instead of a FWD impulse. To test this concept, one of the sensors of the FWD was placed on the shaker located in the utility box under the slab (Figure 2.6). A 30-msec pulse was applied to the shaker using a signal generator. The raw voltage from the FWD and the reference geophones are shown in Figure 2.13. The two curves follow each other quite well, except that the voltage measured by the reference geophone is slightly higher. This difference in the amplitude is due to the fact that the reference geophone has a higher sensitivity. The abrupt change in the slope of the curves coincide with the completion of the 30 msec impulse. The actual displacement from the two geophones are shown in Figure 2.14. The results indicate that the two geophones experience similar deflections.

This method of calibration can be used for all the geophones of the FWD over a wide range of deflections. The only changes needed are the amplitude of the impulse. The advantage of this

method is that the calibration and verification is easier as compared to the SHRP or Texas method. Another added advantage is that the whole deflection time history can be obtained for estimating the dynamic modulus.

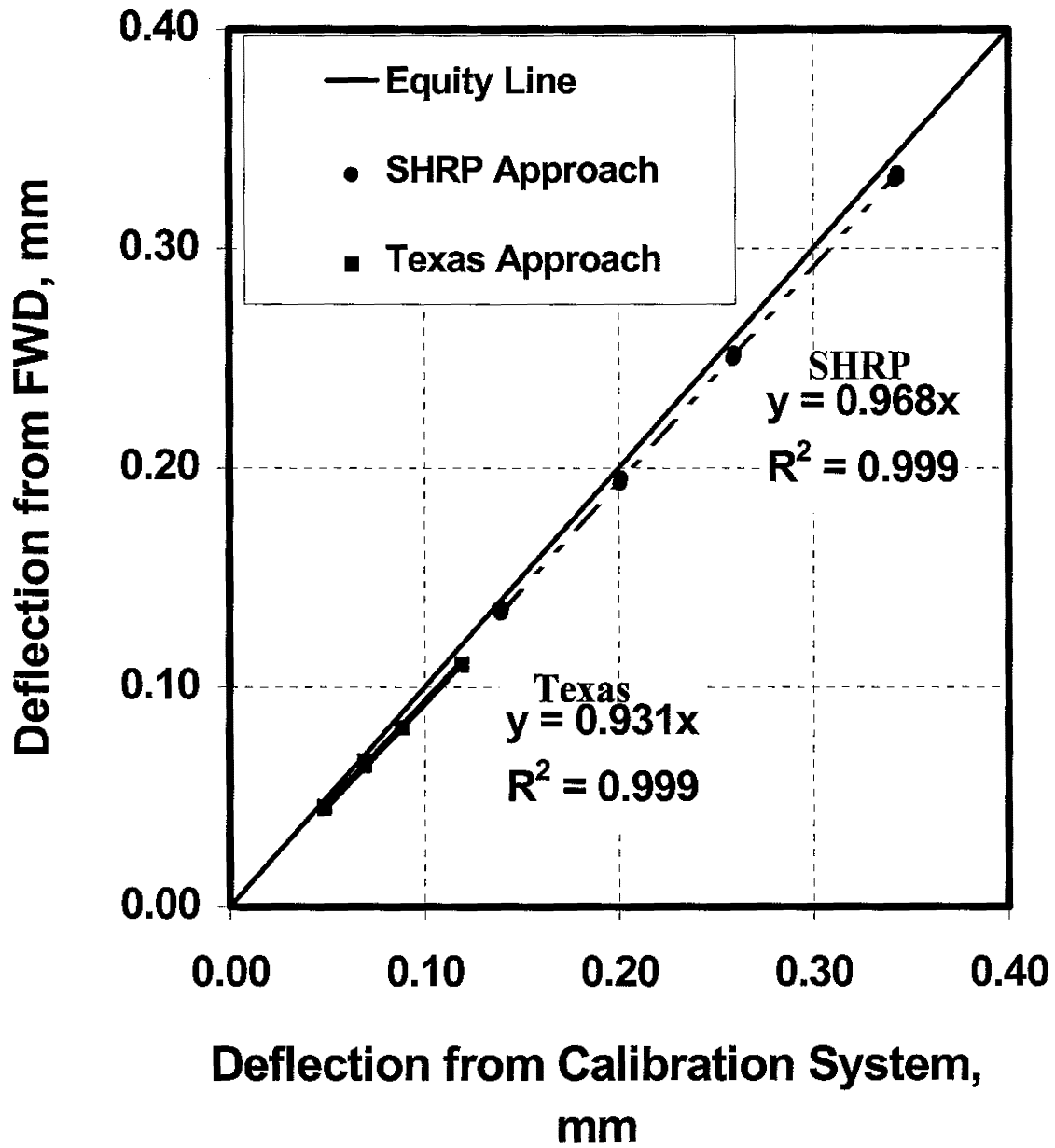


Figure 2.12 Comparison of Calibration Factors from SHRP and Texas Protocols

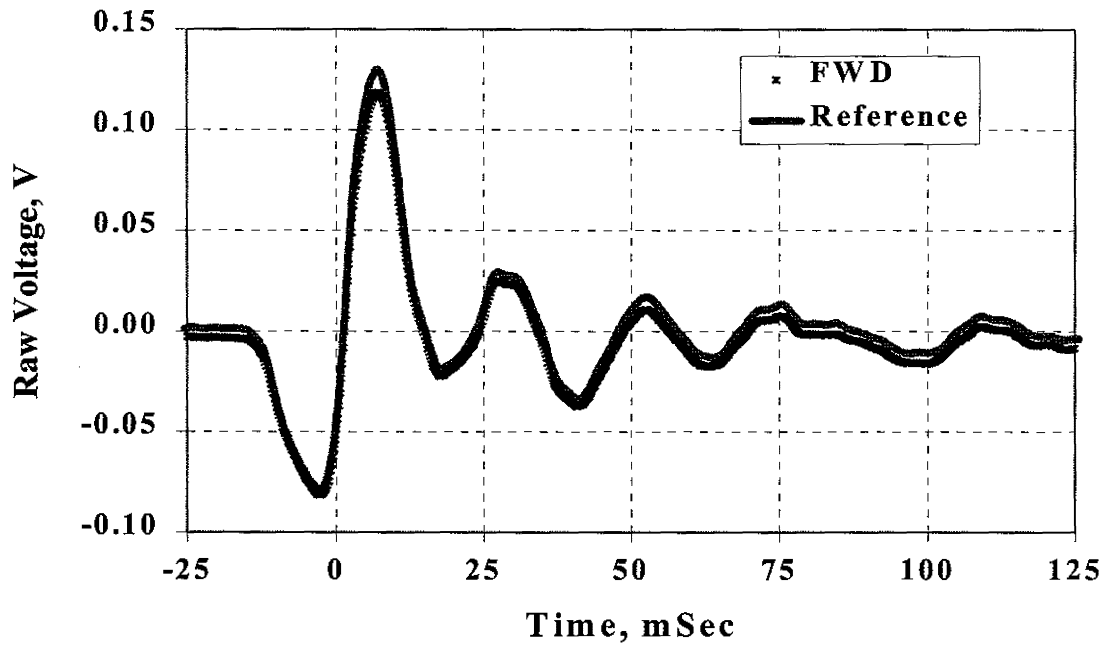


Figure 2.13 Comparison of Raw Geophone Outputs Under a 30 mSec Impulse

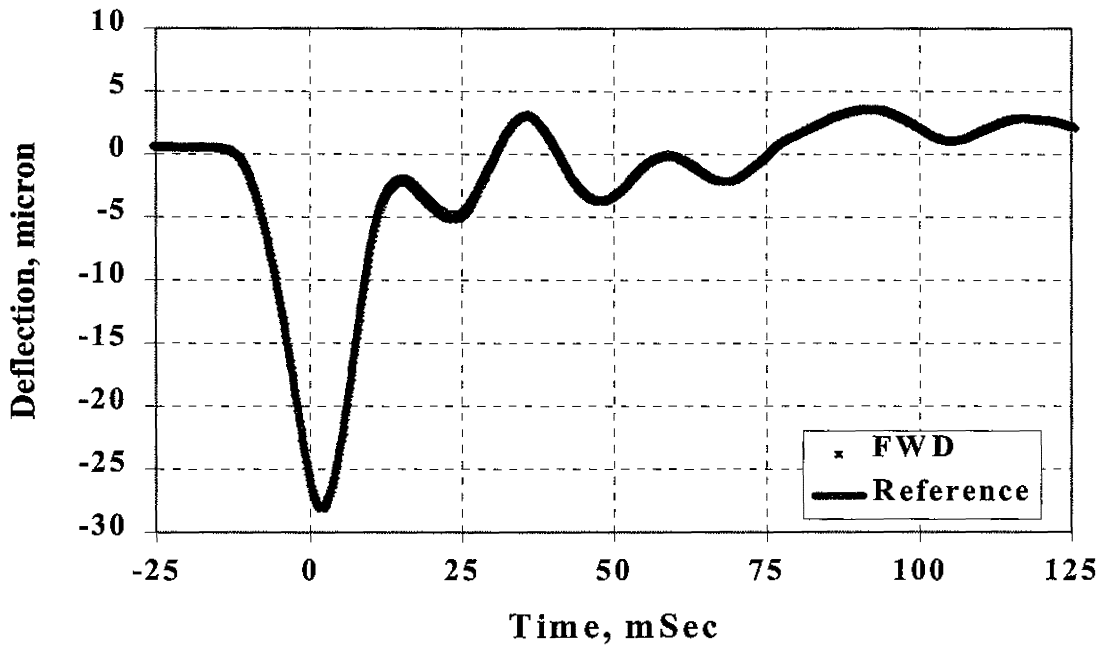


Figure 2.14 Comparison of Deflections Obtained from Geophones Under 30 mSec Impulse

Chapter 3

Portable Seismic Pavement Analyzer

The Portable Seismic Pavement Analyzer (PSPA) has been developed at UTEP (Baker et al., 1995). The PSPA uses wave propagation techniques to estimate the modulus and thickness of PCC or AC pavement layers. A standard calibration procedure does not exist for the PSPA because it has been recently developed. Since the use of this device is rapidly increasing, a calibration procedure for the sensors used in the PSPA is needed.

A schematic of the PSPA is shown in Figure 3.1. The device contains two accelerometers as receivers and a source hammer. A typical test with the PSPA consists of impacting the pavement with the source, and monitoring the propagation of seismic energy sensed by the accelerometers. The recorded data are interpreted in two ways.

First, the Ultrasonic Surface Wave (USW) method or the Ultrasonic Body Wave (UBW) method are used for determining the modulus of the layer. In these methods, the interpretation of the results consists of directly or indirectly determining the velocity of waves propagating between the two accelerometers. In this case, the focus of the calibration procedure is to ensure that the travel time measured between the two PSPA accelerometers is not altered by electronic components of the PSPA or affected by the method used to mount the sensors. In other words, if the two accelerometers are placed the same distance from the source, the difference in travel time between them should be equal to zero. Technically, this translates to ensuring zero phase shift between the response of the two accelerometers over the range of frequencies of interest.

Second, the Impact-Echo (IE) method is used to determine the thickness. In that method, the resonant frequency associated with the wave energy trapped within the top layer is of interest (Nazarian et al., 1997). Therefore, one should ensure that the characteristics of the accelerometer or the mounting system are not interfering or contaminating the response from the pavement.

An understanding of the data analysis procedure is essential to following the process used in calibrating the device. In the following section, a brief description of the data analysis of the PSPA is included. A detailed description of the device can be found in Baker et al. (1995).

Description of PSPA Data Analysis Procedures

To perform a test, the surface of the layer is impacted with a source capable of imparting high-frequency waves to the pavement. The response of the pavement to this impact at two locations on the pavement is detected by two sensors. Typical records from two sensors placed 75 mm and 225 mm from the point of impact are shown in Figure 3.2. The arrivals of different types of seismic energy are marked on each record. The UBW method consists of determining the arrivals of these waves in the time-domain. If one is only interested in calibrating the system for the UBW method, one can perform tests on a thick slab of a material with known properties (such as aluminum). The calibration factor is then determined by comparing the known travel time with the one measured with the PSPA. This was not done here because the USW method requires a more sophisticated calibration method, which when performed, assures that the system is also calibrated for the UBW method.

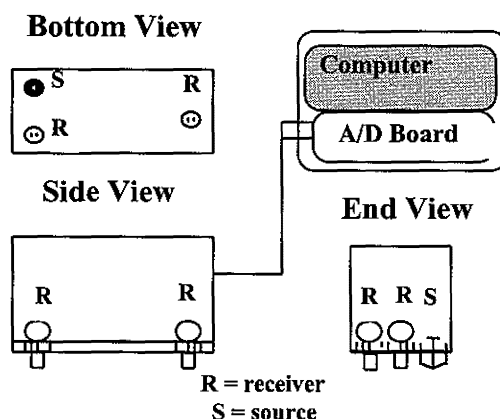


Figure 3.1 Schematic of Portable Seismic Pavement Analyzer

The USW method has an advantage over the UBW in terms of robustness and in terms of providing modulus along a specified thickness (Nazarian et al., 1997). By performing a fast Fourier transform on the two signals similar to those shown in Figure 3.2, and by dividing the two transformed signals by one another, one obtains a phase spectrum (i.e., variation in phase with frequency). As a standard representation, such a phase is wrapped as shown in Figure 3.3a. To relate the phase to modulus, the unwrapped phase is used and fitted by a straight line for the frequency range corresponding to wavelengths shorter than the thickness of the layer (Figure 3.3b). As indicated by Baker et al. (1995), the slope of the line, m , can be directly related to Young's modulus, E , using

$$E_{USW} = 2 \frac{\gamma}{g} (1 + \nu) \left[(1.13 - 0.16\nu) \frac{360\Delta X}{m} \right]^2 \quad (3.1)$$

where ν is Poisson's ratio, and ΔX is the sensor spacing. Parameters' γ and g are the unit weight and acceleration of gravity, respectively.

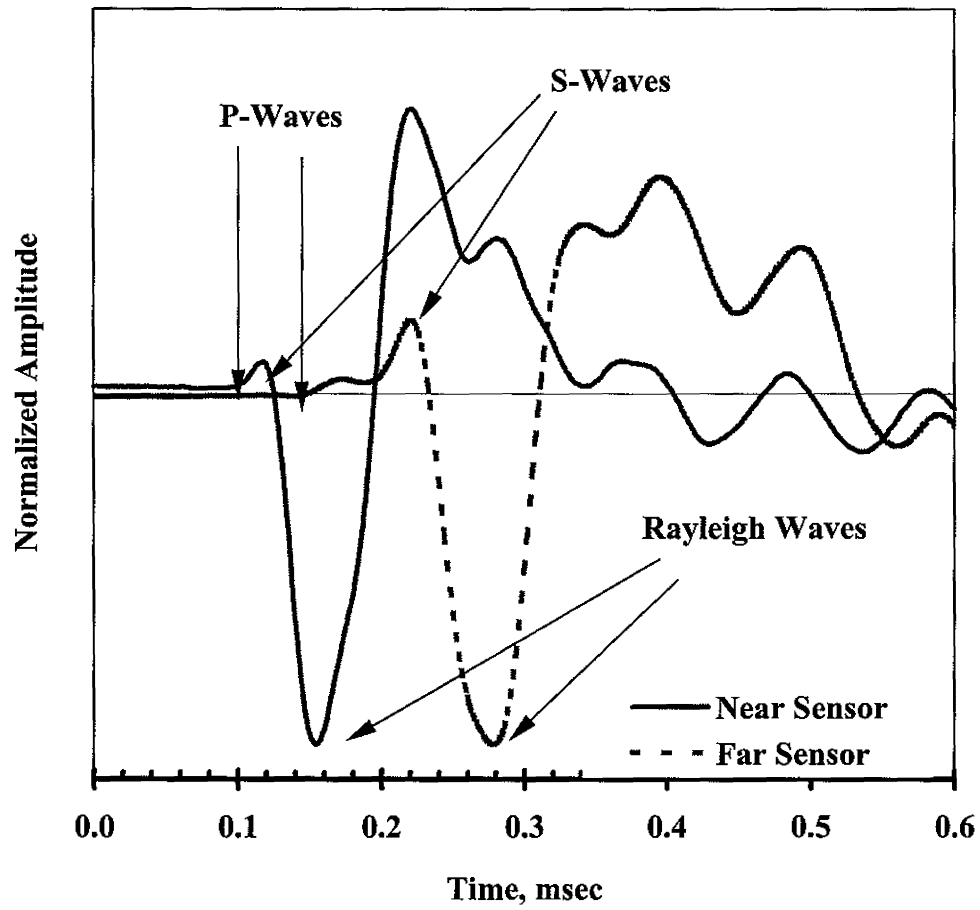
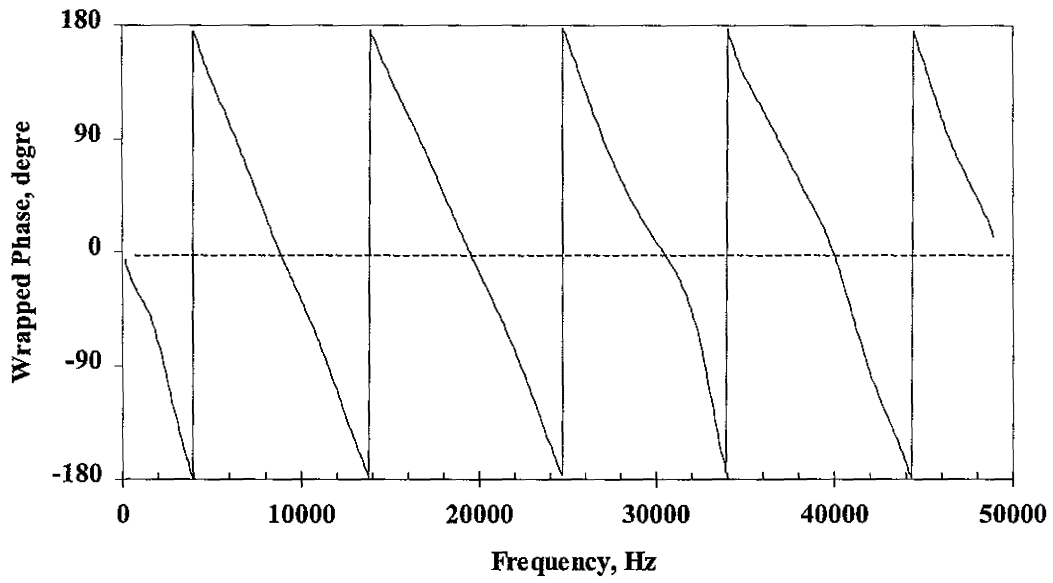
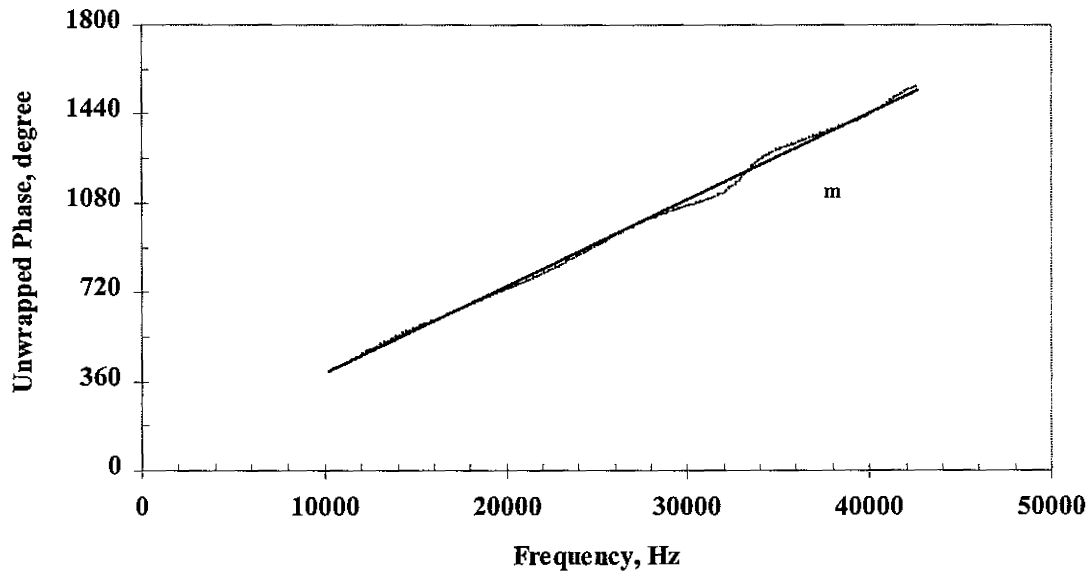


Figure 3.2 Typical Time Records from High-Frequency Seismic Field Tests



a) wrapped



b) unwrapped

Figure 3.3 Spectral Functions from USW Tests

Alternatively, one can construct a dispersion curve, as shown in Figure 3.4, and determine the variation in the modulus of the top layer from:

$$E_{USW} = 2 \frac{Y}{g} (1 + \nu) [(1.13 - 0.16\nu) V_{ph}]^2 \quad (3.2)$$

where V_{ph} is the average phase velocity of the top layer.

To calibrate the PSPA for the USW method, one should compare the phase difference between the two sensors, and ensure that any phase difference at any given frequency due to differences in mounting of the sensor or differences in manufacturing the accelerometers are accounted for. In other words, one should ensure that any phase shift measured in Figure 3.3a is due to propagation of surface waves in the PCC or AC, and not due to differences in manufacturing.

The Impact-Echo (IE) method, as applied to concrete, was primarily developed at the National Institute of Standards and Technology and Cornell University (Sansalone and Carino, 1989). Upon impact of a slab's surface, seismic waves that propagate within the slab are generated. Some of the energy is transmitted to the layers underlying the concrete and the remainder is reflected from the boundary of the concrete and underlying layers. The reflected energy is again reflected at the top of the concrete layer. Here, almost all of the energy is reflected because of the significant mismatch between the stiffness of air and concrete. The thickness of the slab, H , can be determined from

$$H = (V_p \cdot t_r) / 2, \quad (3.3)$$

where V_p is the compression wave velocity determined using the ultrasonic-body-wave or ultrasonic-surface-wave method and t_r is the travel time between two consecutive reflection arrivals. The process is made significantly simpler when the signal is Fourier transformed into the frequency domain to obtain the amplitude spectrum. The thickness can be determined from

$$H = V_p / 2f_r. \quad (3.4)$$

A typical frequency-response spectrum obtained from a test site is shown in Figure 3.5. The major peak (at about 12 kHz) corresponds to a standing wave within the thickness of the layer and is called the return (resonant) frequency. The large amplitude low-frequency signal corresponds to the hold down mechanisms of the sensors, and can be readily removed upon a proper calibration of the system. This process will be discussed shortly.

In summary, the accelerometers of PSPA measure the propagation of the wave in the pavement surface layers for the UBW, USW as well as IE method. However, the analysis of the data is different for each method. In the USW method, the phase spectrum is used for the modulus calculation, therefore, a phase shift between the two accelerometers is of importance and should be estimated through calibration. If the phase shift at each frequency, through the calibration for USW method, is accounted for, this automatically ensures proper calibration for the UBW method. On the other hand, the IE method uses peak amplitude observed in the accelerometer signal as an indication of thickness of the surface layer, therefore, the amplitude spectrum of the first accelerometer should also be calibrated.

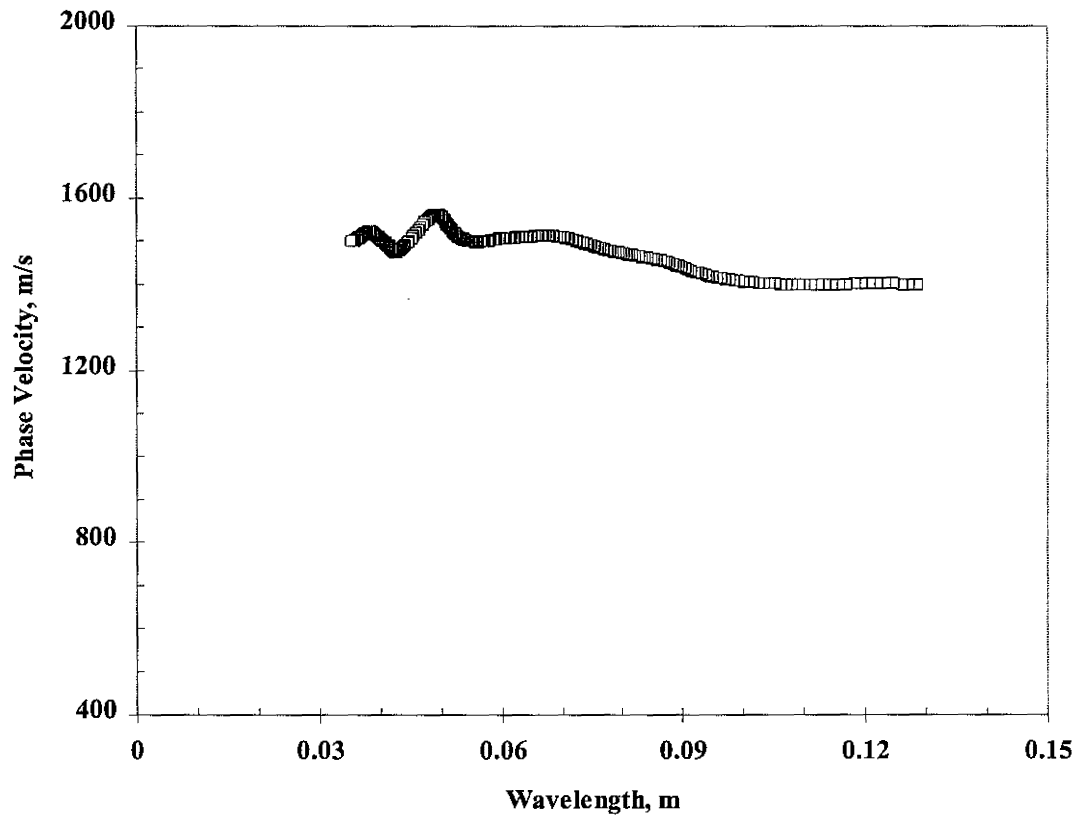


Figure 3.4 Typical Dispersion Curve from an Asphalt Concrete Layer

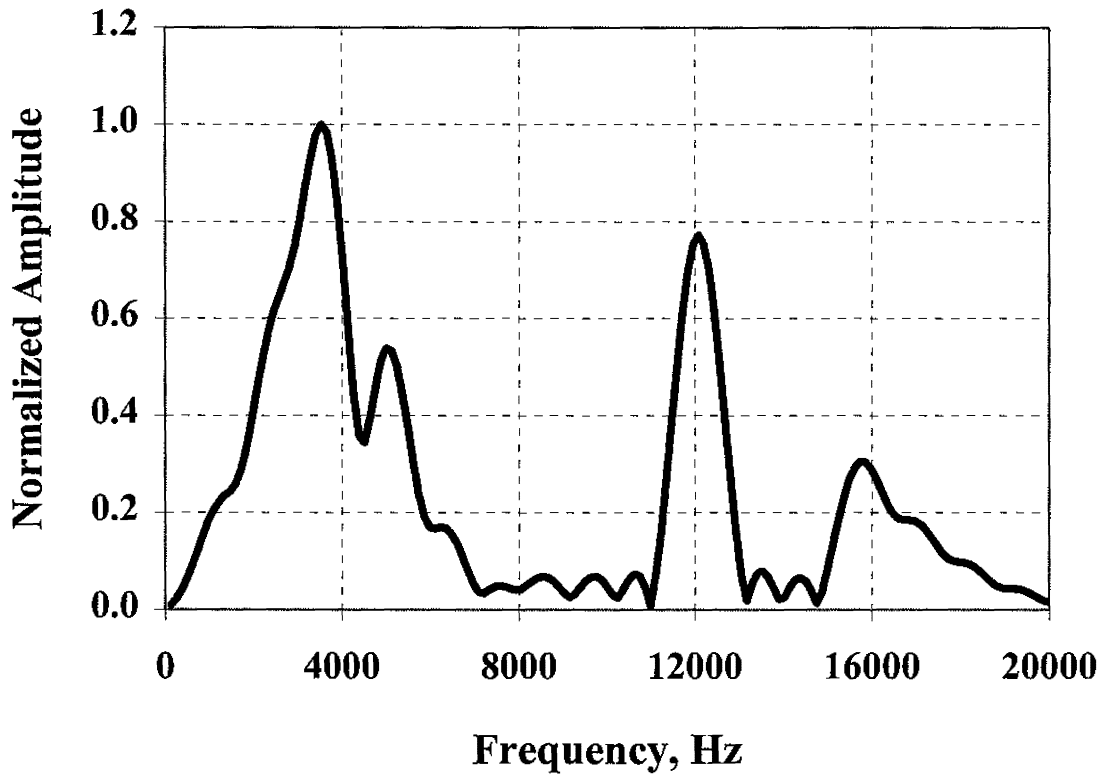


Figure 3.5 A Typical Frequency Response Obtained with IE Method

Proposed Calibration of Accelerometers

Phase Shift Calibration

The setup required for calibrating the PSPA is shown in Figure 3.6. The setup consists of a rather heavy metal frame that can hold the PSPA in place. A high-frequency shaker, also embedded in a rather heavy frame, is also needed. A combination of a piezoelectric and electromagnetic shakers which works in the range of frequencies of 10 Hz to 70 KHz was found suitable for this task. The shaker is equipped with a built-in accelerometer with NIST-traceable calibration. The shaker assembly, which can be leveled as needed, is moved under each of the two accelerometers of the PSPA. The outputs of the built-in accelerometer (directly) and the PSPA accelerometer (just before entering into the data acquisition board of the PSPA) are connected to a dynamic signal analyzer for real-time analysis. The shaker is excited in a swept-sine mode in a range of frequencies of 10 Hz to 100 kHz using a built-in feature of the dynamic signal analyzer.

Dynamic Signal Analyzer with Random Function Generator

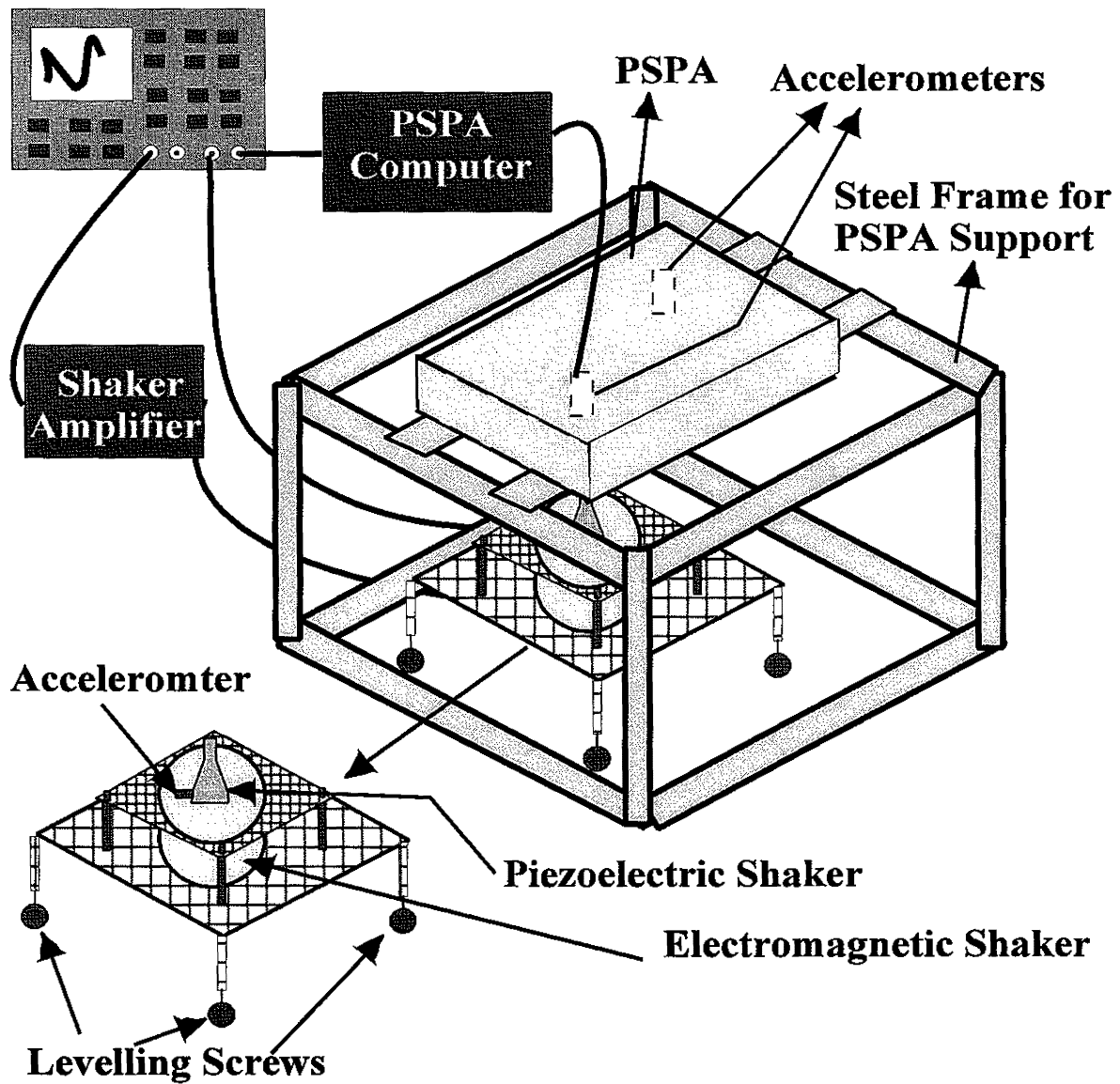


Figure 3.6 A Schematic Diagram of PSPA Calibration System

To eliminate the need for disassembling the PSPA for calibration, the behavior of each of the two accelerometers is compared with the shaker's built-in accelerometer first. Assuming that the characteristics of the calibration system do not change, by comparing the calibration of the two PSPA accelerometers relative to the built-in accelerometer, one can determine the phase shift calibration. The calibration curve, is the ratio of the transfer functions of accelerometers 1 and 2 obtained in that manner. The calibration results in the range of frequencies of 100 Hz to 20 KHz are of interest.

Typical characteristics of the PSPA accelerometer, before being mounted in the device are shown in Figure 3.7. The accelerometer was directly mounted on top of the high frequency shaker. The variation in the ratio of the response of the PSPA accelerometer and that of the shaker's built-in accelerometer as a function of frequency is demonstrated. Up to a frequency of about 7 kHz, the response is flat and slightly larger than 10. This indicates that the two accelerometers have similar responses, with the PSPA sensor being about 10 times more sensitive. In the same range, the phase is about 180 degrees. This indicates that the two accelerometers have different polarities (e.g., up direction is negative voltage for one and positive for the other). This occurs because the shaker is mounted upside down. Several vertical lines extended between -180 degrees and 180 degrees occur because at isolated points the phase is minutely above 180 degrees. In those cases, the phase is translated to about -180 degrees.

At about a frequency of about 9 kHz, a sharp peak in amplitude spectrum is observed in Figure 3.7. The peak in the amplitude spectrum is accompanied by a 180-degree shift in phase spectrum. The frequency of about 9 kHz, which corresponds to a natural frequency of the system, is in fact the resonance frequency of the built-in accelerometer. In general, the response within the range of 100 Hz and 50 kHz correspond to a typical single-degree-of-freedom system with a resonant frequency of about 9 KHz. A minor peak about the frequency of 10 kHz concurs with the natural frequency of the piezoelectric shaker.

The response of the same accelerometer mounted in place in the PSPA sensor box is compared with the shaker's built-in accelerometer in Figure 3.8. The response is affected by the mounting system, the nature of the accelerometer and the electronic circuitry of the PSPA. The low frequency, high amplitude peak primarily corresponds to the mounting assembly of the PSPA. The wide peak of the amplitude ratio and the gradual decrease in phase indicate that the system is highly damped. Fortunately, the natural frequency is about 1700 Hz which is outside the range of interest in the PSPA analysis. A comparison of the results from before and after accelerometer mounting suggests that the calibration of the accelerometers should definitely be performed after they have been placed inside the PSPA.

To demonstrate the use of these curves, the response of two accelerometers mounted in a typical PSPA are compared in Figure 3.9. The amplitude spectra from the two curves are similar in the range of frequencies of 100 Hz to 1000 Hz. The peak amplitude for accelerometer 2 is higher than that of accelerometer 1, because of higher fixed gain applied to accelerometer 2. The frequency associated with the peak amplitude for accelerometer 1 is lower than that of accelerometer 2. The phase spectra are also similar except in the ranges of about 2 kHz to 4 kHz, where the peak responses are registered. To adjust the results for the differences in phase shift, the ratio of the two response curves is determined (Figure 3.10). The phase measured at each frequency in Figure 3.10 should be subtracted from the phase of transfer function obtained during field tests. To facilitate this task, a polynomial is fitted to the measured phase spectrum. Typical poles and zeros obtained from the curve

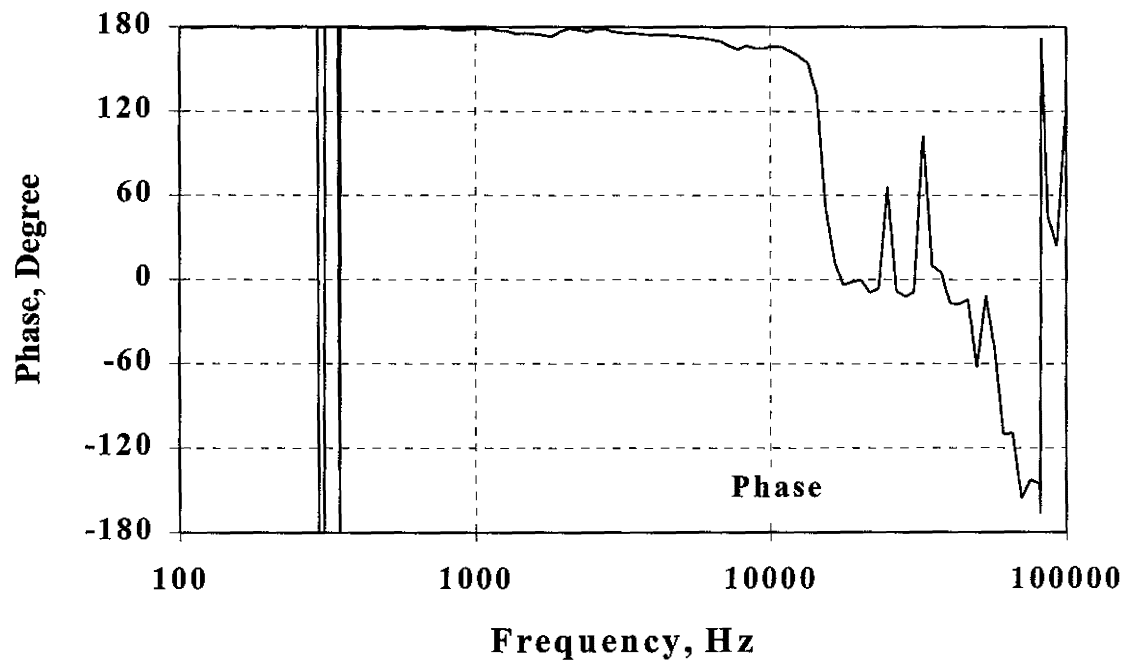
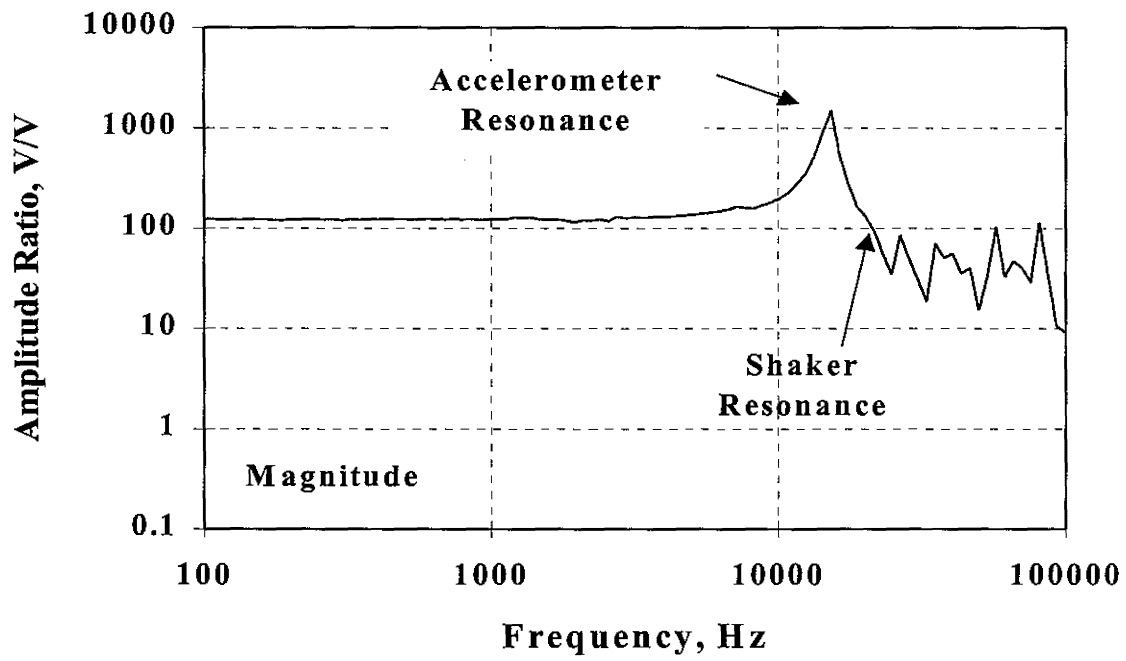


Figure 3.7 Response of Accelerometer Outside PSPA Holder

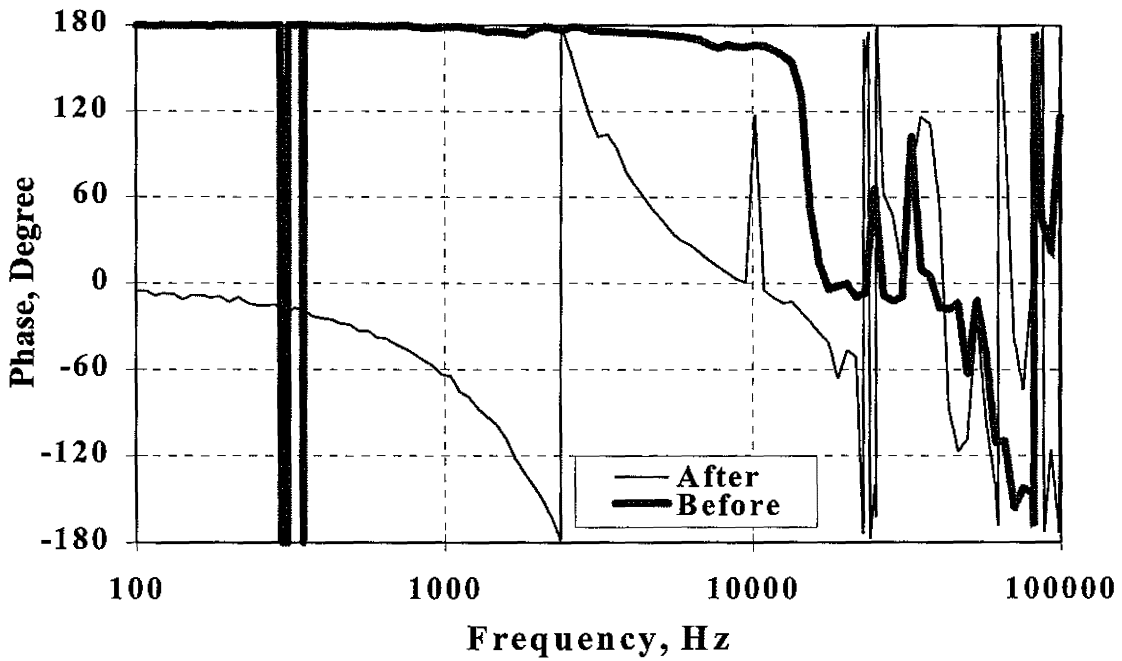
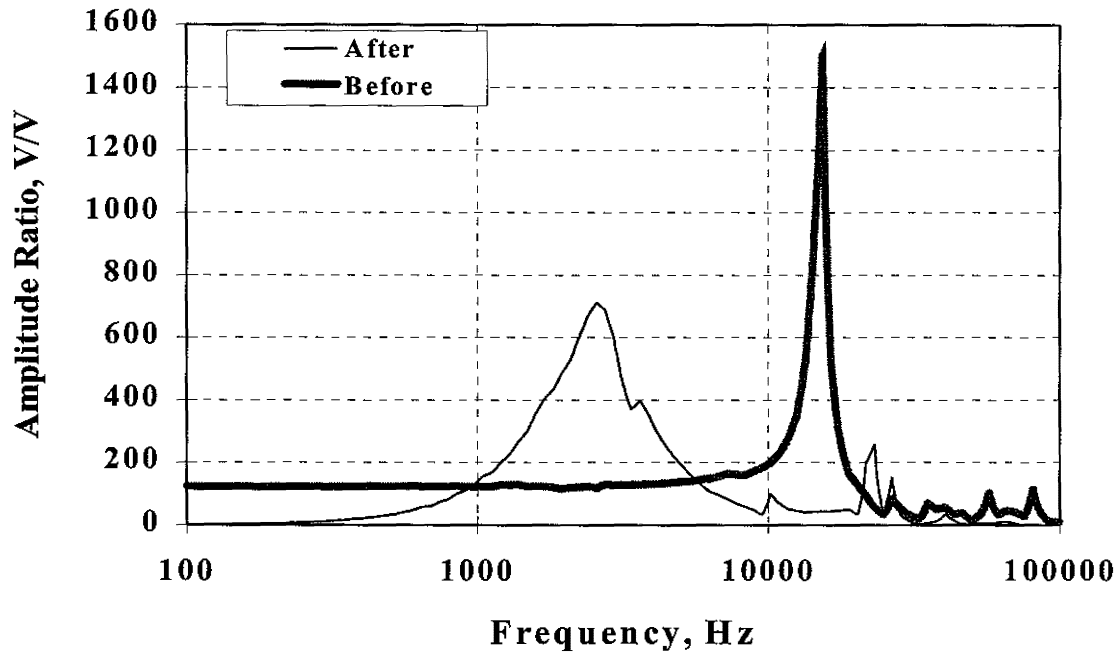


Figure 3.8 Responses of a Typical PSPA Accelerometer before and after Placed inside the Sensor Holder

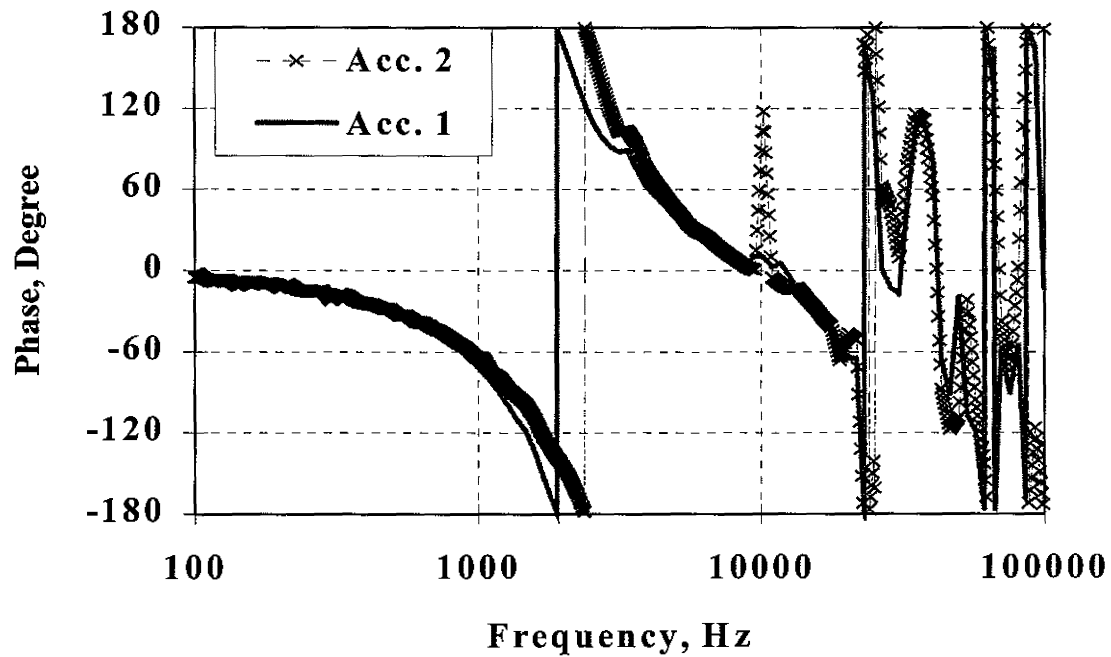
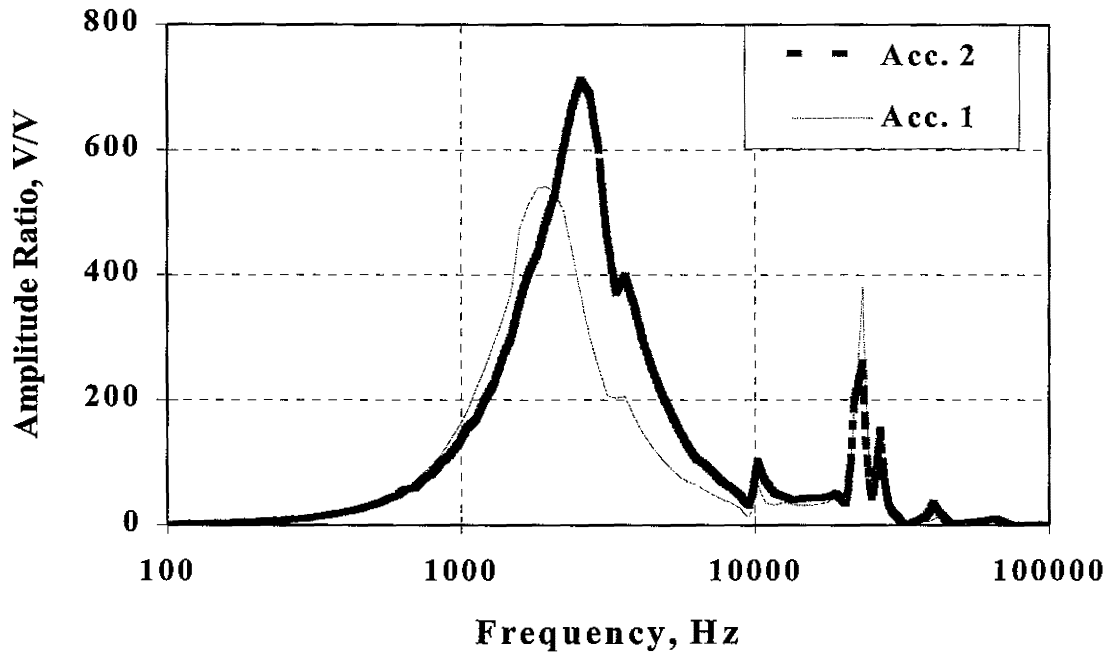


Figure 3.9 Comparison of Response of Accelerometers 1 and 2 of PSPA

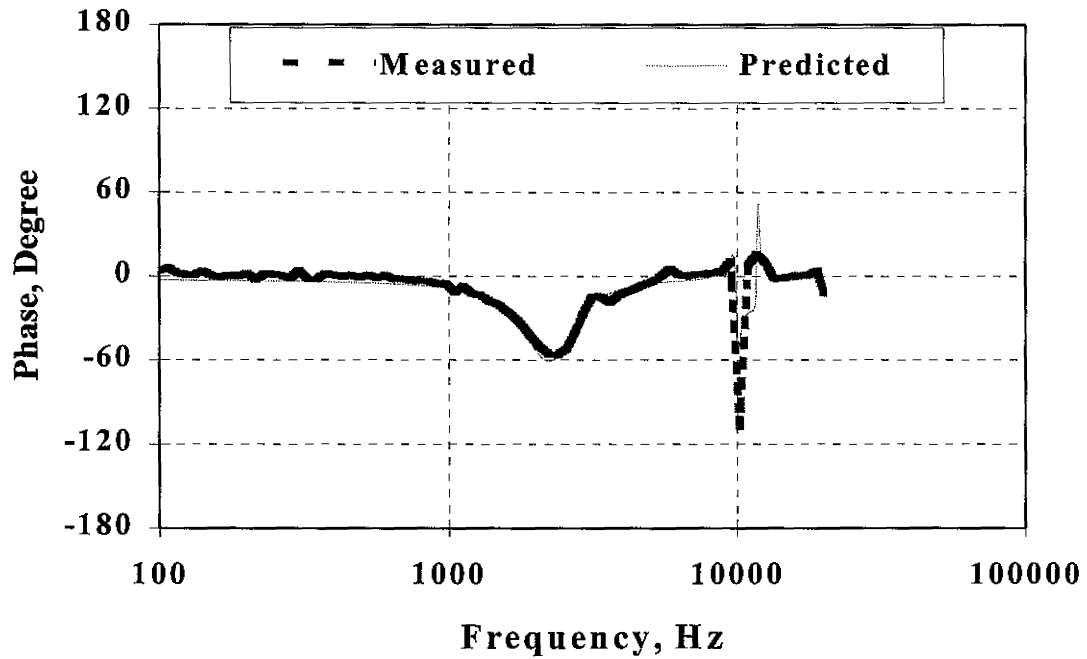
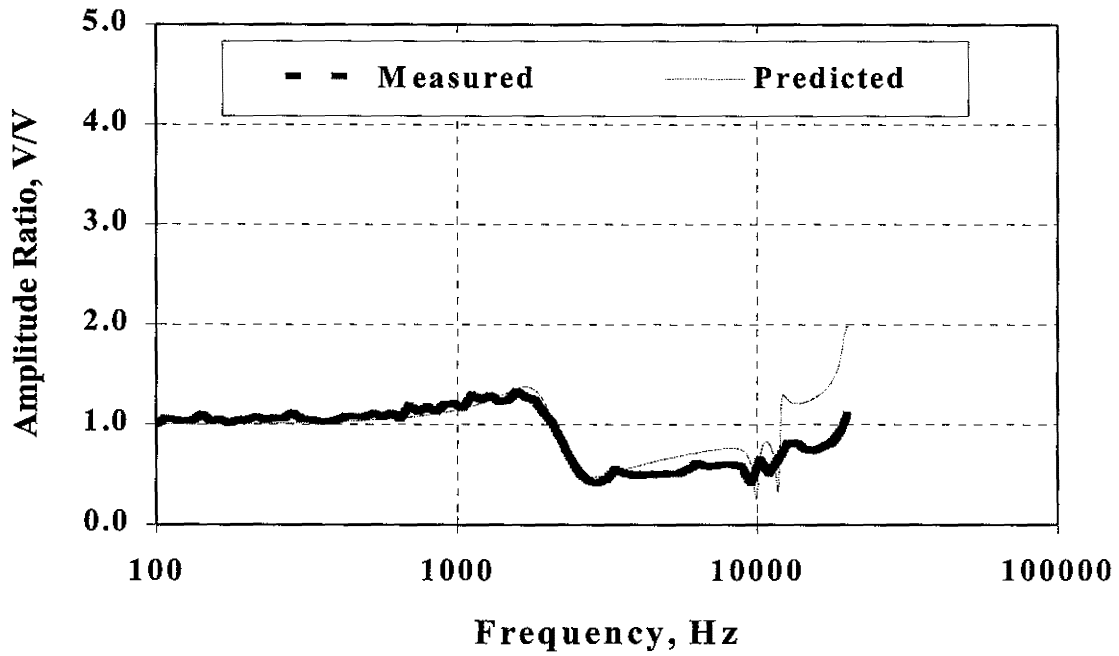


Figure 3.10 Ratio of Frequency Response Curves of Accelerometer 1 and 2

fitting are shown in Table 3.1. The curve fitting capabilities of the dynamic signal analyzer are used. The poles and zeros can be incorporated in the PSPA data reduction program.

Table 3.1 Poles and Zeros Obtained from Curve Fitting of the Data of Figure 3.10

Number	Zeros	Poles	Gain
1	-57.8981	-13483.3	7.37E-08
2	0.0	-4475.25	
3	-3264.86+7494.14i	-2052.59	
4	-3264.86-7494.14i	-563.725+1784.03i	
5	92.616+9798.3i	-563.725-1784.03i	
6	92.616-9798.3i	37.9211+9982.56i	
7	13391.9+13454.7i	37.9211-9982.56i	
8	13391.9-13454.7i	-4193.56+18913.3i	
9	-2985.89+17385.8i	-4193.56-18913.3i	
10	-2985.89-17385.8i	0	

Amplitude Calibration

The amplitude calibration of the accelerometer for the IE method can be performed using the same setup. However, the steps involved in the analysis and data reduction are slightly different. The test setup for the analysis is shown in the Figure 3.11. The calibration is carried out in two steps. A proximator is used first as a reference sensor. The response of the shaker's built-in accelerometer is compared with the response of the proximator. In that manner, the amplitude calibration of the shaker's built-in accelerometer is assured. In the second phase, the response of the PSPA accelerometer is compared with that of the embedded accelerometer. The response obtained from first phase is integrated twice because proximator measures deflection and accelerometer measures acceleration. The integrated response is then multiplied by the calibration factor of the proximator. This modified response is multiplied by the response spectrum of the second phase to obtain the amplitude calibration of the PSPA for the analysis of the IE results. This two step calibration is required so that the PSPA accelerometer does not have to be disassembled for calibration.

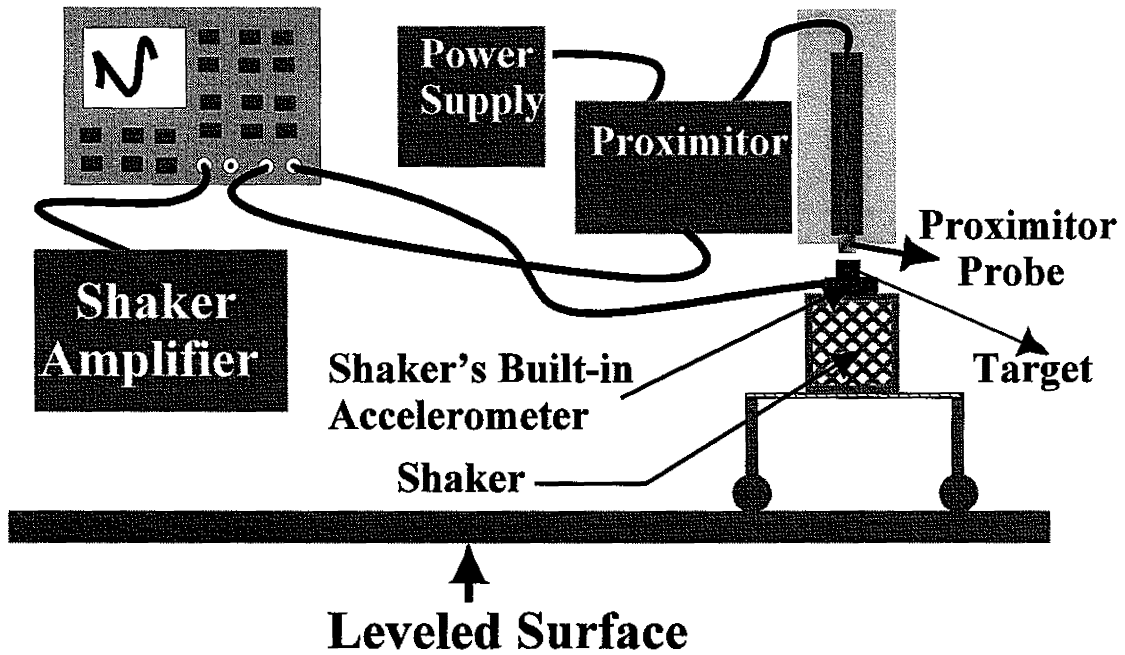


Figure 3.11 A Schematic of Test Setup for Amplitude Calibration of Accelerometer

The response spectra from the calibration of the shaker's built-in accelerometer with the proximator are shown in Figure 3.12. The response is quite linear up to a frequency of about 20 kHz. After that frequency, a large resonance is observed. The range of interest typically lies between frequencies of 4 kHz and 20 kHz (thicknesses of 600 mm to 60 mm, respectively). The phase spectrum is constant value of about -180 degrees up to a frequency of about 1 KHz, above which a gradual increase is observed. The phase spectrum resembles one of a highly damped system (perhaps the shaker). In the IE method, the phase is of small concern and the amplitude spectrum is significant.

The magnitude and phase spectra determined from the calibration of the PSPA accelerometer and the shaker's built-in accelerometer are shown in Figures 3.13. The method used to determine this graph is identical to the one described in Figure 3.9 for accelerometer 1. As a matter of fact, those results can be directly used in this process as well as for the calibration of phase.

By multiplying the spectra shown in Figure 3.13 by those shown in Figure 3.12, the actual calibration curve for the IE method is determined. Such a curve is shown in Figure 3.14. The curve fitting capabilities of the dynamic signal analyzer can be used to fit the curve. The poles and zeros obtained from fitting the curve can be provided to the PSPA manufacturers for input in their data reduction program. The poles and zeros obtained from the curve fitting of the data shown in Figure 3.14 is included in Table 3.2. The fitted and measured spectra are compared in Figure 3.14. The fit, particularly for the amplitude is quite good.

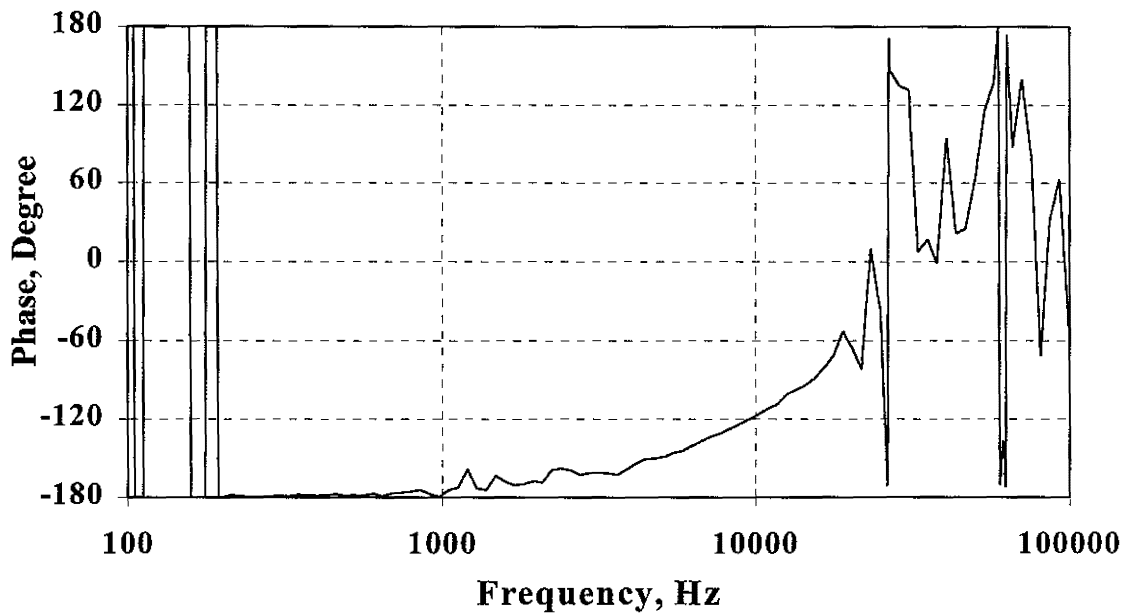
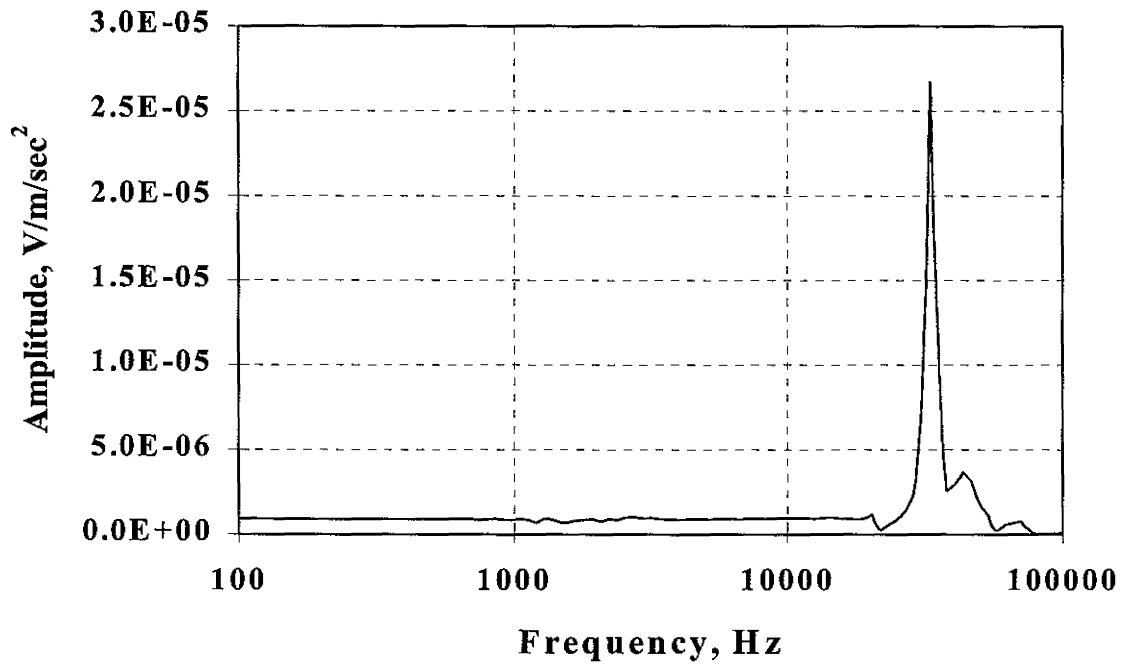


Figure 3.12 A Typical Frequency Response of Built-in Accelerometer of Piezo Shaker

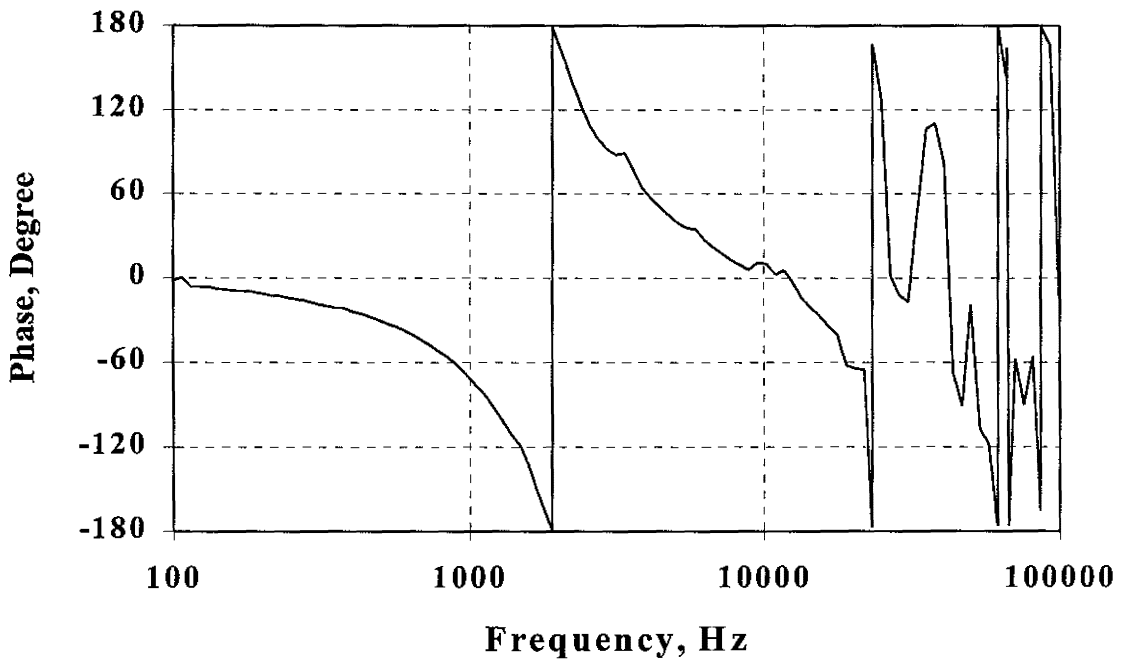
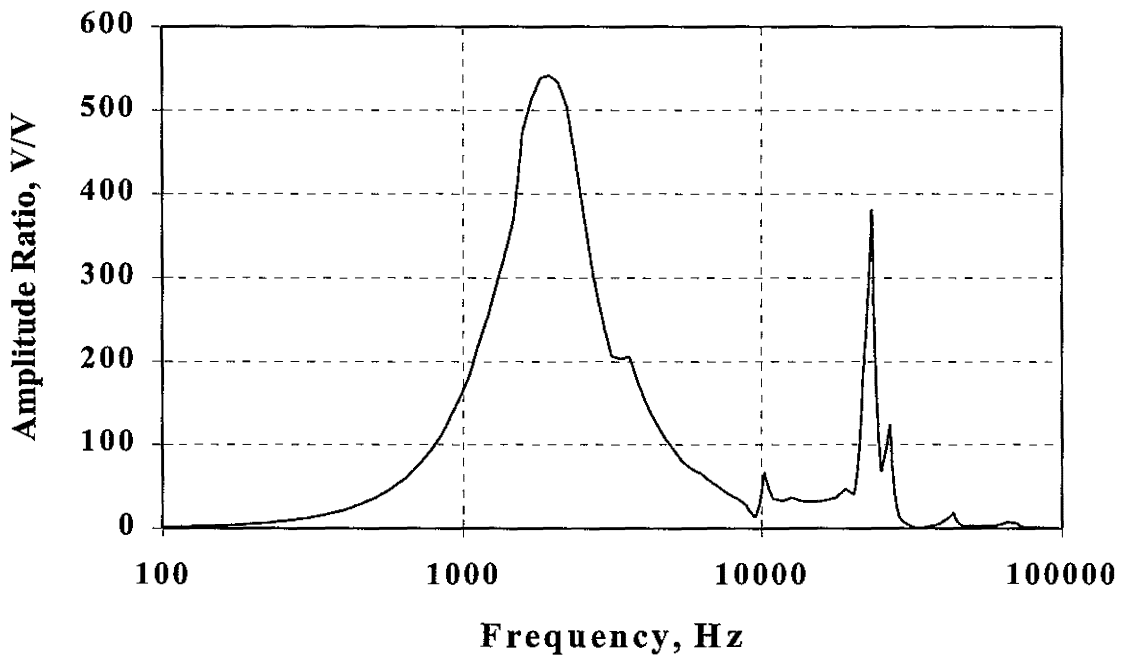


Figure 3.13 A Typical Frequency Response of PSPA Accelerometer

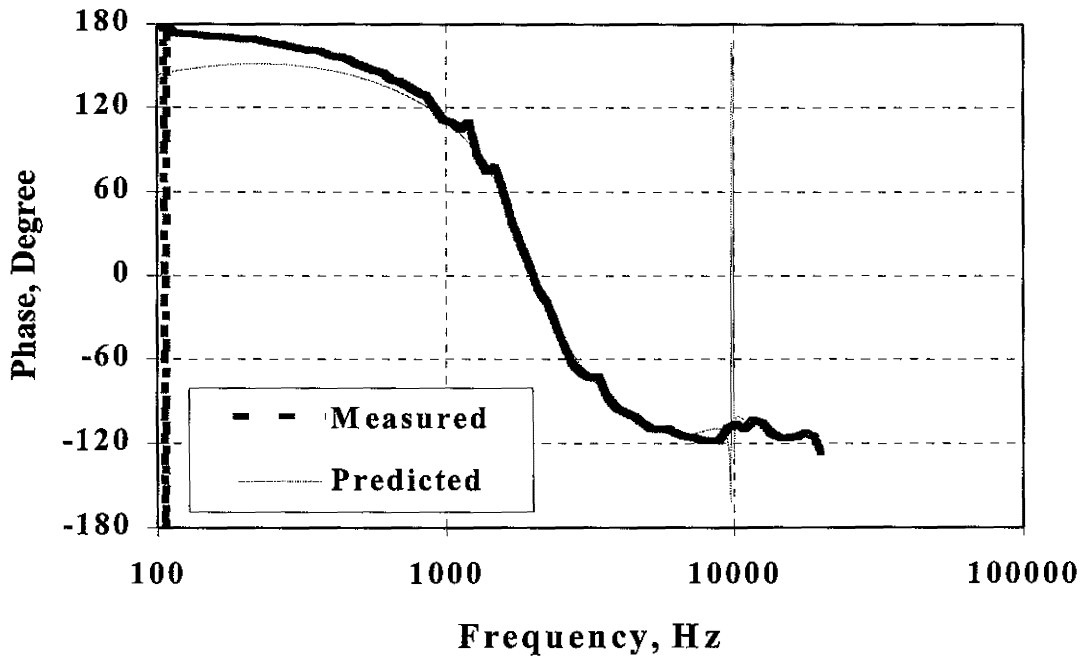
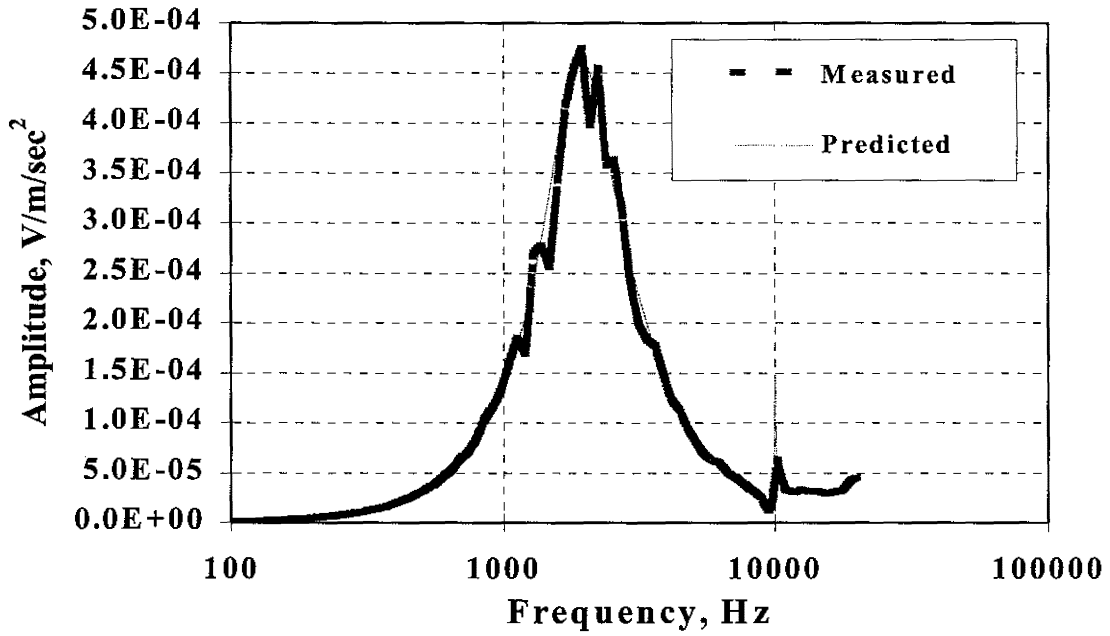


Figure 3.14 Calibration Curves for PSPA Accelerometer

Table 3.2 Poles and Zeros Obtained from Curve Fitting of Spectra Shown in Figure 3.14

Number	Zeros	Poles	Gain
1	3189.91	1685.22	3.23E-05
2	9359.49	27077.7	
3	-3780.26+2669.41i	-648.619+2929.41i	
4	-3780.26-2669.41i	-648.619-2929.41i	
5	-149.63+10582.9i	-279.185+11961.9i	
6	-149.63-10582.9i	-279.185-11961.9i	
7	100.972+13656.8i	-181.474+15829.9i	
8	100.972-13656.8i	-181.474-15829.9i	
9	453.977+16558.4i	-7895.45+25999.9i	
10	453.977-16558.4i	-7895.45-25999.9i	

To indicate the use of the calibration results, the calibration spectra shown in Figure 3.14 was applied to the results from the IE tests shown in Figure 3.5. The outcome, which is shown in Figure 15, exhibits that the results are better pronounced when the impact of the mounting and the electronic components are subtracted from the raw IE spectra.

In summary, the results from this study indicate that the calibration of the accelerometers, used in PSPA, can be easily performed in the laboratory. Since the equipment is portable, there is no need to develop a field calibration test procedure.

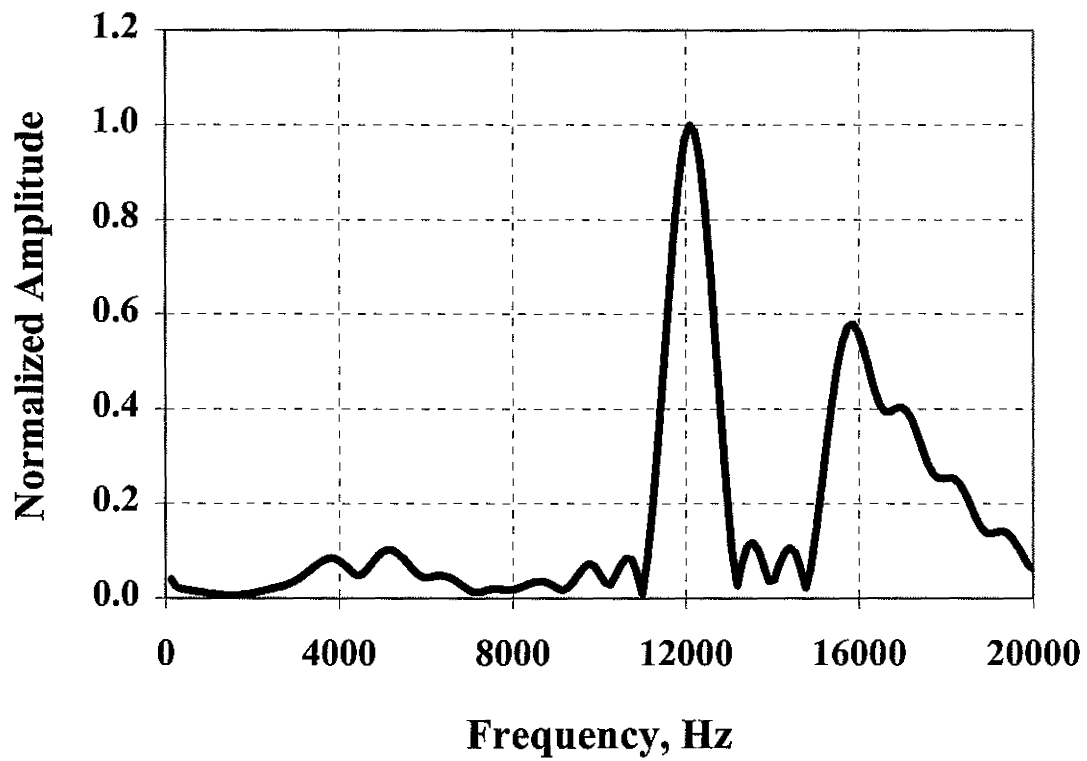


Figure 3.15 Calibrated Response of PSPA Accelerometer

Chapter 4

Seismic Pavement Analyzer

The Seismic Pavement Analyzer (SPA) is similar to the PSPA in terms of principles of operation. However, it is more comprehensive. As for the PSPA, a standard calibration procedure for the SPA did not exist, and had to be developed under this project.

A schematic of the SPA is shown in Figure 4.1. The major components include eight receivers (five accelerometers and three geophones), the receiver mounting members, two pneumatic impact sources, and a raise-lower mechanism. These are mounted on a light trailer for towing behind a vehicle.

In addition to the tests performed with the PSPA, the SASW and Impulse Response (IR) tests can be performed with the SPA. The IR technique is used to determine the modulus of subgrade reaction for rigid pavements and overall modulus of flexible pavements. The Spectral-Analysis-of-Surface-Waves (SASW) method can determine the shear modulus profile of a pavement section.

To facilitate the description of the calibration process, the data analysis and collection procedures are briefly described first. A detailed description of the device can be found in Nazarian et al. (1993).

Description of SPA Data Analysis Procedure

A typical test at one point with the SPA consists of the following steps. The testing sequence, which is initiated through the computer, starts by lowering the sensors to the pavement. The high-frequency source is then activated. The time histories of the three accelerometers closest to the high-frequency source, as well as the load cell connected to this source, are acquired first. The source is fired four to seven times. For the last three impacts of the source, the output voltages of the load cell and the receivers are saved and averaged (stacked) in the frequency domain. The initial impacts are used to adjust the gains of the pre-amplifiers. The gains are set for optimization of the dynamic range.

The same procedure is followed again, but the first three accelerometers are replaced by the last three accelerometers. The middle accelerometer (third closest accelerometer to the source) is active in both sets of experiments.

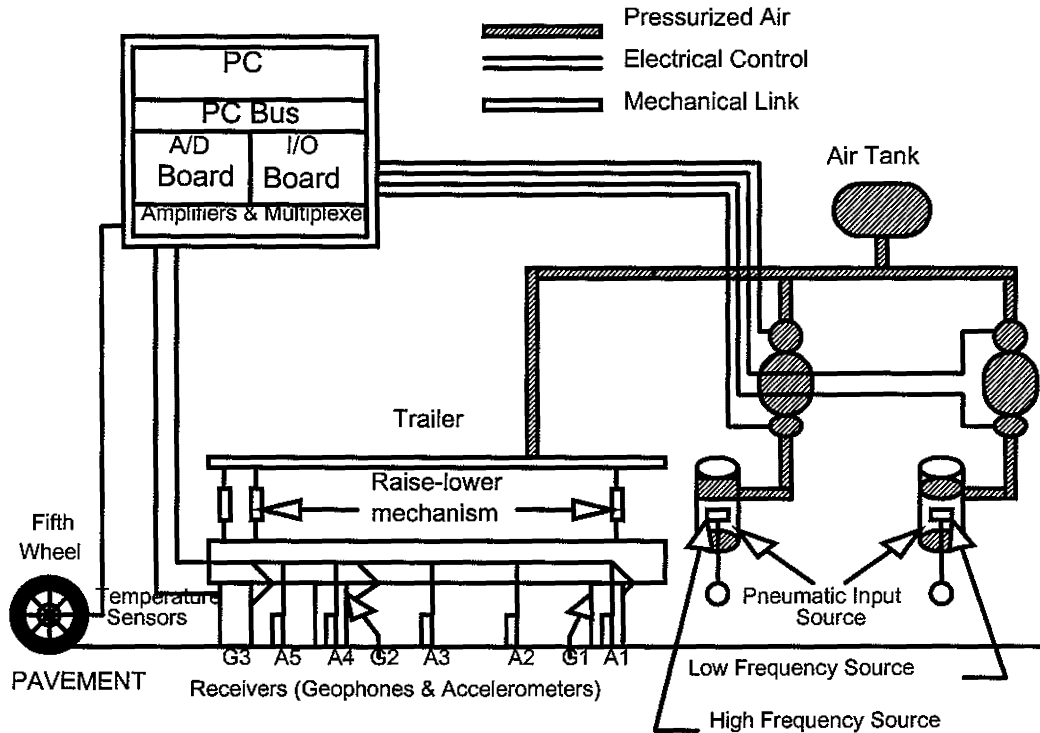


Figure 4.1 A Schematic of Seismic Pavement Analyzer

Typical voltage outputs of the load cells and the accelerometers are shown in Figure 4.2. To ensure that an adequate signal-to-noise ratio is achieved in all channels, signals are normalized to a maximum amplitude of one. In this manner, the main features of the signals can be easily inspected.

In the next step of data collection, the low-frequency load cell and the three geophones are recorded. The procedure described above for each of the accelerometer banks is utilized. A typical output of the three geophones is shown in Figure 4.2c in the normalized fashion. The data collected in this step has to be processed using signal and spectral analyses. These processes are described in the next section. For the sake of brevity, the UBW, USW and IE methods are not repeated herein. The reader is referred to the previous chapter.

Impulse-Response Method

This method uses the voltage output from the first geophone (the geophone closest to the source, G1) and the low-frequency load cell (see Figure 4.2c). The output of the load cell and geophone are transformed into the frequency domain using a fast-Fourier Transform (FFT) algorithm. The ratio of the load and the particle velocity at each frequency is then determined. This function is then integrated to obtain the stiffness spectrum.

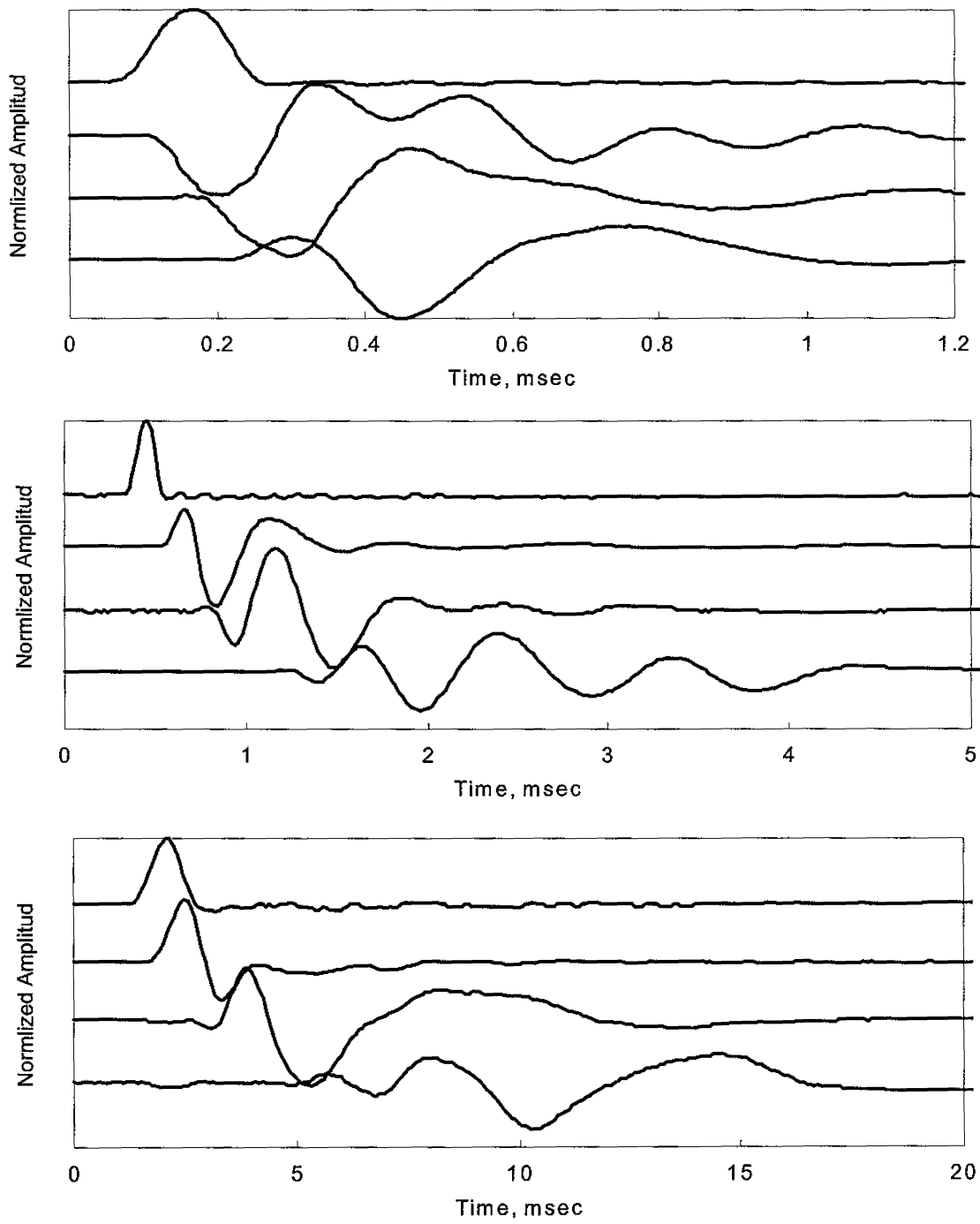


Figure 4.2 Typical Normalized Time Records Obtained with SPA

Typical stiffness spectra are shown in Figure 4.3. The results of interest are a “static stiffness” (stiffness close to zero), and the damping ratio. The higher the subgrade quality is, the larger the static stiffness will become. A higher rate of an increase in stiffness with frequency is an indication of a lower damping ratio. In other words, a flat stiffness spectrum corresponds to a pavement system with a high damping ratio.

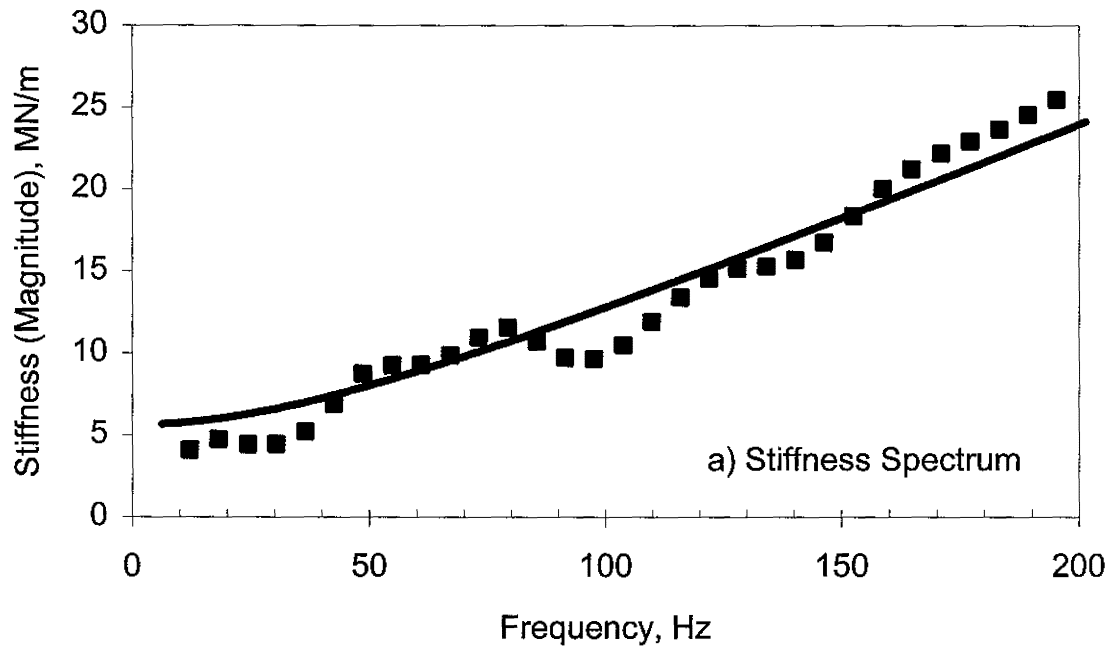


Figure 4.3 Typical Spectral Functions Used in Impulse-Response Test

Spectral-Analysis-of-Surface-Wave (SASW) Method

In the SASW testing, a dispersion curve of the pavement section is measured and inverted to obtain shear modulus profile of a pavement section. The initial steps involved in obtaining a dispersion curve are similar to those described for the USW method. Time records from two adjacent sensors are Fourier-transformed. Spectral analysis is applied to obtain the phase information of the transfer function and the coherence function. From the fitted phase spectrum, the dispersion curve (phase velocity versus wavelengths) is determined. This process is repeated for all receiver spacings.

Finally, the representative dispersion curve is obtained by combining the dispersion curves from different spacings using a L1-norm curve-fitting process. The details of this process can be found in (Nazarian et al., 1995).

Four sets of phase spectra from accelerometers are utilized. They are phase spectra between accelerometers 1 and 2 (spacing of 75 mm not shown here, see Figure 3.9); accelerometers 2 and 3 (spacing of 150 mm); accelerometers 3 and 4 (spacing of 300 mm); and accelerometers 4 and 5

(spacing of 600 mm). In addition to the accelerometer records, records from Geophones 2 and 3 (spacing of 1200 mm) are used. The phase spectra and the coherence functions from one of site are shown in Figure 4.5.

The next step is to determine the final dispersion curve. The dispersion curves obtained from all receiver spacings are combined as shown in Figure 4.6. A curve is fitted to this data to obtain the "ideal dispersion curve," which is representative of the raw data, is used in the inversion process. Finally, an inversion process determines the final Young's modulus profile for a site from this curve. The modulus profile at the example site is shown in Figure 4.7.

To ensure that the shear wave velocity profile is realistic, the dispersion curve should be accurately constructed. The first step in the construction of an accurate dispersion curve is to confirm that the phase spectra from different spacings are accurate. Therefore, as for the USW method in the PSPA, one should calibrate the sensors to eliminate any phase shift due to electronics or sensor placement between the sensor pairs.

The above discussion suggests that the five accelerometers, three geophones and two load cells of the SPA should be calibrated for accurate and precise determination of pavement properties. The calibration procedures developed in the last two chapters can be used for the calibration of SPA sensors with only few modifications. Two geophones and five accelerometers need to be calibrated for the phase shift similar to that of PSPA. The accelerometer involved in the IE test and the geophone involved in the IR test should also be calibrated for the amplitude. The high and low frequency load cells need to be calibrated similar to that of FWD. Specifically, accelerometer A1 needs to be calibrated for amplitude, and accelerometers A1 through A5 for phase shift. Similarly, geophone G1 needs to be calibrated for amplitude, and geophones G2 and G3 for phase shift. The calibration procedure for each sensor is described in the next section.

Proposed Calibration of Accelerometers

Phase Shift Calibration

The setup required for calibrating the SPA accelerometers is shown in Figure 4.8. The setup is similar to that of FWD with the only exception that the low frequency shaker is replaced by a high frequency shaker. The accelerometer to be calibrated is lowered on top of the piezo-shaker using raise-lower mechanism of the SPA. The outputs of the built-in accelerometer (directly) and the SPA accelerometer (just before entering into the data acquisition board of the SPA) are connected to a dynamic signal analyzer. The shaker is excited in a swept-sine mode in a range of frequencies of 10 Hz to 100 kHz using a built-in feature of the dynamic signal analyzer.

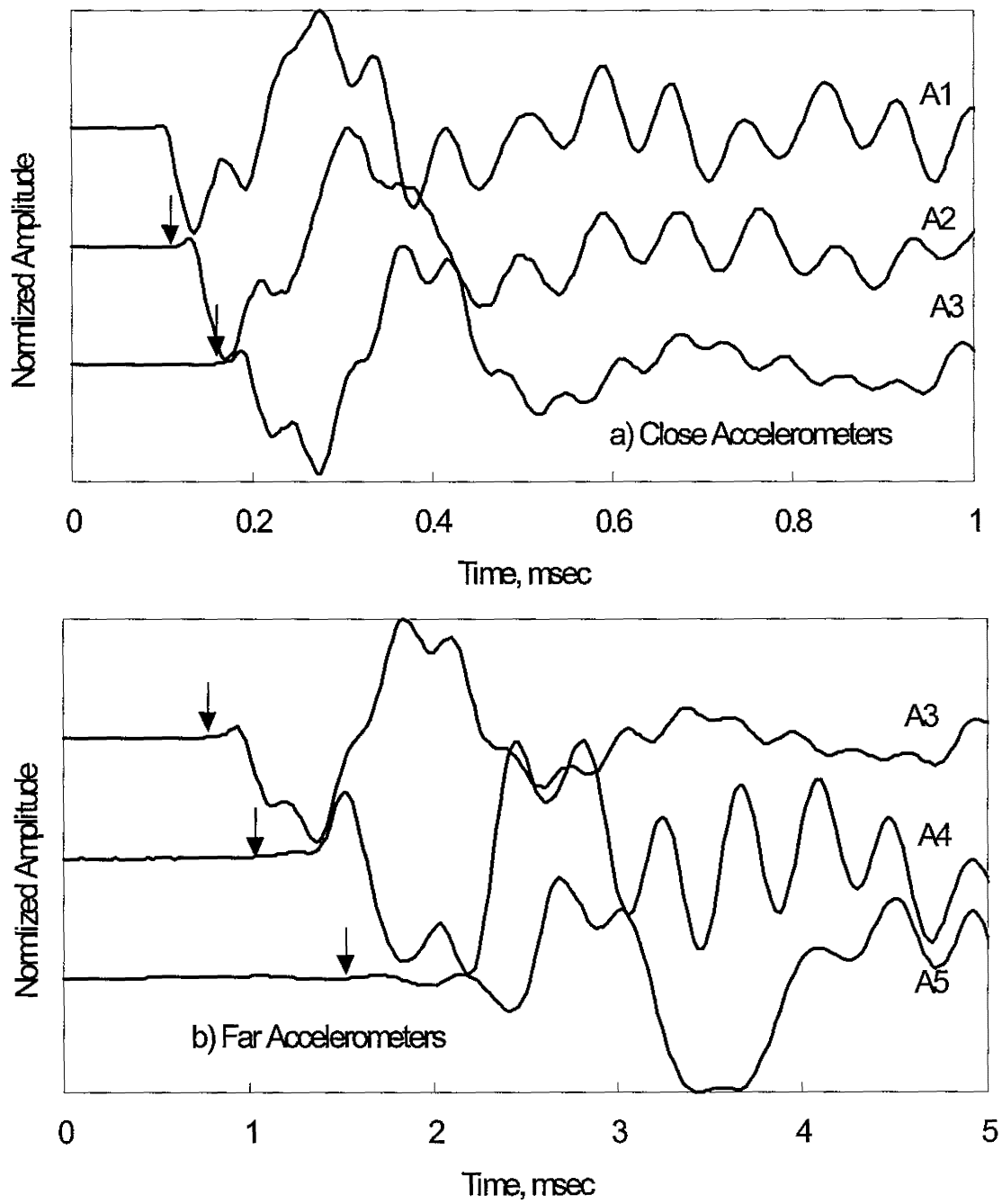


Figure 4.4 Typical Amplified Signal Used in Ultrasonic-Body-Waves Test

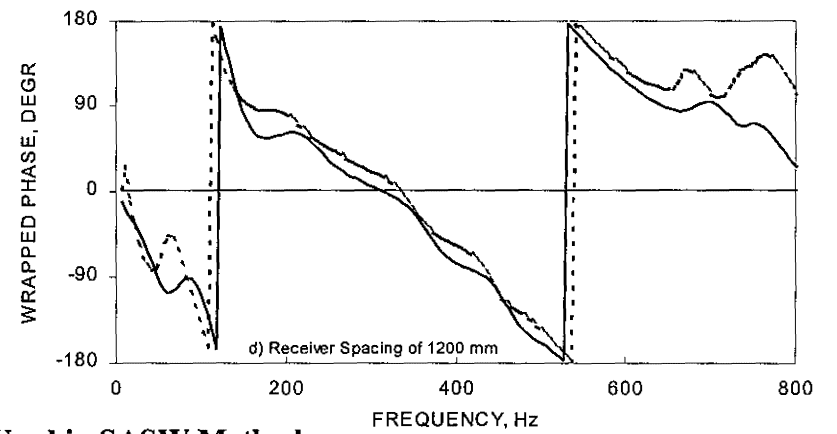
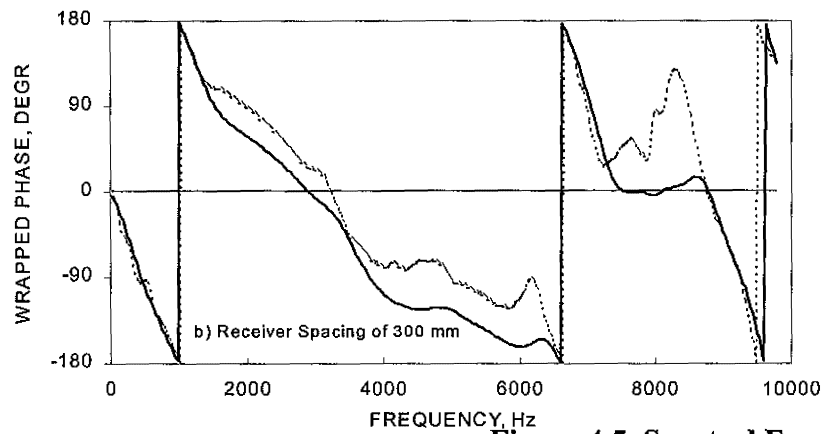
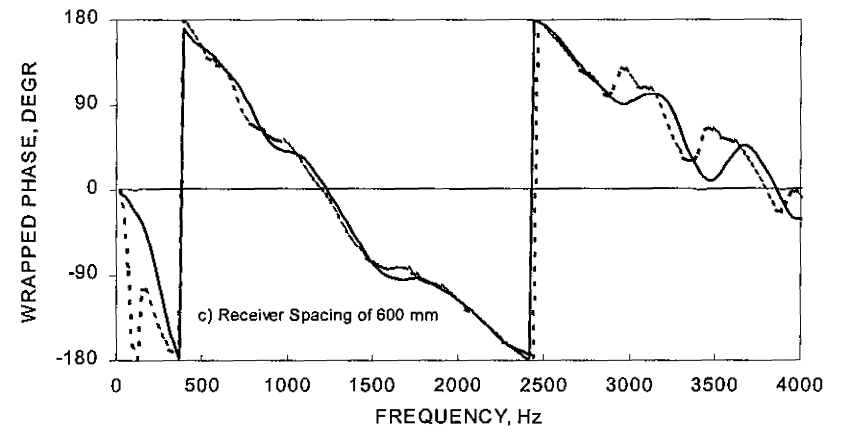
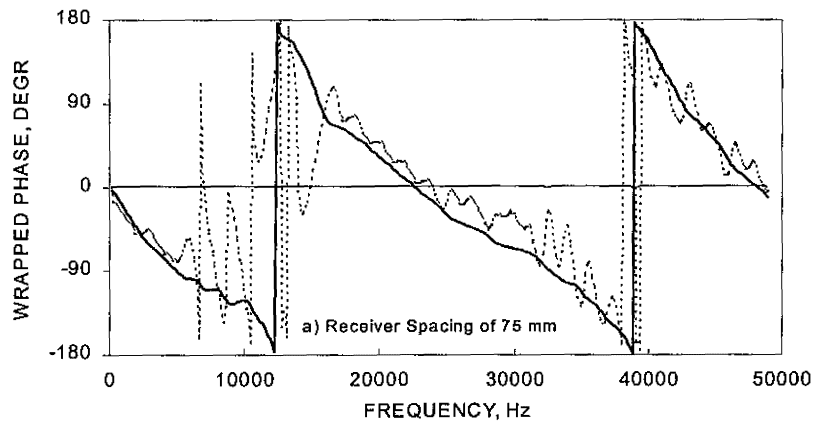


Figure 4.5 Spectral Functions Used in SASW Method

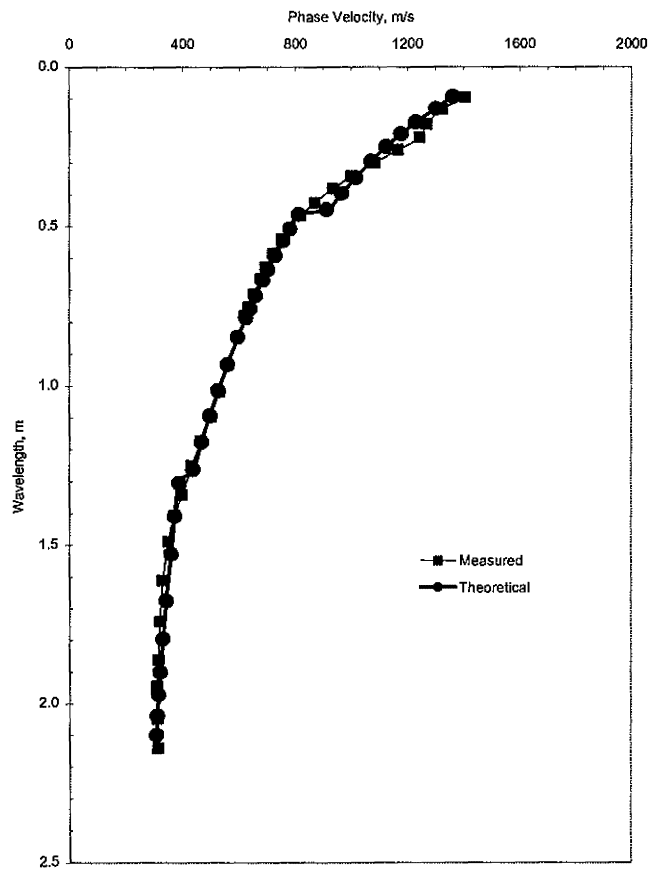


Figure 4.6 Typical Dispersion Curves from SASW Testing

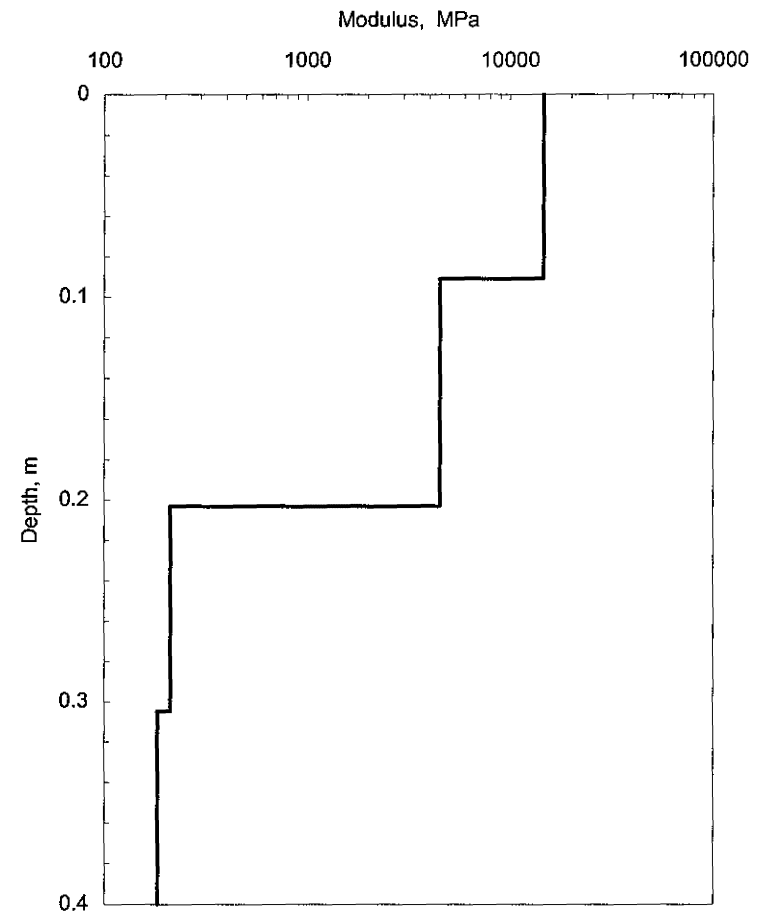


Figure 4.7 Typical Modulus Profile from SASW Tests

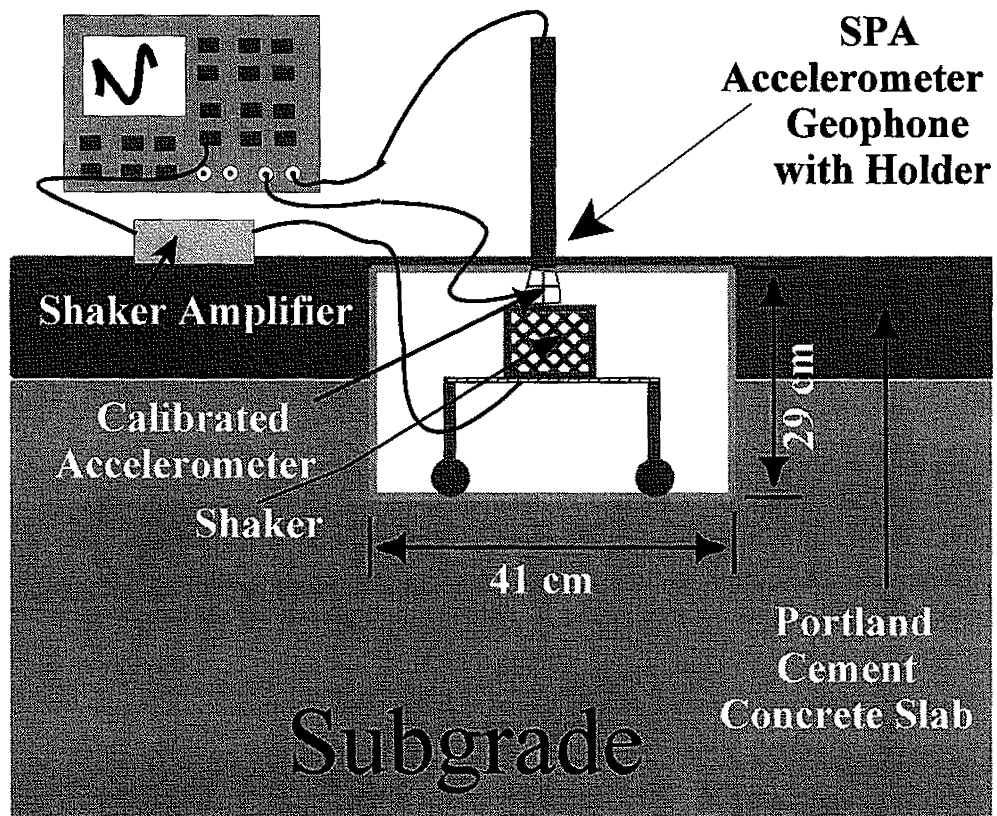


Figure 4.8 A Schematic of Field Calibration of SPA Accelerometer or Geophone

To eliminate the need for disassembling the SPA sensors for a calibration, the behavior of each accelerometer is compared with the shaker's built-in accelerometer first. By dividing the calibration curves relative to the shaker's accelerometer for each adjacent pair of SPA accelerometers, one can determine the phase shift calibration for them. The calibration results in the range of 100 Hz to 30 kHz are of interest.

The phase spectra of accelerometers 2 and 3 of SPA are compared in Figure 4.9. The two spectra are almost identical up to a frequency of 5 KHz. At frequencies greater than 5 kHz, the phase values show similar trends with some variation.

The phase spectrum associated with the difference between the two spectra of accelerometers 2 and 3 (shown in Figure 4.9) is depicted in Figure 4.10. The phase shift between the two accelerometers is almost zero up to a frequency of 2,500 Hz. Past this frequency, because of differences in the resonant frequencies of the accelerometer systems, a relative phase shift of up to 100 degrees is observed. If such phase shifts are not considered in the analysis, localized errors in velocity of less than 12% (for a typical AC layer) and less than 6% (for a typical PCC layer) should be anticipated. Because of the averaging process involved in determining the final dispersion curve, the global impact is less pronounced.

The phase measured at each frequency in Figure 4.10 should be subtracted from the phase of transfer function obtained during field tests. To facilitate this task, a polynomial is fitted to the measured phase spectrum. Typical poles and zeros, obtained from the curve fitting routines built in the dynamic signal analyzer, are shown in Table 4.1. In a similar manner, phase spectra for accelerometer pairs 1 and 2, 3 and 4, and 4 and 5 can be obtained.

Table 4.1 Poles and Zeros Obtained from Fitting a Curve to Data Shown in Figure 4.10

Number	Poles	Zeros	Gain
1	-27843.2	-15012	1.43E+00
2	-256.776+8576.7i	-1183.18+7981.07i	
3	-256.776-8576.7i	-1183.18-7981.07i	
4	-365.857+12921.9i	-1270.28+15157.1i	
5	-365.857-12921.9i	-1270.28-15157.1i	

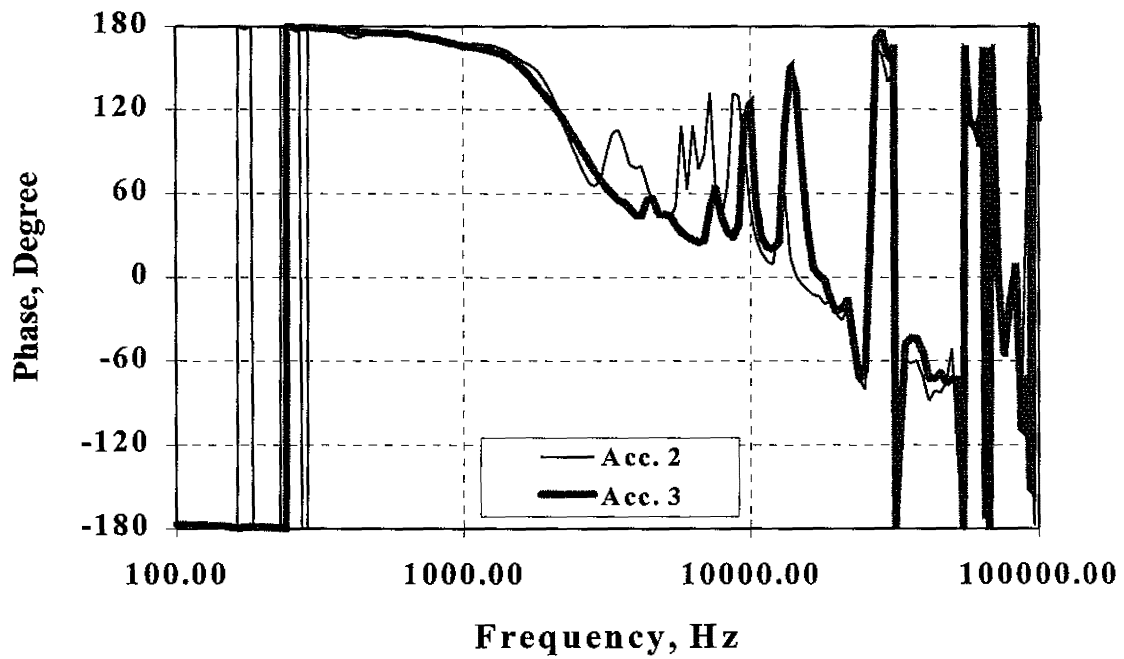


Figure 4.9 Comparison of Phase Spectra of Accelerometers 2 and 3 of SPA

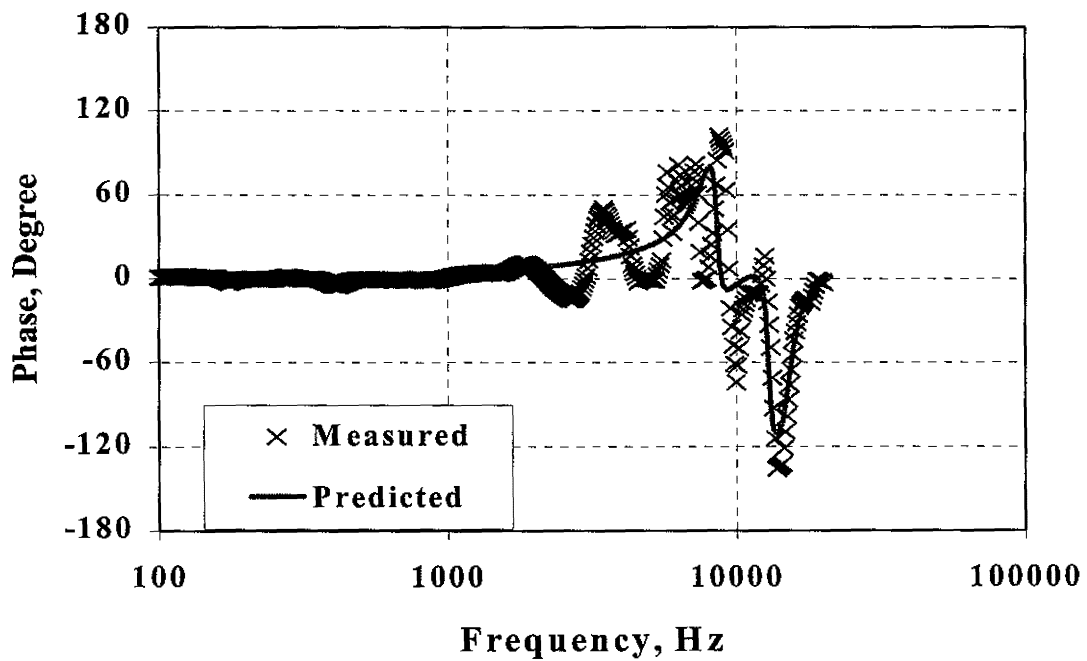


Figure 4.10 Phase Calibration Spectrum for Accelerometers 2 and 3 Pair

Table 4.2 Poles and Zeros Obtained from Fitting a Curve to Data Shown in Figure 4.12

Number	Poles	Zeros	Gain
1	1685.22	3189.91	3.23E-05
2	27077.7	9359.49	
3	-648.619+2929.41i	-3780.26+2669.44i	
4	-648.619-2929.41i	-3780.26-2669.44i	
5	-279.185+11961.9i	-149.63+10582.9i	
6	-279.185-11961.9i	-149.63-10582.9i	
7	-181.474+15829.9i	100.972+13656.8i	
8	-181.474-15829.9i	100.972-13656.8i	
9	-7895.45+25999.9i	453.977+16558.4i	
10	-7895.45-25999.9i	453.977-16558.4i	

Amplitude Calibration

The amplitude calibration of the accelerometer 1 of SPA can be performed using the same setup used for phase calibrations. The calibration process is carried out in two steps, very similar to that described for the PSPA accelerometer. A proximitator is used as a reference sensor to verify the amplitude calibration of the shaker’s built-in accelerometer (see Figure 3.12).

In the second phase, the response of the SPA accelerometer is compared with that of the built-in accelerometer. The amplitude ratio spectrum of accelerometer 1 relative to the shaker’s accelerometer is shown in Figure 4.11. A resonant frequency of about 3 kHz is observed. Several small amplitude peaks corresponding with the natural frequency of the accelerometers and shaker can also be seen in the range of frequencies of 10 kHz to 20 kHz.

The amplitude calibration spectrum of accelerometer A1 is obtained by multiplying the spectra shown in Figures 3.12 and 4.11. The result is shown in Figure 4.12, and the poles and zeros obtained from curve fitting of the data are shown in the Table 4.2.

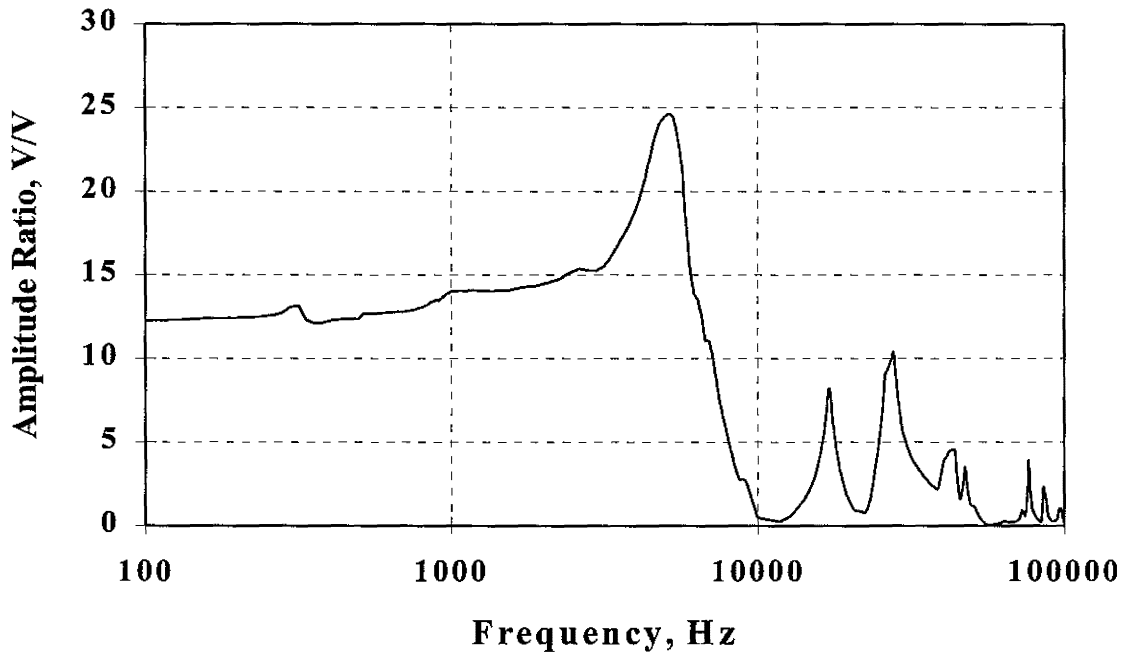


Figure 4.11 Amplitude Ratio Spectrum of Accelerometer 1 of SPA

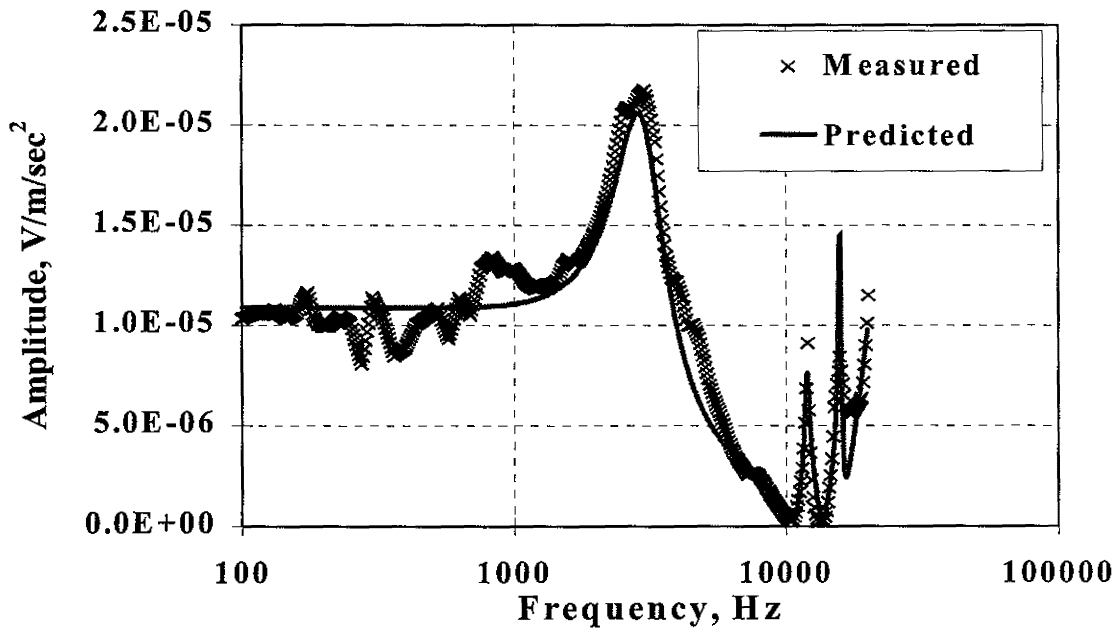


Figure 4.12 Amplitude Calibration of SPA Accelerometer 1

Proposed Calibration of Geophones

Phase Shift Calibration

The phase shift calibration should be carried out between geophones 2 and 3. These are the two geophones that are used in the SASW method. The calibration procedure is identical to that of the SPA accelerometer, with one exception. The calibration process is carried out between frequencies of 10 Hz and 2000 Hz.

The phase spectra between the high frequency shaker's sensor and the two geophones are compared in Figure 4.13. Small differences can be observed between the two curves. The phase calibration spectrum, which as usual is obtained by dividing the two phase spectra of Figure 4.13, is included in Figure 4.14. The phase shift values throughout the spectrum deviate very little from zero.

Amplitude Calibration

Geophone 1 should be calibrated for amplitude in order to be utilized accurately in the IR test results. The procedure followed here is almost identical to that described for calibrating the FWD geophones. The only difference is that the calibration up to a frequency of 200 Hz is necessary.

As a quick review, the first step is to verify the calibration of the built-in geophone with a proximator (see Figure 2.4). In the second step, geophone 1 of the SPA is lowered on top of the shaker and is calibrated under a swept sine condition.

The variation in the amplitude ratio spectrum of the SPA geophone with respect to the calibration geophone is shown in Figure 4.15a. The SPA geophone is about 5 to 10 times more sensitive than the calibration geophone in the range of frequencies of 1 Hz to 500 Hz. As usual, the peak at about 1.5 kHz corresponds to the resonant frequency of the sensor assembly.

The phase spectrum associated with the amplitude ratio spectrum shown in Figure 4.15a is included in Figure 4.15b. The phase varies between ± 20 degrees in the range of frequencies of 1 Hz to 500 Hz. At about a frequency of 1500 Hz an abrupt change in the phase is observed that can be contributed to the resonant frequency of the geophone assembly.

By multiplying the spectra shown in Figure 2.5 by those of Figure 4.15, the calibration spectra for geophone 1 of the SPA is obtained. Such curves are shown in Figure 4.16. These spectra can be conveniently incorporated into the analysis of the IR data by fitting curves to them. The natural frequency, damping ratio and gain of the geophone shown are 5.75 Hz, 0.85 and 210 mv/m/sec, respectively. The fitted curves are compared with the measured data in Figure 4.16. The results are quite comparable.

Proposed Calibration of Load Cells

The calibration of the high- and low-frequency load cells is carried out very similar to those of the FWD load cell. The only difference is that only one of the three load cells used in the calibration of the FWD is used. The schematic of the setup for this task is shown in Figure 4.17. As before, a load cell is sandwiched in between two plates. For calibrating the high frequency load cell, the top

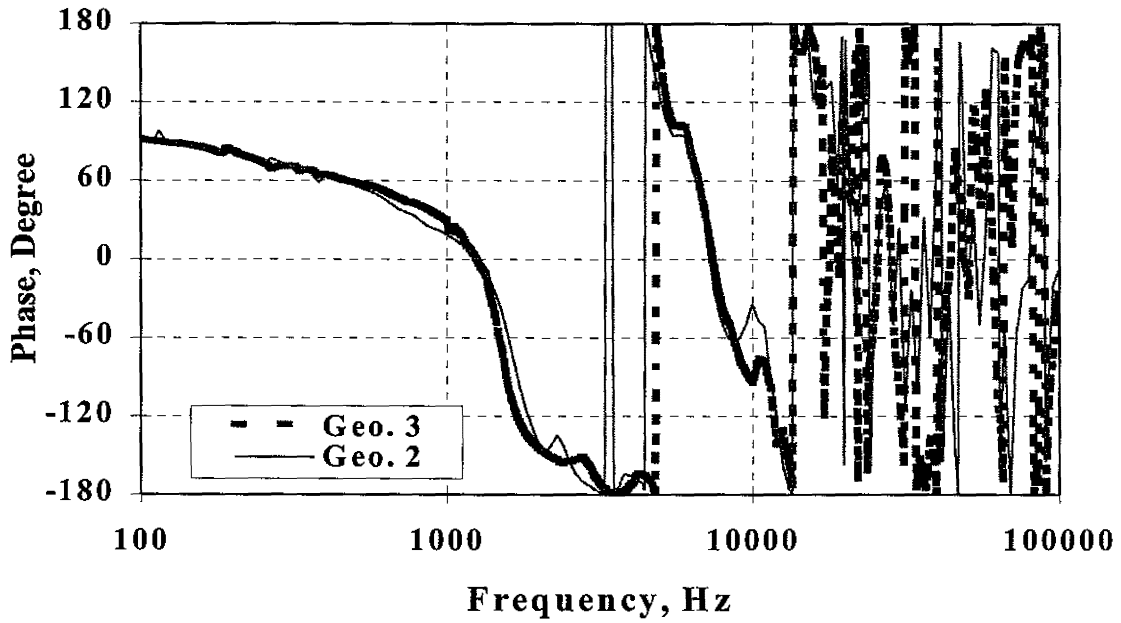


Figure 4.13 Comparison of Response of Geophones 2 and 3 of SPA

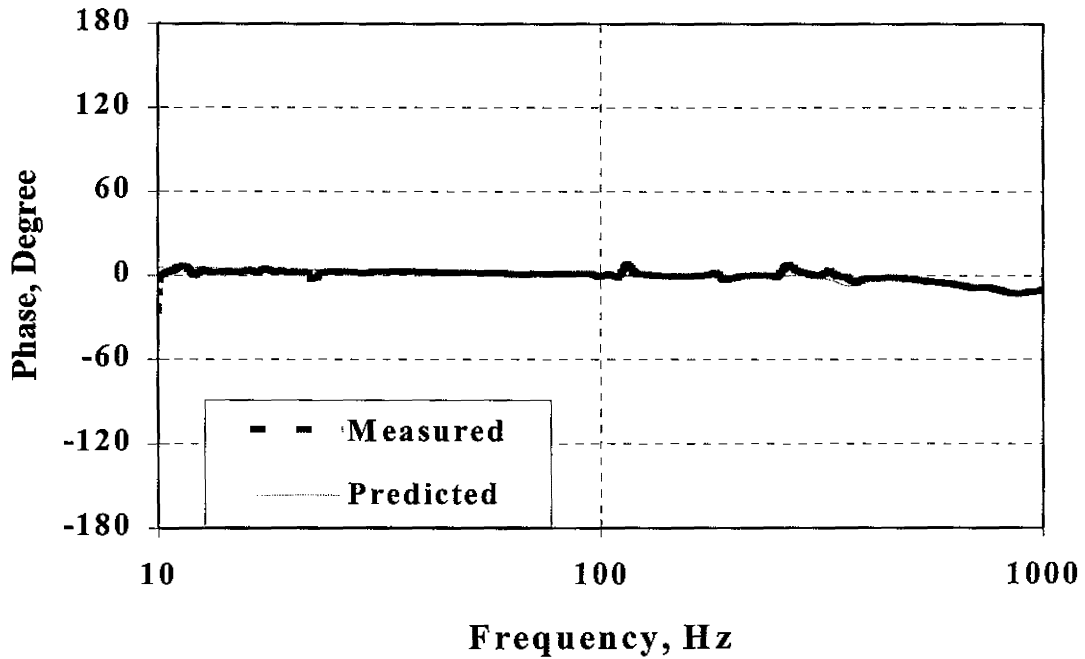


Figure 4.14 Ratio of Frequency Response Curves of Geophones 2 and 3

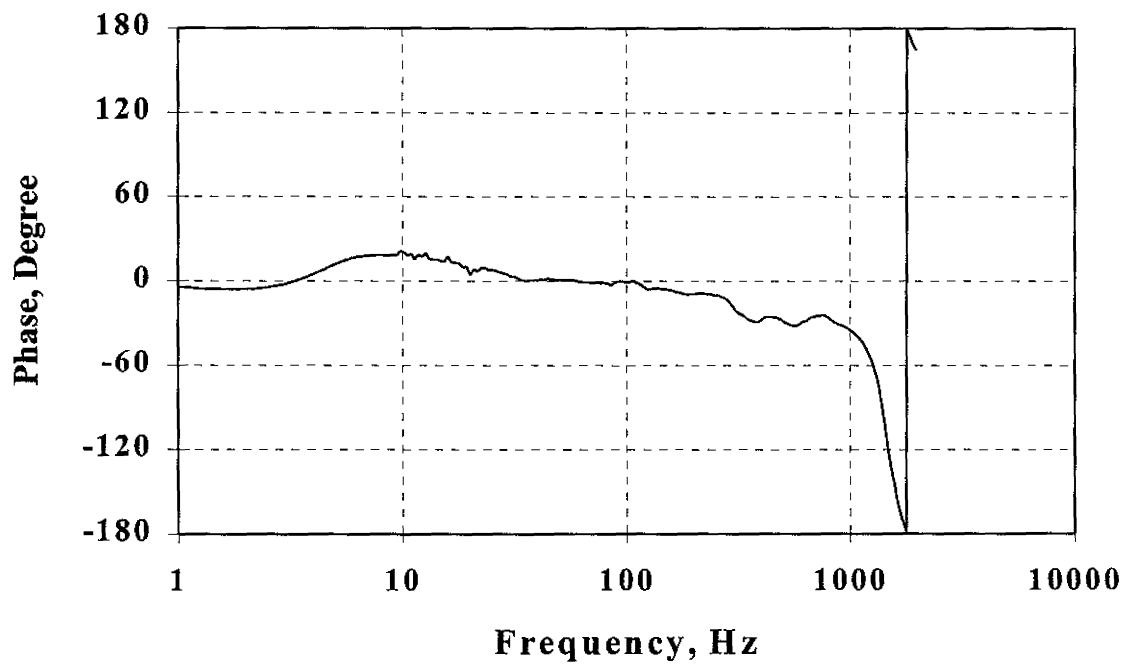
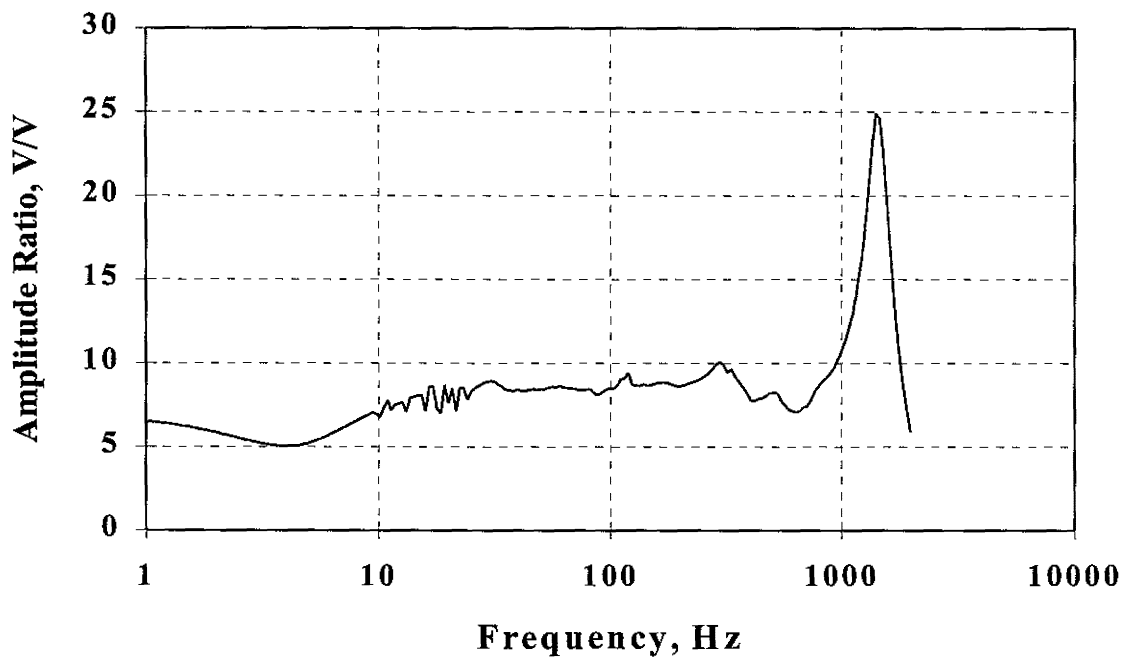


Figure 4.15 Field Calibration of SPA Geophone 1

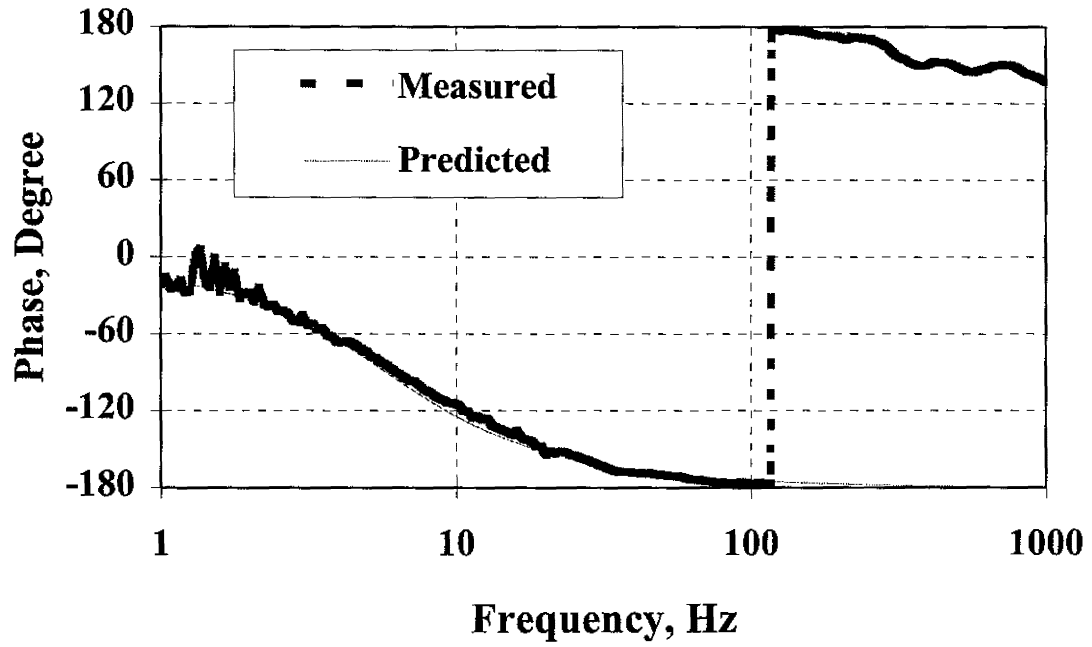
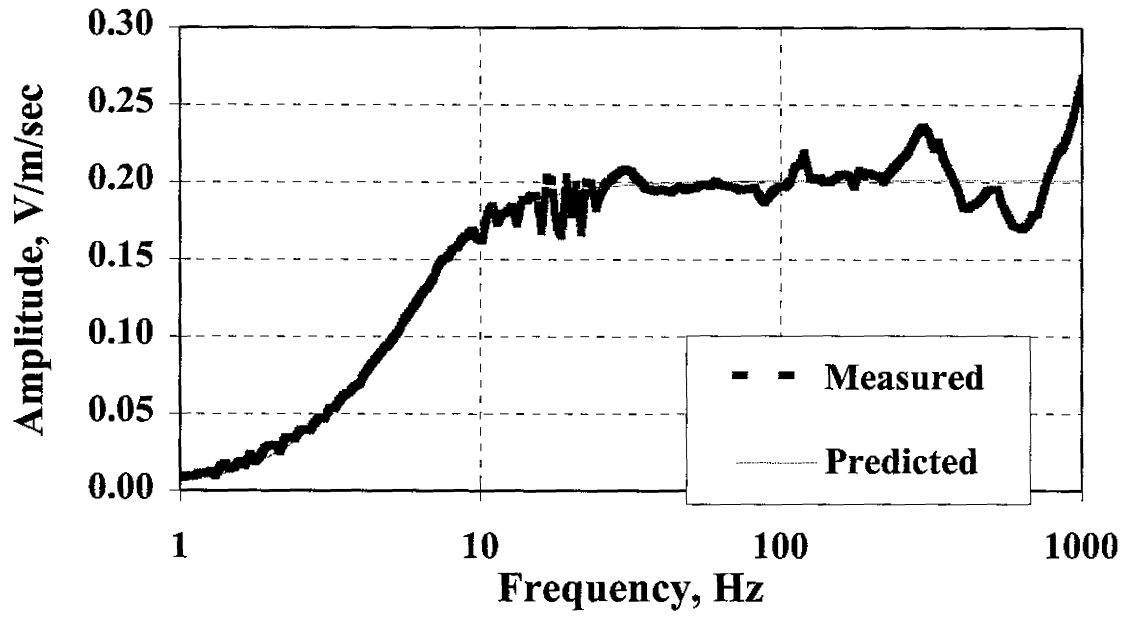


Figure 4.16 Calibration Amplitude Spectra for Geophone 1 of SPA

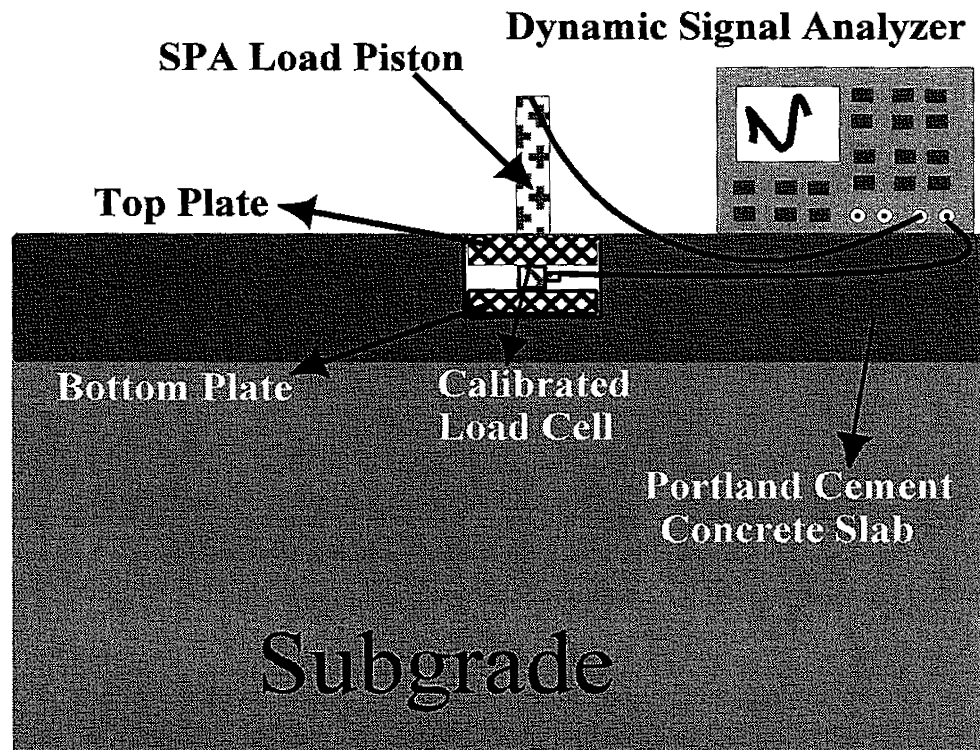


Figure 4.17 A Schematic of Test Setup for SPA Load Cell Calibration

plate is removed, and the reference load cell is directly impacted. Once again, the calibration of the reference load cell is verified under an MTS system, as discussed in Chapter 2.

The calibration is carried out at four pressure levels. At each pressure level, the load is measured with the SPA and reference load cell about 10 times. A typical load time-histories from the reference and SPA low-frequency load cells are shown in Figure 4.18. The two systems yield similar results. By comparing the peak loads from the SPA and the reference load cell one can develop the calibration curve.

The variation in output of the SPA low-frequency load cell as a function of the load imparted to the reference load cell is shown in Figure 4.19. The two variables are well correlated since the R^2 -value is about 0.99. The reference load cell exhibits larger variability in the values than the SPA load cell. This is an indication that with need to improve the seating of the reference load cell on the slab. The calibration value for the low-frequency load cell consisting of the impacts of the electronic components and the mounting system is about 91 mv/KN.

Similarly, the calibration curve for the high-frequency load cell is shown in Figure 4.20. Slightly more scatter in the results is observed for this process. The R^2 -value is about 0.97. The calibration value for the high frequency load cell is about 1193 mv/KN. We again believe that we need to improve the seating of the reference load cell to minimize the scatter in the results. Some effort in that direction is under way.

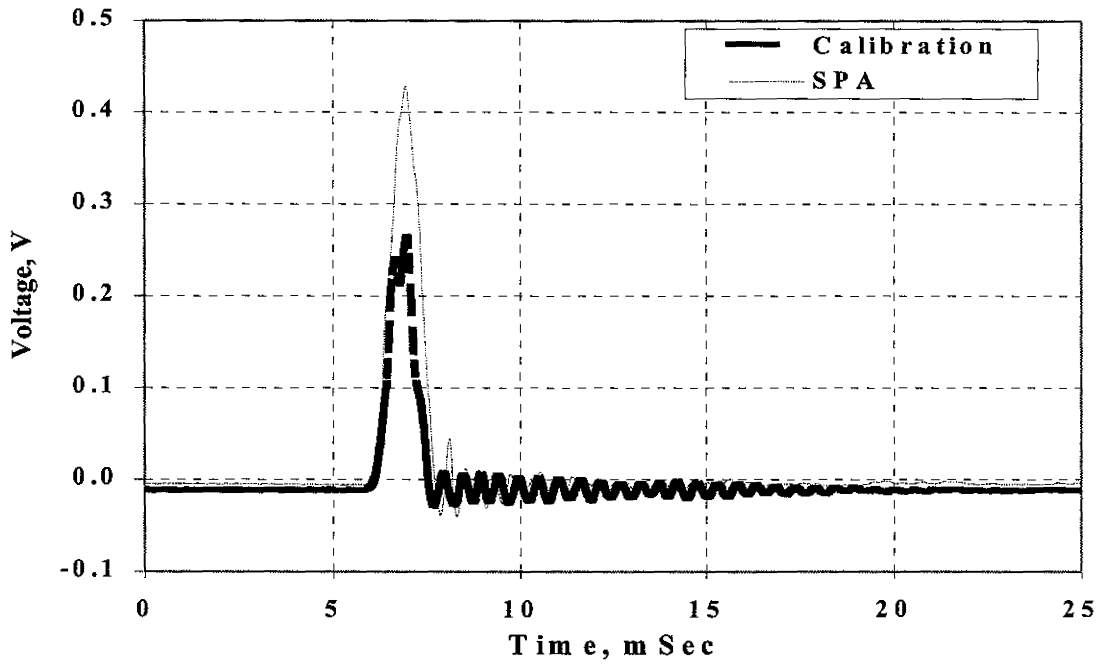


Figure 4.18 A Typical Load Time-History from the Calibration and SPA Load Cells

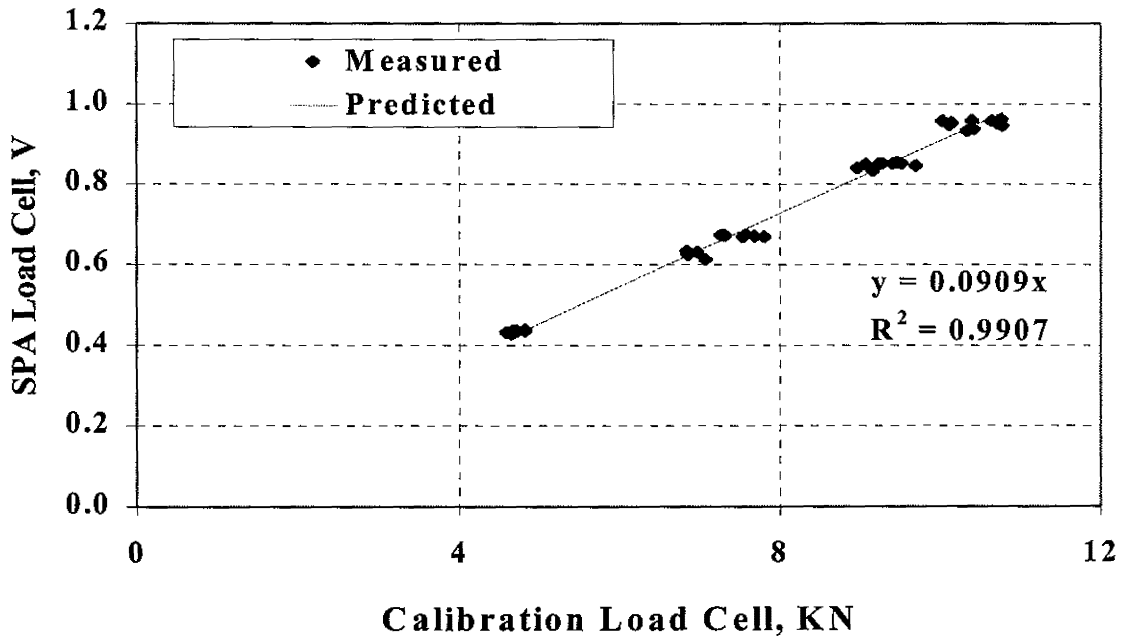


Figure 4.19 A Typical Calibration Curve of SPA Low-Frequency Load Cell

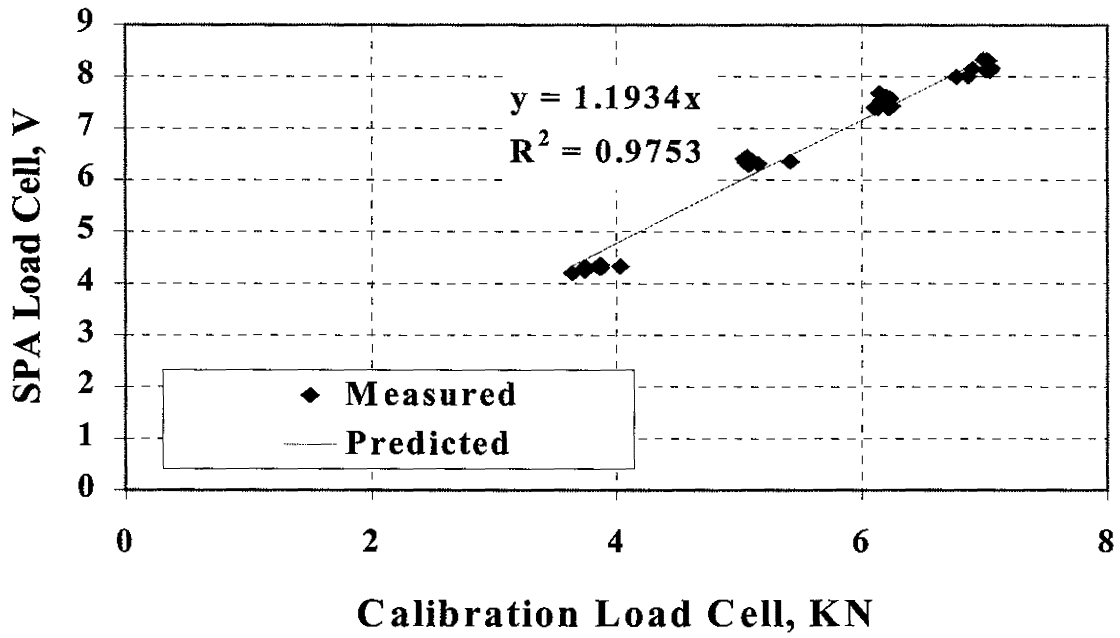


Figure 4.20 A Typical Calibration Curve of SPA High-Frequency Load Cell

References

- Baker, M.R., Crain, K., and Nazarian, S. (1995), "Determination of Pavement Thickness with a New Ultrasonic Device," Research Report 1966-1, Center for Highway Materials Research, The University of Texas at El Paso, El Paso, TX, 53 p.
- Nazarian, S., Yuan, D., Weissinger, E. (1997), "Comprehensive Quality Control of Portland Cement Concrete with Seismic Methods," Transportation Research Record 1575, Transportation Research Board, Washington, D.C.
- Nazarian S., Yuan D., and Baker M. (1995), "Rapid Determination of Pavement Moduli with Spectral-Analysis-of-Surface-Waves Method," Research Report 1243-1, The University of Texas at El Paso, 76 p.
- Nazarian, S., Baker, M. R., and Crain, K. (1993), "Fabrication and Testing of a Seismic Pavement Analyzer," Report H-375, Strategic Highway Research Program, Washington, DC, Dec., 156 pp.
- Nazarian, S., Tandon, V. and Briggs, R. C. (1991), "Development of an Absolute Calibration System for Nondestructive Testing Devices," Transportation Research Record 1293, Transportation Research Board, Washington, D.C.
- Nazarian S. and Stokoe, K.H., II (1986), "A Theoretical Sensitivity Study of the Falling Weight Deflectometer Device on Determining Moduli of Farm-to-Market Roads," Technical Memorandum IAC936-4, Center for Transportation Research, The University of Texas at Austin.
- Sansalone M., and Carino, N.J. (1989), "Detecting Delamination in Concrete Slabs with and without Overlay the Impact-Echo Method," ACI Materials Journal, Vol. 86, No. 2, Mar.-Apr., pp. 175-184.
- Tandon, V. (1990), "Development of an Absolute Calibration System for Nondestructive Testing Devices," Master of Science Thesis, Department of Civil Engineering, The University of Texas at El Paso, El Paso.

This page replaces an intentionally blank page in the original.

-- CTR Library Digitization Team

Appendix A
Specifications of Equipment Used

This page replaces an intentionally blank page in the original.

-- CTR Library Digitization Team

Table A.1 Specifications of Matching Network (Manufactured by Wilcoxon Research, Inc.)

Description	Units	Values
Model		N7C
Input Voltage, maximum	Vrms	42
F4 Channel		
Current, Maximum (Circuit Breaker)	amps rms	1.5/2.5
Fixed Output	Vrms	42
Frequency Range	Hz	10 - 5000
F7 Channel		
Voltage Output (Switch Position A)	Vrms	300
Frequency Range	Hz	1 - 25
Voltage Output (Switch Position B)	Vrms	500
Frequency Range	Hz	1 - 13
Voltage Output (Switch Position C)	Vrms	800
Frequency Range	kHz	1 - 5

Table A.2 Specifications of F4 Electromagnetic Shaker system (Manufactured by Wilcoxon Research, Inc.)

Description	Units	Values
Model		F4/Z820WA
Usable Frequency Range	Hz	10 - 7500
Maximum Continuous Current	amp rms	1.5
Maximum Continuous Current w/ Air Cooling	amps	2.5
Nominal Electrical Impedance	Ohms	25
DC Electrical Resistance	Ohms	13
Resonance Frequency, blocked	Hz	30
Forced Air Cooling Pressure, Maximum	psi	25

Table A.3 Specifications of Electromagnetic Shaker System Accelerometer (Manufactured by Wilcoxon Research, Inc.)

Description	Units	Values
Accelerometer Model		F4
Voltage Sensitivity	mV/g	100
Frequency Response (±0.5dB)	Hz	10 - 2000
Frequency Response (±1.0 dB)	Hz	6 - 3000
Frequency Response (±3.0dB)	Hz	3 - 6000
Power Requirements, Voltage Source	VDC	18 - 30
Current Regulating Diode	mA	2 - 10
Bias Output Voltage, Nom.	VDC	12
Output Impedance	Ohms	<100
Electrical Noise Broadband 2.5 Hz - 25 kHz, nom	mg	700
Electrical Noise Spectral 10 Hz	$\mu\text{g}/\sqrt{\text{Hz}}$	100
Electrical Noise Spectral 100 Hz	$\mu\text{g}/\sqrt{\text{Hz}}$	10
Electrical Noise Spectral 1000 Hz	$\mu\text{g}/\sqrt{\text{Hz}}$	1

Table A.4 Specifications of F4 Electromagnetic Shaker System Force Gage (Manufactured by Wilcoxon Research, Inc.)

Description	Units	Values
Impedance Head Model (Force Gage)		Z820WA
Voltage Sensitivity	mV/lb	100
Frequency Response (±0.5 dB)	Hz	10 - 2000
Frequency Response (±1.0 dB)	Hz	6 - 3000
Frequency Response (±3.0 dB)	Hz	3 - 6000
Power Requirements, Voltage Source	VDC	18 - 30
Current Regulating Diode	mA	2 - 10
Bias Output Voltage, Nom.	VDC	12
Output Impedance	Ohms	<100
Electrical Noise Broadband 2.5 Hz - 25 kHz, nom	mlb	500
Electrical Noise Spectral 10 Hz	$\mu\text{lb}/\sqrt{\text{Hz}}$	60
Electrical Noise Spectral 100 Hz	$\mu\text{lb}/\sqrt{\text{Hz}}$	10
Electrical Noise Spectral 1000 Hz	$\mu\text{lb}/\sqrt{\text{Hz}}$	1
Mass Below Force Gage (including stud)	gram	140
Effective Stiffness	lb/in	>500,000,000

Table A.5 Specifications of Piezoshaker system (Manufactured by Wilcoxon Research, Inc.)

Description	Units	Values
Model		F7
Usable Frequency Range	Hz	500 - 20,000
Maximum Input Voltage	V rms	800
Capacitance	μ F	0.010
Weight with Sensing Transducer	grams	1134
Contact Area (Diameter)	mm	15.2
Input Connector		Bendix SPOZA-8-3P
Cable Supplied	m	3

Table A.6 Specifications of Piezoshaker system Transducers (Manufactured by Wilcoxon Research, Inc.)

Description		Units	Values
Model			Z7
Accelerometer	Charge Sensitivity	pC/g	6
	Voltage Sensitivity	mV/g	12
	Capacitance	pF	500
	Frequency Range	Hz	1 to 14,000
Force Gage	Charge Sensitivity	pC/N	49
	Voltage Sensitivity	mV/N	25
	Capacitance	pF	2000
	Frequency Range	Hz	1 to 40,000
	Mass Below Force Gage	grams	20

Table A.7 Specifications of Arbitrary Waveform Generator (Manufactured by Wavetek San Diego, Inc.)

Description	Units	Values
Model Number		75
Waveform Resolution	points	8192 x 4095
Amplitude Range (50 ohms)	Vp	±0.005 - 5
Amplitude Range (open circuit)	Vp	±0.01 - 10
Offset Range (50 ohms)	V	+5 to -5
Maximum Offset Range (open circuit)	v	±10
Resolution	digits	3
Sample Rate Range	Hz	0.02 - 2 E+6
Frequency Resolution	digits	4
Input Impedance	KW	100
Vibration	Hz	5 - 55
Power	rms	90 - 128, 180 - 256
Shock	g	30

Table A.8 Specifications of Vibration Exciter (Manufactured by MB Electronics. A Division of Textron Electronics, Inc.)

Description	Units	Values
Model Number		EA 1250
Frequency Range	cps	5 - 10000
Frequency Range Usable to	cps	20000
Force Vector	lbs	15
Vector Capability	in./sec	70
Displacement	in.	0.5
Max. Acceleration with Internal Accelerometer	g	49
Moving Weight with Internal Accelerometer	lbs	0.255
First Resonance	cps	8900
Power ($\pm 5\%$)	V	9
Power ($\pm 5\%$)	A	4.2
Power	W	28
Driver Coil Resistance	ohms	0.65

Table A.9 Specifications of High Resolution Accelerometer (Manufactured by PCB Piezotronics, Inc.)

Description	Units	Values
Model		352A
Voltage Sensitivity	mV / g	1000
Frequency Range ($\pm 5\%$)	Hz	5 to 8000
Frequency Range ($\pm 10\%$)	Hz	3 to 10000
Resonant Frequency	kHz	≥ 25
Amplitude Range	$\pm g$ pk	4
Resolution (broadband)	g pk	0.0001
Mechanical Shock Limits	$\pm g$ pk	1000
Amplitude Linearity	%	± 1
Transverse Sensitivity	%	≤ 5
Base Strain Sensitivity	g/m^e	≤ 0.001
Excitation Voltage	VDC	20 to 30
Constant Current Excitation	mA	2 to 20
Output Impedance	ohms	≤ 300
Output Bias Voltage	VDC	8 to 14

Table A.10 Specifications of Power Amplifier (Manufactured by Wilcoxon Research, Inc.)

Description	Units	Values
Model Number		PA7C
Amplifier Channels		2
High Pass Filter for F4 Channel	Hz	15
High Pass Filter for F7 Channel	Hz	440
Power per Channel	W	115
Combined Channels Power (into 8 ohms)	W	230
Total Harmonic Distortion (20 Hz to 20 kHz)	%	<0.020
Intermodulation Distortion (Into 8 ohms, 1-115 W)	%	<0.005
Frequency Response (Into 8 ohms, at 1 W, -3dB)	Hz	1 - 50000
Input Impedance	KOhms	2.5
Input Limit	Vrms	2.2
Power Consumption (both Channels)	VA	840
AC Power Line	V	120
AC Power Line	Hz	60

Table A.11 Specifications of High Resolution Accelerometer (Manufactured by PCB Piezotronics, Inc.)

Description	Units	Values
Model		352A78
Voltage Sensitivity	mV / g	100
Frequency Range ($\pm 5\%$)	Hz	5 to 15000
Frequency Range ($\pm 10\%$)	Hz	3 to 18000
Resonant Frequency	kHz	≥ 45
Amplitude Range	$\pm g$ pk	50
Resolution (broadband)	g pk	0.001
Mechanical Shock Limits	$\pm g$ pk	5000
Amplitude Linearity	%	± 1
Transverse Sensitivity	%	≤ 5
Base Strain Sensitivity	g/m^e	≤ 0.001
Excitation Voltage	VDC	20 to 30
Constant Current Excitation	mA	2 to 20
Output Impedance	ohms	≤ 300
Output Bias Voltage	VDC	8 to 14